PIP4K HAS A CATALYTIC INDEPENDENT ROLE IN MODULATING PIP5K AND THE PI3K PATHWAY

A Dissertation

Presented to the Faculty of Weill Cornell Graduate School

of Medical Sciences

in Partial Fulfillment of the Requirements for the Degree of

Doctor of Philosophy

by

Diana G. Wang

August 2018

PIP4K HAS A CATALYTIC INDEPENDENT ROLE IN MODULATING PIP5K AND THE PI3K PATHWAY

Diana Grace Wang, Ph.D.

Cornell University 2018

Phosphatidylinositol-4-phosphate-5-kinase (PIP5K) and phosphatidylinositol-5-phosphate-4-kinase (PIP4K) are two families of lipid kinases that catalyze production of phosphatidylinositol-4,5-bisphosphate ($PI(4,5)P_2$). The majority of cellular $PI(4,5)P_2$ is produced by PIP5Ks, using PI(4)P as a substrate. In a non-canonical pathway, PIP4Ks catalyze the conversion of PI(5)P into $PI(4,5)P_2$, but the importance of PIP4K has remained unclear.

Unexpectedly, we find that PIP4K has a kinase independent role in regulating cellular $PI(4,5)P_2$ levels. We demonstrate that PIP4Ks act as negative regulators of PIP5Ks and that depletion of PIP4K causes hyperactivation of PIP5Ks. Increased cellular $PI(4,5)P_2$ generation by PIP5Ks promotes flux through the PI3K pathway, and these effects are reversed by reconstitution with kinase-dead PIP4K. This novel role for PIP4Ks provides an additional mechanism by which these kinases regulate cellular metabolism, which has the potential to be exploited by therapeutics.

BIOGRAPHICAL SKETCH

Diana Grace Wang was born in 1990 in Cold Spring, NY to Helen and Li Wang. She grew up in LaGrangeville, NY, and also spent two years of elementary school in Manassas, VA. Diana attended Arlington High School, and spent her free time swimming or playing the violin. She took her first biology class senior year of high school.

In 2008, Diana arrived at Massachusetts Institute of Technology (MIT) in Cambridge, MA. Her first research experience was in the lab of Leonard Guarente, studying the role of sirtuins in Alzheimer's Disease. Next, she worked in the lab of Tyler Jacks to study lung cancer genetics. The summer before graduating, Diana worked at Merck in the vaccines development group. She was grateful for the opportunities to explore various biomedical fields. Diana graduated from MIT in May, 2012 with a Bachelors of Science in Biology and concentration in Economics.

A month after graduation, Diana moved to New York City to begin the Tri-Institutional MD/PhD program. Under the direction of Dr. Lewis Cantley, Diana began her dissertation research on phosphatidylinositol lipids. For four years, she focused on understanding the functions of the family of phosphatidylinositol-5-phosphate-4-kinases (PIP4Ks). Her experience as part of the Cantley lab PIP4K team was rewarding on many levels. The group encountered many obstacles, and tested many paradigm shifting hypotheses. Although she is sad to leave her lab and labmates, she is looking forward to the opportunities that lie ahead.

ACKNOWLEDGEMENTS

First, I want to thank my early mentors at MIT, Dr. Tyler Jacks and Dr. Eric Snyder. With their patience and encouragement, I embarked on this path to become a physician-scientist.

I would like to thank my thesis advisor, Dr. Lewis C. Cantley. He inspires everyone in lab to be creative and look for paradigm shifting discoveries. His passion for understanding PIP4K is contagious, and I am grateful for his support through all my experimental endeavors. The Cantley Lab has been a wonderful place to grow and learn. I was surrounded with so many talented post-docs and grad students in my lab. There is the PIP4K team/family: Dr. Marcia Paddock, Dr. Jared Johnson, Dr. Hyeseok Shim, Dr. Jonathan Yang, Dr. Mark Lundquist, Dr. Marcus Goncalves, and Dr. Evan Noch. We have shared moments of excitement after stumbling across new findings, and shared more moments of confusion. I must also mention past and present post-docs that were generous with their time and wisdom: Dr. Gina DeNicola, Dr. Florian Karreth, Dr. Valbona Luga, Dr. Yuxiang Zheng, Dr. Cindy Hodakoski, Dr. Ben Hopkins, and Dr. Ben Stein. Thank you to all the past and present Cantley lab technicians who have kept the lab up and running. In particular, I want to thank Oksana, Solomon, and Janet for helping me at the bench.

Next, I want to acknowledge the wonderful members of the Meyer Cancer Center for helpful discussions and mentorship, including Dr. Lukas Dow, Dr. Elena Piskounova, and Dr. John Blenis.

I am grateful to have met collaborative colleagues in the field, who have evolved into mentors. I would like to thank Dr. Tamas Balla, Dr. Jeremy Baskin, and Dr. Seth Fields, for sharing their expertise.

I want to thank my committee members for their advice and insight—Dr. Lukas Dow, Dr. Fred Maxfield, Dr. Sohail Tavazoie, and Dr. Jonathan Yang. I need to acknowledge the people who have logistically made my training possible—thank you to the BCMB program, Dr. Olaf Anderson, Dr. Ruth Gotian and the rest of the Tri-I program administrators, and to the NIH MSTP grant T32GM07739.

Finally, I want to thank my friends and family. There is a special place in my heart for my thirteen classmates, the incoming MD-PhD class of 2012. I've also had a wonderful support group in NYC, consisting of friends from college and high school. I want to thank Cosmo, who has taken me on so many adventures over the years. Finally, I would like to thank my entire family for their continued support— Li Wang, Helen Wang, Vinson Wang, Carol Li, Pom, and Dora.

TABLE OF CONTENTS

LIST OF FIGURES

LIST OF TABLES

LIST OF ABBREVIATIONS

^{3}H	tritium
3xHA	three tandem human influenza hemagglutinin
3xFLAG	three tandem FLAG epitopes
Akt	AK thymoma, protein kinase B (PKB)
ATP	Adenosine triphosphate
CCLE	cancer cell line encyclopedia
cDNA	complementary DNA
CME	clathrin mediated endocytosis
CMV	cytomegalovirus
CRISPR	clustered regularly interspaces short palindromic repeats
Da	Dalton
DAG	diacylglycerol
DMEM	Dulbecco's modified eagles media
DMSO	dimethylsulfoxide
EBSS	Earle's balanced salt solution
EDTA	ethylenediamine tetraacetic acid
EE	early endosome
EGTA	ethyleneglycol tetraacetic acid
FBS	fetal bovine serum
FOXO1/3A	forkhead box O 1/3A
gDNA	genomic DNA
GFP	green fluorescent protein
GSK3	glycogen synthase kinase 3
GST	glutathione S-transferase

GTP	guanine triphosphate
GWAS	genome wide association study
HA	human influenza hemagglutinin
HPLC	High pressure liquid chromatography
IB	immunoblot
IF	immunofluorescence
IgG	immunoglobulin
IP	immunoprecipitate
IP_3	inositol 1,4,5-trisphosphate
iRFP	infrared RFP
KD	kinase dead
LE	late endosome
M	Molar
MAPK	mitogen-activated protein kinase
miRNA	microRNA
MOI	multiplicity of infection
mTOR	mechanistic target of rapamycin
OCRL	Lowe occulocerebrorenal syndrome protein
PA	phosphatidic Acid
PBS	phosphate buffered saline
PCR	polymerase chain reaction
PDK1	phosphoinositide dependent kinase 1
PH	pleckstrin homology
PHD	plant homeodomain
PI	phosphatidylinositol
PI3K	phosphatidylinositol 4,5-bisphosphate 3'-OH kinase

$PI(3,4,5)P_3$	PIP3, phosphatidylinositol 3,4,5-trisphosphate
PI(4)P	phosphatidylinositol 4-phosphate
$PI(4,5)P_2$	phosphatidylinositol 4-5-bisphosphate
PI(5)P	phosphatidylinositol 5-phosphate
PIP	phosphatidylinositol phosphate
PIP4K	phosphatidylinositol 5-phosphate 4'-OH kinase
PIP5K	phosphatidylinositol 4-phosphate 5'-OH kinase
PLC	phospholipase C
PLD	phospholipase D
PRAS40	proline-rich AKT substrate, 40 kDa
PTEN	phosphatase and tensin homologue
RFP	red fluorescent protein
RNA-seq	ribonucleic acid sequencing
RNAi	RNA interference
RPMI	Roswell Park Memorial Institute medium
RTK	receptor tyrosine kinase
shRNA	short hairpin RNA
SILAC	stable isotope labeling using amino acids in cell culture
siRNA	small interfering RNA
TOR	target of rapamycin
TKD	triple knockdown
TKO	triple knockout
TLC	thin layer chromatography
WB	western blot

CHAPTER ONE: INTRODUCTION: PIP4K AND PHOSPHATIDYLINOSITOL LIPIDS IN REGULATION OF DIVERSE BIOLOGICAL PROECESSES

1.1 GENERATION OF CELLULAR PI(4,5)P_2

Phosphatidylinositol (PI) is a 1,2-diacylglycerol lipid connected to a *myo*-inositol head group, which can be phosphorylated at the 3, 4, and 5 positions, to generate phosphatidylinositol-phosphates (PIPs, phosphoinositides). PIPs are highly dynamic, through reactions catalyzed by kinases and phosphatases, or hydrolyzed by phospholipases (Figure 1.1).

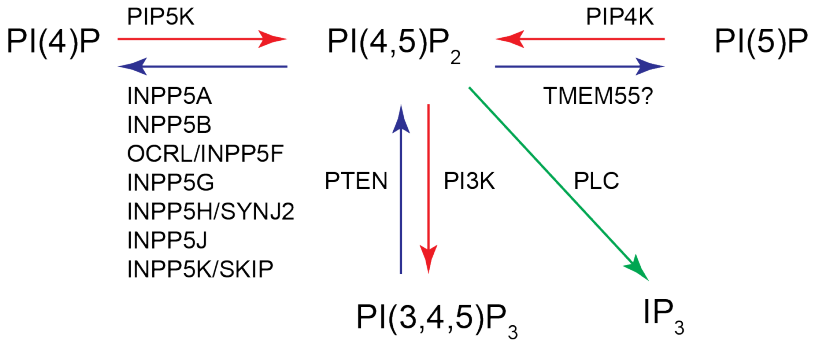

Figure 1.1 Pathways to generate PI(4,5)P_2.
The PIP5K family uses PI(4)P as a substrate to generate PI(4,5)P_2. The reaction can be reversed by many different 5-phosphatases. The PIP4K family catalyzes the conversion of PI(5)P to PI(4,5)P_2. There has been one report of a 4-phosphatase named TMEM55A/B. PI(3,4,5)P_3 is converted to PI(4,5)P_2 in the presence of PTEN, a 3-phosphatase. PI(4,5)P_2 can be hydrolyzed by phospholipase C (PLC) to create inositol-1,4,5-trisphosphate (IP_3). Red arrow indicate reactions mediated by lipid kinases. Blue arrows indicate reactions mediated by lipid phosphatases. Green arrow indicates hydrolysis by phospholipase.

Phosphatidylinositol-5-phosphate-4-kinase (PIP4K) and phosphatidylinositol-4-phosphate-5-kinase (PIP5K) are two families of lipid kinases that catalyze production of phosphatidylinositol-4,5-bisphosphate ($PI(4,5)P_2$)[1,2]. The majority of cellular $PI(4,5)P_2$ is produced by PIP5Ks, using PI(4)P as a substrate. Both the substrate and product of PIP5K are highly abundant phosphoinositides. The PIP5K family is referred to as the "Type 1 PIP-kinases" and is conserved from unicellular eukaryotes. Knockout of the yeast paralog of PIP5K, *MSS4*, is lethal[3]. PIP5K biology has been extensively studied and the focus of multiple reviews[4-7].

In the non-canonical pathway for $PI(4,5)P_2$ synthesis, PIP4Ks catalyze the conversion of PI(5)P into $PI(4,5)P_2$. This function emerged in metazoans[8] and the PIP4K family is referred to as the "Type 2 PIP-kinases." In 1997, the Cantley Lab discovered the phosphatidylinositol-5-phosphate-4-kinase (PIP4K) family, and in doing so, identified the in-vivo presence of a new phosphoinositide, PI(5)P[9]. The importance of PIP4K and its substrate PI(5)P remains poorly understood.

1.2 OVERVIEW OF PIP4K

PHENOTYPES FROM PIP4K KNOCKOUT STUDIES PROVIDE EVIDENCE THAT PIP4K FAMILY MEMBERS ARE NOT REDUNDANT

The three members of the PIP4K family, PIP4K$\alpha/\beta/\gamma$, are encoded by *PIP4K2A*, *PIP4K2B*, and *PIP4K2C*. Murine knockout models of PIP4K family members have been generated over the years, revealing complex roles of these enzymes in metabolism (Table 1.1).

Murine knockout of *Pip4k2b* increases insulin sensitivity, as measured through an insulin tolerance test[10]. *Pip4k2b*$^{-/-}$ mice did not exhibit changes during glucose tolerance tests, which suggests that insulin-sensitive tissues have an exaggerated response to insulin in the setting of normal pancreatic insulin release. Upon examination of different insulin-sensitive tissues, there is higher Akt activation in skeletal muscle, and to a lesser extent, liver. Murine knockout of other isoforms of PIP4K do not modulate insulin sensitivity[11].

Co-deletion of *Pip4k2b* and *Trp53* is embryonically lethal, although it is unclear which tissues are affected during embryogenesis, and what the mechanism may be[12]. Nonetheless, there are significant efforts to exploit the relationship between PIP4K and p53, in hopes of restraining tumorigenesis in cancers driven by loss of p53. *Pip4k2a* knockout mice did not have obvious phenotypes, although there are ongoing efforts to characterize the function of this enzyme in the nervous system. Interestingly, concomitant loss of *Pip4k2a* and *Pip4k2b* allels results in perinatal lethality, due to defects in autophagy during

autophagosome-lysosome fusion[12,13]. As a result, mouse embryonic fibroblasts from *Pip4k2a*$^{-/-}$; *Pip4k2b*$^{-/-}$ mice accumulate lysosomes and autophagosomes, and exhibit enhanced transcriptional programs for lysosomal biogenesis[13].

Murine knockout of *Pip4k2c* increases mTOR activity in multiple tissue types, leading to systemic inflammation[11]. Various tissues examined had increased immune infiltrates, and pro-inflammatory cytokines were elevates in the serum. Interestingly, there is one isoform in *Drosophila,* dPIP4K. We would predict that loss of all three mammalian isoforms of PIP4K should phenocopy loss of the sole isoform in Drosophila. Surprisingly, deletion of *dPIP4K* decreases TOR activity, resulting in smaller larvae[14]. Since loss of PIP4Kγ increases mTOR signaling, this paradox raises the possibility that PIP4Kγ has dominant negative functions on PIP4Kα/β.

There is published evidence that *Pip4k2b*$^{-/-}$; *Pip4k2c*$^{-/-}$ is embryonically lethal[11], and unpublished evidence that *Pip4k2a*$^{-/-}$; *Pip4k2c*$^{-/-}$ mice are viable, but difficult to breed. We conclude that in certain settings, PIP4K isoforms may have redundant functions or dominant negative effects. The family of enzymes appear critical for development and survival of higher level organisms.

Table 1.1 Phenotypes of murine knockouts of PIP4K isoforms

Gene knockout	Viability	Phenotype
Pip4k2a$^{-/-}$	yes	None?
Pip4k2b$^{-/-}$	yes	Lamia et al. 2004
Pip4k2c$^{-/-}$	yes	Shim et al. 2016
Pip4k2a$^{-/-}$ *Pip4k2b* $^{-/-}$	perinatal lethality	Emerling et al. 2013
Pip4k2b$^{-/-}$ *Pip4k2c* $^{-/-}$	embryonic lethality	----
Pip4k2a$^{-/-}$ *Pip4k2c* $^{-/-}$	yes	None?

CURRENT UNDERSTANDING OF BIOCHEMICAL FEATURES OF PIP4K ISOFORMS

PIP4Kα, PIP4Kβ, and PIP4Kγ, have varying levels of activity and are enriched in different subcellular locations[15-21].. PIP4Kα is about 1000- fold more active than PIP4Kγ, and PIP4Kα is about 10- fold more active than PIP4Kβ, summarized by α>>β>>γ[8].

All three PIP4K members have been crystallized and deposited into the protein data bank (PDB, www.rcsb.org) under accession codes PIP4K2A: 2YBX; PIP4K2B: 3X01; PIP4K2C: 2GK9. The structure of PIP4Kβ is described as homodimers, with a series of beta sheets at the amino terminus. The first beta sheet has residues mediating bond formation at the homo-dimer interface (Figure 1.3). The series of beta sheets of each subunit line up to create a flat, positively charged interface that is proposed to mediate membrane binding[22]. Each

subunit has enzymatic activity, but it is unclear if monomers exist *in-vivo*, and if enzymatic properties are altered upon dimerization. All three isoforms are predicted to homodimerize and heterodimerize[8,21], and PIP4Kγ is crystallized as a tetramer with all four catalytic pockets facing the same side of the complex. It is predicted that additional dimers can associate, thereby producing hexamers, octamers, and higher order oligomers. However, the relative abundance of these different higher order species is not known. PIP4K achieves specificity for PI(5)P through its activation loop[23]. Swapping the PIP4K and PIP5K activation loops changes their substrate specificity, such that PIP4K uses PI(4)P as a substrate, and vice-versa. In fact, exchanging one amino acid was able to change substrate specificity[24].

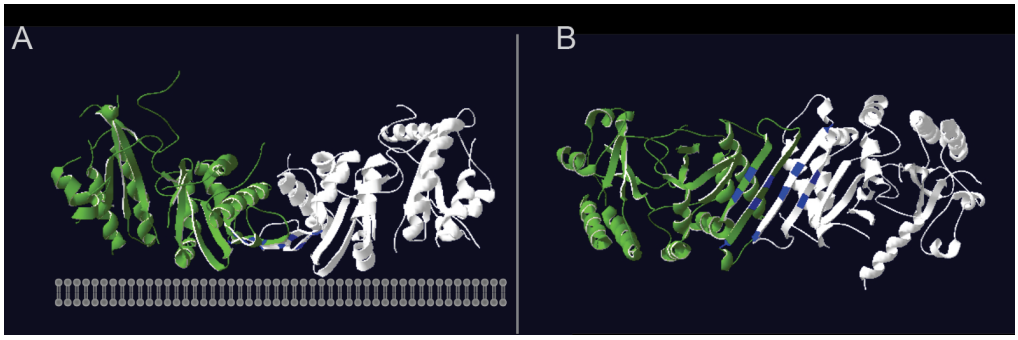

Figure 1.2 Crystal structure of PIP4Kβ.
All three PIP4K isoforms have been crystallized and deposited on PDB. The PIP4Kβ structure is representative of the entire family. **(A)** PIP4Kβ is crystalized as a homodimer. Unique ribbon color indicates each subunit. A flat, positively charged interface mediates interactions with membranes. **(B)** Membrane facing view to examine positively charged beta sheets. Basic residues are colorized in blue.

Localization studies utilizing transient overexpression of fluorescently tagged PIP4K isoforms, or CRISPR mediated recombination of fluorescent tags at endogenous genomic loci reveal that both PIP4Kα and PIP4Kβ are found in the plasma membrane and nucleus, and PIP4Kγ is enriched in multiple endomembrane compartments[25-28]. In one study, PIP4Kβ was found to be enriched in the nucleus, and modulated the abundance of nuclear PIP4Kα through direct interactions[21]. In another study, PIP4Kβ was found to be enriched in the endoplasmic reticulum (ER) upon fractionation of murine brain tissue[29]. In a separate report, the phosphorylation state of PIP4Kγ was correlated with differential localization to the Golgi or ER[26]. It is possible that localization of these enzymes varies amongst different tissue types, and shuttles between compartments in response to cues such as the nutrient state.

The PIP4K family is thought to provide a minor pool of total cellular $PI(4,5)P_2$. Instead, it is postulated that these enzymes are critical for maintenance of levels of PI(5)P, their substrate[30]. In order to understand the mechanistic underpinnings of how PIP4Ks modulate cellular processes, it is important to consider existing mechanistic paradigms through which phosphoinositide lipids and their lipid kinases can direct vesicle trafficking and cellular signaling. A plethora of proteins have been identified that bind with high affinity and selectivity to specific phosphoinositides. This is a shared feature underlying the mechanisms discussed in the next two sections.

1.3 PIP4K IN REGULATION OF VESICLE TRAFFICKING

Cellular phosphoinositides act as markers of membrane identity, and are tightly regulated in time and location to facilitate vesicle trafficking events[2]. Phosphoinositides have a role in many processes: endocytosis, endosome maturation, vesicle motility, vesicle fusion/fission, and exocytosis[31,32].

For example, in clathrin mediated endocytosis (CME), $PI(4,5)P_2$ recruits adaptor proteins during early steps of clathrin-coat formation[33]. In order to complete endocytosis, dynamin is recruited to the neck of membrane pits to coordinate microtubule bundles to generate force for membrane scission. Next, conversion of $PI(4,5)P_2$ to PI(4)P by the phosphatase synaptojanin facilitates dynamin-driven membrane fission[34] (Figure 1.3).

There is evidence that PIP4K regulates CME. Loss of *dPIP4K* increases rates of CME, and photoreceptor accumulation on Rab5 positive endosomes[35]. There is partial co-localization of dPIP4K with Rab5, which marks early endosomes (EE). Recently, PIP4Kγ was reported to alter Notch1 passage through recycling endosomes[27]. Also, an unbiased kinome RNAi screen found loss of PIP4K isoforms disrupts trafficking between the Golgi Apparatus and the endoplasmic reticulum[36]. It appears that PIP4K may affect many aspects of endosome maturation and vesicle trafficking.

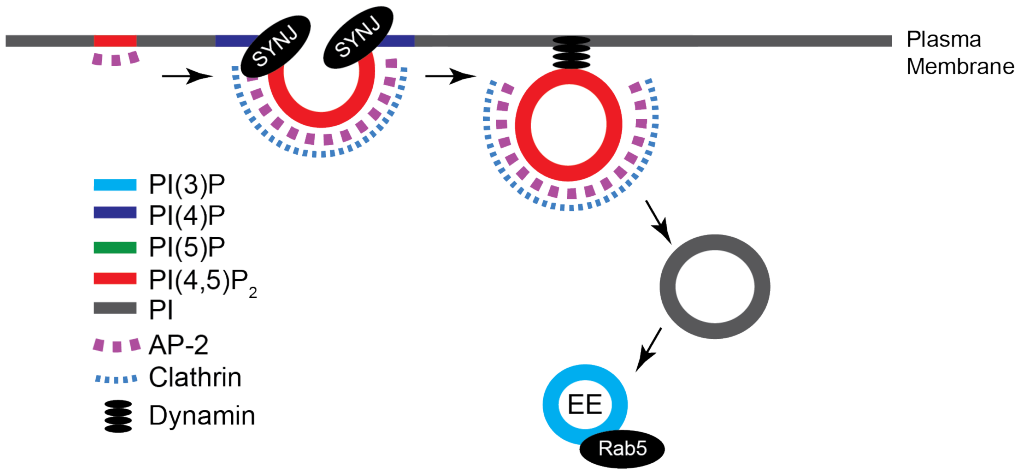

Figure 1.3 Phosphoinositides regulate clathrin-mediated endocytosis. To initiate clathrin-mediated endocytosis (CME), adaptor proteins, such as AP-2, recognize PI(4,5)P_2 for generation of clathrin-coated pits. Synaptojanin (SYNJ), a 5-phosphatase, limits diffusion of PI(4,5)P_2 in the membrane by converting it to PI(4)P. To complete CME, Dynamin is needed for scission. Early endosomes (EE) become enriched for PI(3)P, which recruits Rab5 during endosome maturation.

During autophagy, late endosomes and autophagosomes fuse with lysosomes for degradation and recycling of vesicle contents. During autophagosome-lysosome fusion, PI(4)P is thought to be required, independent of its ability to act as a precursor for PI(4,5)P_2[37]. Loss of OCRL, a lysosomal 5-phosphatase that PI(4,5)P_2 to PI(4)P, produced a similar defect in autophagy, supporting the model that autophagosome fusion requires PI(4)P[38] (Figure 1.4). In a different membrane setting, vesicle fusion during exocytosis is promoted by PI(4,5)P_2, through its ability to directly interact with synaptotagmin-1[39].

Vicinanza et al. found that PI(5)P recruits autophagy effector proteins to promote autophagosome clearance of mutant huntingtin

protein[40]. Overexpression of active PIP4Kγ impaired autophagy, presumably through eliminating PI(5)P on autophagosomes, since overexpressing catalytic-dead PIP4Kγ did not have this effect. In another report, deletion of *Pip4k2a* and *Pip4k2b* in mice caused a defect in autophagosome-lysosome fusion[13]. Since both PI(4)P and $PI(4,5)P_2$ are critical for autophagosome-lysosome fusion, these lipids could be supplied by PIP4K and OCRL, summarized by PI(5)P→ $PI(4,5)P_2$→ PI(4)P. It is likely that only a subset of autophagosome-lysosomal fusion events require PIP4K, since yeast, which lack PIP4K, successfully accomplishes autophagy.

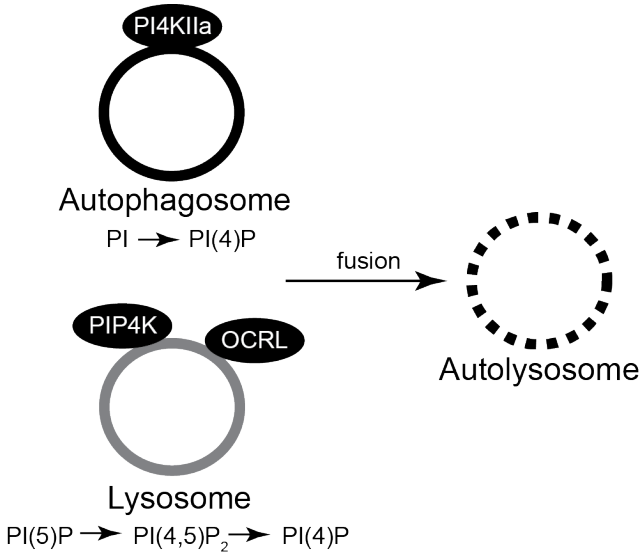

Figure 1.4 Model for PIP4K regulation of autophagosome-lysosome fusion.
Loss of PIP4K causes defects in autophagosome-lysosome fusion. This may be one pathway to form lysosomal PI(4)P. Defects in autolysosome formation occur when lysosomes or autophagosomes lose their ability to generate PI(4)P.

Phosphoinositides bind to cytoskeletal adaptor proteins to direct movement of membranous structures. Interactions between plasma membrane $PI(4,5)P_2$ and cytoskeletal adaptor proteins drive changes in plasma membrane dynamics[41]. $PI(4,5)P_2$ has the ability to induce membrane ruffling or actin comets depending on the context in which it becomes enriched[42-44]. Cell migration and invasion are directed through cytoskeletal reorganization, and these characteristics influence how cancers grow and metastasize[45-48].

There is evidence that PIP4K can control features of the cytoskeleton, through regulation of PI(5)P. Lipid droplets are thought to have PI(5)P on their surface, and interactions between PI(5)P and Septin 9 mediate anterograde lipid droplet trafficking along microtubules[49]. In many reports, increased PI(5)P promotes cell migration through activation of Rac1, a well described small G-protein which directs actin polymerization[50-53]. There may be also be catalytic-independent mechanisms through which PIP4K controls the cytoskeleton, since knockdown of PIP4K2C, but neither PIP4K2A nor PIP4K2B, was shown to protect against arsenite-induced mitotic spindle defects[54].

There is much evidence that PIP4K mediates changes in vesicle trafficking. So far, the primary focus of these studies has been the consequence of losing PIP4K catalytic function. Dissecting the roles of PI(5)P and PI(5)P-derived PI(4,5)P2 in control of vesicle trafficking events warrants further investigation.

1.4 PIP4K IN REGULATION OF SIGNALING

Cellular phosphatidylinositols are tightly regulated to recruit PIP-binding effector proteins that control the initiation, propagation, and termination of signaling events.

Stimulation of a variety of membrane receptors activates the hydrolysis of $PI(4,5)P_2$ by PLC to generate the second messengers, inositol 1,4,5-trisphosphate (IP_3) and diacylglycerol (DAG) (Figure 1.5). IP_3 binds IP_3 receptors (IP_3Rs) on the endoplasmic reticulum that increases intracellular Ca^{2+} channels and activation of PKC. Stimulation of receptor-tyrosine kinases (RTKs) such as the insulin receptor (IR) activates PI3K conversion of $PI(4,5)P_2$ into $PI(3,4,5)P_3$ and subsequent recruitment of the protein kinases, PDK-1 and Akt (Figure 1.5). Many signaling cascades are downstream of PDK-1 and Akt, resulting in altered cellular metabolism. One important consequence is the translocation of GLUT4 to the plasma membrane, which enhances glucose uptake[55].There is crosstalk between various pathways, for complex feedback loops[56,57]. Notably, mTORC1 is activated downstream of PI3K activation, and promotes silencing of IRS-1 as a mechanism of negative feeback[58].

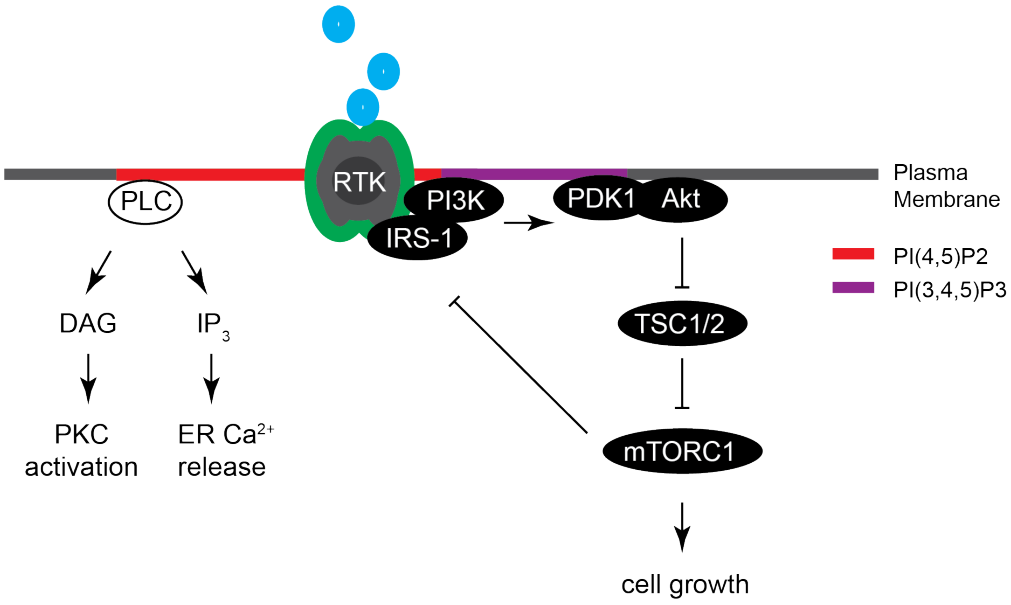

Figure 1.5 PI(4,5)P_2 mediates important signaling cascades
Upon cell stimulation by various factors, PLC cleaves PI(4,5)P_2 to generate second messengers DAG and IP_3. These molecules control many pathways, through activation of PKC and increasing intracellular Ca2+. Activation of receptor tyrosine kinases (RTKs) potently activates the PI3K pathway, which converts PI(4,5)P_2 to PI(3,4,5)P_3. Many effector proteins are recruited by this lipid, and subsequently activated. Notably, the PI3K pathway can activate Akt, which phosphorylates TSC1/2, thereby de-repressing mTORC1.

PIP4K has been reported to modulate PI3K/Akt signaling. TCR activation and engagement of insulin mimetics have been shown to upregulate PI(5)P[59,60]. In response to insulin stimulation, *Pip4k2b* knockout mice have enhanced glucose clearance and increased activation of Akt in liver and muscle tissue[10]. Conversely, overexpression of PIP4Kβ decreases activation of the PI3K pathway, which is attributed to the ability of PIP4K to inhibit a PI(3,4,5)P_3 phosphatase [61]. These studies reveal a paradox in which deletion of an

enzyme that generates PI(4,5)P_2, the substrate for PI3K, results in more, rather than less, PI3K activity.

There is evidence that PIP4K has catalytic-dependent mechanisms to affect the PI3K pathway. Increased levels of PI(5)P enhance activation of Akt in many systems, and is highly reproducible. During *Shigella flexneri* infection, Ipgd, a virulence factor with 4-phosphatase activity, is delivered into cells to cause a dramatic increase in PI(5)P[62]. This lipid is thought to directly activate host cell PI3K[63]. PI(5)P has also been described to mediate oxidative stress induced activation of Akt[64].

mTOR, a downstream component of the PI3K/Akt pathway, is intricately linked to PIP4K. *Pip4k2c* knockout mice exhibit increased mTOR signaling in multiple tissues, resulting in increased inflammation[11]. On the other hand, loss of dPIP4K conferred the opposite phenotype, with decreased mTOR signaling and smaller larvae size[14]. To add to the complexity, mTORC1 can directly phosphorylate PIP4Kγ, which is involved in negative feedback onto mTORC1[26].

To increase the complexity of our understanding of why PIP4K may modulate the PI3K/Akt pathway, one group reported that deletion of PIP4Kα decreases Akt signaling and plasma membrane PI(3,4,5)P_3 during exponential growth in serum-replete media[65]. However, they also employed an auxin-degron system to acutely eliminate PIP4Kα over the course of hours, which revealed the opposite effect—acute loss of PIP4Kα *increases* Akt signaling. The authors were unable to explain the differences between acute and prolonged depletion of PIP4Kα. We

speculate that acute loss of PIP4K is predicted to increase PI(5)P levels, which would increase Akt activation. Prolonged loss of PIP4Kα may cause nutrient stress through impaired autophagy, and influence mTOR feedback onto the PI3K pathway.

Lastly, PIP4K may be involved in modulating the response to the second messenger, IP_3. IRBIT is an IP_3R binding protein, that blocks IP_3 binding to IP_3R[66,67]. There is evidence of a direct interaction between IRBIT and PIP4Kα as well as between IRBIT and PIP5Kα[68]. This raises that possibility that IRBIT modulates ion channels and Ca^{+2} signaling through interactions with PIP4K and PIP5K, which provide local $PI(4,5)P_2$.

1.5 DEVELOPMENT OF INHIBITORS OF PIP4K

High throughput screening assays for small molecule inhibitors of PIP4K have been developed[69], and many groups have described and validated candidate PIP4K inhibitors[70,71]. Use of these inhibitors has been limited and confounded by the possibility of off-target effects, since these molecules demonstrate IC50s in the μM concentration. Use of a small molecule inhibitor of PIP4Kγ can reduce accumulation of mutant huntingtin protein, but the weakness of this study lies in the their use of a drug in the μM range, over the course of hours[72]. Moreover, it is unclear if the inhibitor has the ability to inhibit PIP4Kγ. Assays to assess potency of inhibitors on kinases rely on measuring the ability of a drug to displace ATP from the kinase. PIP4Kγ is predicted to have a

high Km for ATP, and therefore many non-specific molecules can easily displace ATP, in the absence of strong binding. These putative inhibitors need further optimization to increase potency and specificity.

A major hurtle to validating small molecule inhibitors is the lack reliable cellular readouts for potent on-target PIP4K inhibition. Levels of PI(5)P are difficult to measure, even by high pressure liquid chromatography (HPLC). We lack a surrogate read-out in cells that is sensitive to detect changes in PI(5)P. While this chapter has summarized many of the phenotypes associated with loss of PIP4K, it remains unclear how inhibition of different members of the PIP4K family may produce similar or opposite effects. Also, it is possible that only a subset of the phenotypes previously reported are driven by the enzymatic function of PIP4Ks.

The PIP4K field has primarily focused on how loss of the catalytic function of these enzymes mediate changes in vesicle trafficking and cell signaling. In the work presented in this thesis, we challenge this paradigm and draw attention to one, of possibly many, catalytic-independent functions of the PIP4K family. First, we optimize and validate a toolset for studying the PIP4K family. We observe that loss of PIP4K increases cellular $PI(4,5)P_2$, and explore a novel, catalytic-independent function of the PIP4K family in negatively regulating production of $PI(4,5)P_2$. We find that loss of the catalytic-independent functions PIP4K results in increased PIP5K activity and signaling through the PI3K pathway.

CHAPTER TWO: THE PIP4K FAMILY POSESS A NOVEL, CATALYTIC INDEPENDENT FUNCTION IN REGULATING CELLULAR PI(4,5)P_2

2.1 ABSTRACT

Study of a single mammalian PIP4K family member produces an incomplete picture. To facilitate investigation on the family of PIP4K enzymes, we have generated tools to systematically deplete members of the PIP4K family. We optimize knockdown of single or multiple PIP4K isoforms, in various combinations, using a single lentiviral construct. Second, we used CRISPR to knockout *PIP4K2A*, *PIP4K2B*, and *PIP4K2C*, as an orthogonal method to study PIP4K depletion. Loss of PIP4K in cell lines, through CRISPR and miRNA-based short hairpin RNAs (hereafter miRE), were successfully validated for eliciting previously reported phenotypes.

We characterize how depletion of PIP4K isoforms alters the abundance of various phosphatidylinositol-phosphate lipid species. We find that loss of PIP4K decreases PI(4)P and increases PI(4,5)P_2. Reconstitution with catalytic active or dead PIP4K isoforms restores PI(4)P and PI(4,5)P_2 levels, revealing a novel kinase-independent role for PIP4K in regulating cellular PI(4,5)P_2 levels.

2.2 INTRODUCTION

Deletion of phosphoinositide kinases and phosphoinositide phosphatases can alter the landscape of various phosphoinositide species. Some changes are expected, such as reciprocal changes in the lipid substrate or product. For example, loss of OCRL, a phosphatase which converts $PI(4,5)P_2$ to PI(4)P, causes an increase in cellular $PI(4,5)P_2$[73]. In other settings, deletion of an enzyme does not reveal any changes until a compensatory pathway is also eliminated. For example, insulin-stimulated $PI(3,4,5)P_3$ is eliminated through PTEN, a 3-phosphatase, as well as SHIP1/2, a 5-phosphatase. $PI(3,4,5)P_3$ levels are dramatically increased only when there is loss of both PTEN and SHIP2[74].

Deleting a lipid kinase and examining the nature of compensatory pathways impacted can shed light on the importance of the enzyme. For example, knockout of PI4KIIIalpha results in an upregulation of PIP5K protein levels[75].This allows for preservation of $PI(4,5)P_2$ production, and these results suggest that PI4KIIIalpha is important for supplying PI(4)P to be used for conversion to $PI(4,5)P_2$ by the PIP5Ks.

We asked how levels of phosphoinositide species are altered when PIP4K isoforms are lost. In an effort to ensure potent knockdown or knockout of multiple PIP4K isoforms, we utilized two orthogonal tools. First, we optimized miRE based short hairpin RNAs to target each isoform of PIP4K[76,77], and cloned them in tandem for expression from a single lentiviral construct[78]. We successfully made a panel of cell lines

with potent knockdown of PIP4K. Second, we cloned CRISPR guides and co-transfected constructs into 293T cells.

Phosphoinositides are quantified through metabolic labeling of lipids, lipid extraction, and separation of deacylated head groups through high pressure liquid chromatography. While it is easy to measure the more abundant phosphoinositides, PI(4)P and PI(4,5)P_2 (Figure 2.1), it is difficult to detect and accurately measure the other lipid species. We measured levels of various phosphoinositides, and observed an expected increase in PI(5)P, the substrate of these enzymes. We also observed a paradoxical increase in the product, PI(4,5)P_2, with decreased PI(4)P. We found that levels of PI(4,5)P_2 and PI(4)P were restored upon reconstitution with either kinase active or kinase dead PIP4K isoforms, suggesting a possible model whereby the PIP4K family has a structural role in modulating phosphoinositide homeostasis.

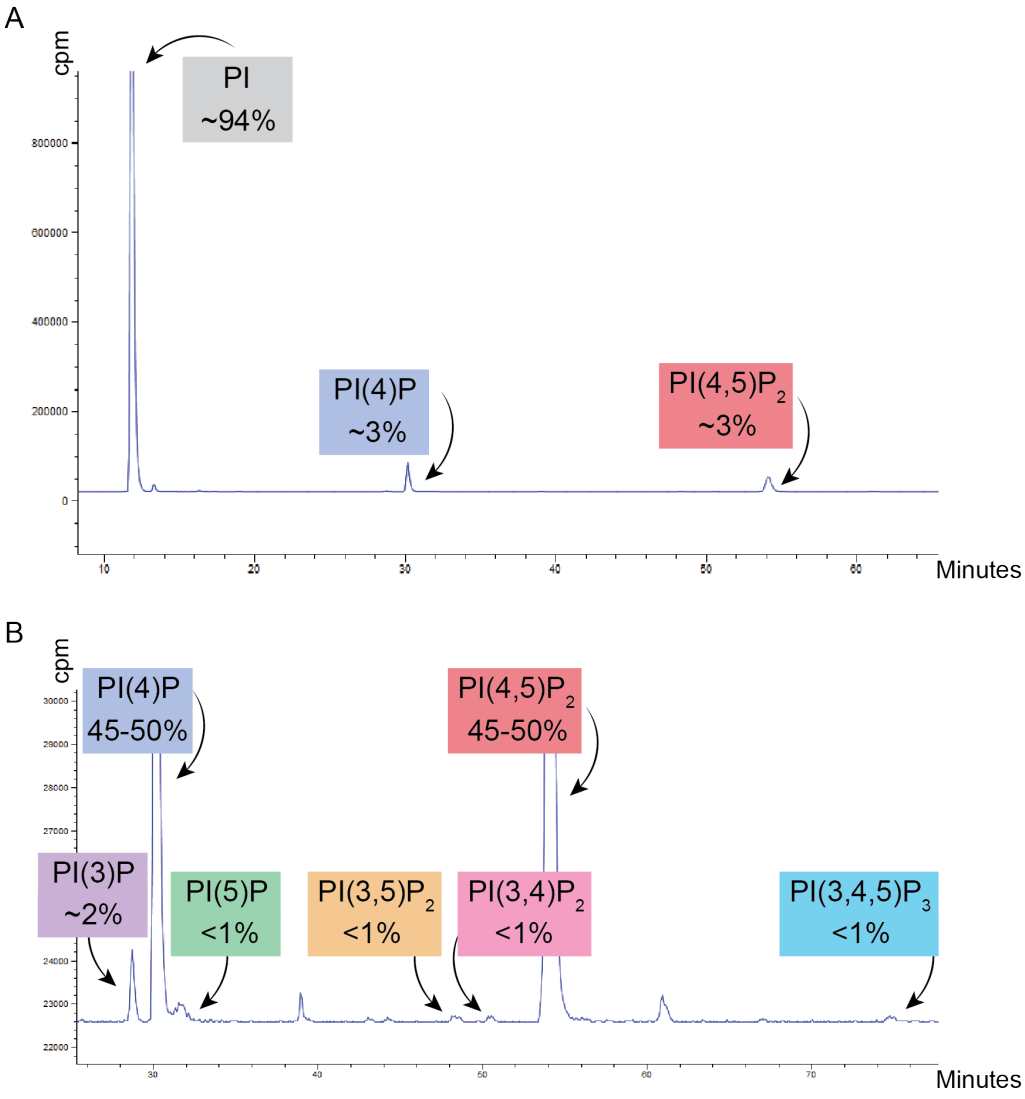

Figure 2.1 Quantification of phosphoinositides
Sample chromatogram of high pressure liquid chromatography (HPLC) separation of cellular phosphatidylinositol lipids. Integration of area under each peak allows for quantification of each lipid species. **(A)** The parental unphosphorylated species, phosphatidylinositol (PI), is in excess to phosphorylated species (phosphoinositides). **(B)** Relative amounts of phosphatidylinositol-phosphate lipids, highlighting the abundance of PI(4)P and PI(4,5)P_2.

2.3 METHODS

Immunoblotting for PIP4K. Cells were lysed in RIPA buffer (Sigma R0278-500mL) supplemented with 1 tablet of protease and phosphatase inhibitor (ThermoFisher, Pierce 88668). After incubation on ice for 20 minutes, lysates were cleared by centrifugation at 14,000 x g and supernatant was quantified using BCA assay (ThermoFisher, Pierce 23225). Lysates were subjected to SDS-PAGE using Novex NuPAGE system (ThermoFisher). Proteins and ladder (EZ-run prestained ladder, Fischer BP36031) were separated on 4-12% Bis Tris Pre-Cast Gels (Life Technologies NP0336BOX , NP0335BOX) or 10% Bis Tris gels (WG1202BOX) using MOPS buffer (ThermoFisher, NP0001). Proteins were transferred to 0.45 μm nitrocellulose membranes (Biorad 1620115) at 350 mA for 1h. Membranes were blocked in 5% non-fat milk in TBST and blotted with the antibodies in table. In order to chemi-luminescently detect antibody binding, membranes were blotted with HRP conjugated secondary antibodies (ThermoFisher, Mouse 45000679; Rabbit NA934-1ML). After another series of TBST washes, membranes were developed using ECL solution (ThermoFisher, Pierce ECL Substrate 32106), and exposed to film. Antibodies were purchased from CST (PIP4K2A CST5527, PIP4K2B CST9694) and Proteintech (PIP4K2C 17077-1-AP).

Immunoblotting for insulin signaling: Cells were normalized for cell number and plated in 6-well dish to achieve ~50% density upon adherence. Cells were serum starved overnight and stimulated with insulin (Sigma I9278) for 10 minutes. Cells were lysed in triton buffer (CST 9803) supplemented with 1 tablet of protease and phosphatase

inhibitor (ThermoFisher, Pierce 88668). After incubation on ice for 5 minutes, lysates were cleared by centrifugation at 14,000 x g and mixed with 4x Loading dye and 2-mercaptoethanol (Biorad 1610747). Lysates were subjected to SDS-PAGE using Novex NuPAGE system. Proteins and ladder (EZ-run prestained ladder) were separated on Bis Tris Pre-Cast Gels (Life Technologie) using MOPS buffer. Proteins were transferred to 0.45 µm nitrocellulose membranes and blocked in 5% BSA in TBST. Antibodies were purchased from Cell Signaling: Akt473 (CST 4058, 4060), total Akt (CST 2920, 4691), PRAS40 (CST 13175), PRAS40 (CST 2691), pGSK s21/9 (CST 9327). Membranes were processed using the LiCor Odyssey system. Images were quantitated using Image Studio Lite software. Significance calculated using ANOVA with Holm-Sidak multiple comparisons to control cell line. *$p<0.05$, **$p<0.1$, ***$p<0.01$, ****$p<0.001$

Cell lines and cell culture. 293T, Hela, PaTu 8988t, MCF7, and BJ cells were cultured using DMEM media (Corning 10-013-CV) supplemented with 10% FBS, glutamine and pyruvate. H1299 and H1975 cells were cultured in RPMI media (Corning 10-040-CV). 3T3s were cultured using DMEM-based media supplemented with 10% FCS. All cells were cultured at 37° C (5% CO2). All cell lines were purchased from ATCC (American Type Culture Collection) and validated and tested for mycoplasma (Lonza LT07-518). Stable cell lines expressing hairpins were generated by virus transduction with 0.8 ug/mL Polybrene (Santa Cruz sc-134220). Puromycin (Life Technologies, A1113803) used in the range of 1 ug/mL to 4 ug/mL. After 4 days of selection, cells were grown in the absence of antibiotics.

Tet-regulated shRNAs were induced with doxycycline (Sigma D3447) at concentrations between 0.5-2.0 μg/mL and replaced every 2 days. Cells were frozen and banked in BAMBANKER media (Wako Diagnostics/Chemicals # 30214681).

Virus production. 293T cells were used to generate lentivirus. Once cells were at 90-95% confluence in a 10cm dish, transfection was performed with lentiviral vectors and accessory plasmids. For each 10cm dish, 750 μL opti-mem + 30 μL lipofectamine 2000 (Life Technologies) were mixed in one tube, 750 μL opti-mem + DNA (6 μg lentiviral vector, 0.67 μg VSVG, 5.33 μg Δ8.2). For lentivirus expressing mir based hairpins, an additional 0.67 μg of sh-DGCR8 was added. DNA mix and lipofectamine mix were combined in a second tubes, mixed, and incubated at room temp for 15 minutes. All 1.5 mL was added dropwise to 293T cells. Virus supernatant was harvested 2 days and 3 days post transfection, then filtered (Whatman 28137-938), and concentrated in an ultracentrifuge at 25,000 rpm for 120 minutes at 4°C (Beckman Coulter # 326823), or with Lenti-X concentrator (Clontech 631231). For production of retrovirus in Sensor assay, human HEK293T Phoenix Eco line was used. Cells were plated, once cells were at 90% confluency, 10 μg of plasmid DNA was transfected with 30 μL of Lipofectamine 2000. Virus was harvested at 48 hours post transfection and filtered before cell transduction.

Cloning of hairpins in doxycycline inducible vectors. Predicted 97-mer oligos were purchased from IDT oligomers and PCR amplified using the primers miRE-Xho-fw (5'-TGAACTCGAGAAGGTATATTGC TGTTGACAGTGAGCG-3') and miRE-Eco-rev (5'-TGAACTCGAGA

AGGTATATTGCTGTTGACAGTGAGCG-3'), and CloneAmp HiFi PCR Premix (Clonetech Cat. No. 639298). 25 μL PCR reactions were performed using 0.05 ng oligonucleotide template, 0.4uM miRE-Xho-fw, 0.4 μM mire-Eco-rev, and 12.5 μL of CloneAmp HiFi PCR Premix. Cycling paramters were 95° for 5min; 30 cycles of 95° for 15 s, 58° for 15 s, and 72° for 20 s; 72° for 5 min. PCR products were purified using a NucleoSpin Gel and PCR Clean-up kit (Clontech cat 740609). Both PCR product and LT3GEPIR vectors were double digested with EcoRI-HF (NEB R3101) and XhoHI (NEB R0146). 20uL digests were performed, with 1uL of each enzyme, 2 μL of CutSmart buffer, and either 5 μg of LT3GEPIR vector or 500 ng of purified PCR product. Both digests were run on a 1.5% DNA gel and appropriate bands were gel excised and purified using the NucleoSpin Gel and PCR Clean-up kit. Using the QuickLigation kit (NEB M2200), 20uL reactions were performed at room temperature using 10uL of 2x Reaction Buffer, 50 ng of LT3GEPIR backbone as well as 5 ng of PCR product. Ligations were transformed in Stbl3 competent cells and grown at 32° overnight. Colonies were screened using the primer miRE-fwd (5'- TGTTTGAAT GAGGCTTCAGTAC-3').

Cloning of tandem hairpins.For generation of multiple miR-E-shRNAs in tandem using the LT3GEPIR vector, a cloning strategy was developed to add miR-E cassettes behind existing miR-E shRNA(s). This strategy to clone "multi" hairpins generates a vector where one promoter drives expression of fluorescent marker followed by shRNAs against multiple PIP4K isoforms. LT3GEPIR vectors containing desired miR-E shRNA(s) were double digested downstream of existing

shRNA(s) with EcoRI-HF (NEB R31010) and MluI-HF (NEB 3198) and PCR purified. The miR-E sequence to be added was PCR amplified with Multi-sh-fw (5'-agg cgcgaagactcaattgaaggctcgagaaggtatattgctg-3') and Multi-sh-rev (5'-cacttttttcaattgacacgtacgcgtattctaccgggta-3'). PCR products were purified, double digested with BbsI/MluI (NEB R0539, R0198, buffer 2.1), and PCR purified once more. Ligations were performed with PCR product and open LT3GEPIR vectors using T4 ligase. Colonies were screened using miRE-fwd.

Transfer of hairpins into constitutive vectors. To transfer hairpins to constitutive vectors, stem-loop sequences were PCR amplified from LT3GEPIR vectors with miRE-transferF: 5'-AACCCAACAGAAGGCT CGAG-3' and miRE-transferR: 5'-ACAAGATAATTGCTCGAATTCT AGCC-3'. PCR products were purified using a NucleoSpin Gel and PCR Clean-up kit. Recipient vector (SGEN, SGEP, LT3REEPIR) were double digested with EcoRI-HF (NEB R3101) and XhoHI (NEB R0146). 20uL digests were performed, with 1 μL of each enzyme, 2 μL of CutSmart buffer, and 5 μg of vector. After incubating at 37° for 6 hours, digests were run on a 1% DNA gel and appropriate bands were gel excised and purified using the NucleoSpin Gel and PCR Clean-up kit. In-Fusion cloning was performed to clone PCR products into open vectors. 10 μL In-Fusion reactions were performed, suing 2 μL of 5x In-Fusion HD Enzyme Premix, 50 ng of vector, and 5 ng of purified PCR product. Reactions were incubated for 15 minutes at 50°C, placed on ice, then transformed in Stbl3 competent cells and grown at 32°C overnight. Colonies were screened using the primer miRE-fwd.

Cloning of Sensor Assay vectors. To test the potency of shRNAs

targeting multiple isoforms of PIP4Kα/β/γ using one vector, we used the SENSOR assay[77]. The assay uses a reporter vector, TtNPT (gift from Lukas Dow), which constitutively expresses a hybrid transcript encoding dTomato with a 3'UTR harboring shRNA target sites with restriction sites for addition of desired shRNA target sequences. Three UTRs for PIP4K shRNA target sites were ordered (IDT ultramers, table) such that each contained sh-RNA targets of a single gene. gBlocks were amplified using primers with overhangs designed for in-fusion cloning to TtNPT vector (Primer sequences in table). TtNPT vector was digested with XhoI and EcoR1, and purified PCR products were cloned using In-Fusion cloning. Colonies were screened using the primer dTomato-fw (5'-CCACCACCTGTTCCTGTACG-3').

Optimization of most potent tandem hairpins using "SENSOR" assay. The assay uses a reporter vector, TtNPT (gift from Lukas Dow), which constitutively expresses a hybrid transcript encoding dTomato with a 3'UTR harboring shRNA target sites with restriction sites for addition of desired shRNA. Three sensor constructs were used, sensor-PIP4K2A, sensor-PIP4K2B, sensor-PIP4K2C. Stable reporter cells (3T3s) were generated using retroviral transduction. The lines were transduced with LT3GEPIR at low MOI. After 3 days of doxycycline addition, dTomato expression was quantified sing flow cytometry. GFP negative control cells were expected to have 100% of dTomato expression (RFP signal intensity). GFP positive cells were expected to have low dTomato expression if hairpin is potent.

Cloning of CRISPR guides targeting PIP4K. Predicted sgRNAs from the CRISPR Design Tool (http://tools.genome-engineering.org) were

ordered with overhangs for cloning into pX458 vector. sgRNA oligomers were annealed in 10 µL reaction (0.5 uL PNK (NEB M0201), 1 uL 10x T7 buffer (NEB M0318), 1µL 100µM forward primer, 1µL 100µM reverse primer) in thermocycler using annealing program with following parameters: 37° for 30 min; 95° for 5 min; ramp down to 25° at 5°/min. Reaction was diluted 1:200. 1 µL was added to ligation with open pX458. Colonies were screened using U6-fwd (5'-GAGGGCCTATTTCCCATGATTC-3').

Generation of PIP4K CRISPR knockout cell lines. CRISPR guides in pX458 were transfected in 293T cells. 293T cells were plated in 6-well dishes. When cells were~50% confluent, 2 µg of plasmid vector was transfected per well, using 300 µL Opti-mem and 5 µL Lipofectamine 2000. For wells with multiple vectors transfected, transfection was modified such that 2 µg of each vector was combined. At 48-96 hours post transfection, GFP positive cells were single-cell sorted in 96-well plates using the Influx sorter at the WCMC Flow Cytometry Core. Two weeks later, wells were scored to contain single cell colony and those wells were transferred to 2x 96-well plates such that there were duplicate plates with successful colonies. Once cells adhered, one of the duplicate plates was aspirated and all wells received 50 µL of Quick Extract DNA extraction solution (Illumina QE09050). Wells were agitated and transferred to PCR plate. DNA extraction was performed according to Quick Extract protocol. To screen for successful PIP4K2A/ PIP4K2B/ PIP4K2C knockouts, nested primers were designed around each cut site. 25 µL PCR reactions were performed using 12.5 µL 2x GoTaq Hotstart Colorless mastermix (Promega M5133), 1 µL 10µM

forward primer, 1µL 10µM reverse primer, and 2 µL DNA. The second, nested, PCR was performed with same recipe, substituting new primers as well as 2 µL of first PCR reaction. PCRs were Sanger sequenced using forward primer from nested reaction and 1 µL of nested reaction PCR product (Genewiz). Genomic PCR primers: 2AoutsideF: AGAGTG GATGGGCAAGAAGC, 2AoutsideR: AAGATGGAGTCATTGCTGTTCA, 2AinsideF: GATTGACTCTCCCTCACCACT, 2AinsideR: CTGTGTACA AGAGCAGAGGTTC; 2BoutsideF: TGCTTGAGCTCAGGACAGTG, 2BoutsideR: ACTAAGACCAAGATGGGGCC, 2BinsideF: GCTGGTG TGGGCAGATTGCT, 2BinsideR: CACTGCTACAGCCTCACACTG; 2CoutsideF: GATTGCCTGCATTCGCTCTG, 2CoutsideR: ATGCTG CTGTTTGGATGGGT, 2CinsideF: GTTCTCATGGCATCTCCAAGG, 2CinsideR: GACTGTTGTGAGCATGAAGTTC.

Cloning of lentiviral reconstitution constructs: A series of cloning vectors were made to achieve the final PIG-3xHA. First, 3-piece Gibson cloning was performed to create the PIG vector. Piece “A” was SGEN backbone cut with ClaI and SalI to excise SFFV, hairpin, and antibiotic selection casettes. Piece “B” was PGK, amplified from SGEN vector (italics overlap piece “A”, bold overlap piece “C” red is XhoI site, DW46-1: *CAAAAATTCAAAATTTTATCGAT*CTACCGGGTAGGGG, DW46-2 **C**CTCGAG**AGATCTAATTC**CGAAAGGCCCGGAG). Piece “C” was the IRES-GFP cassette amplified from pMIG vector (addgene 9044) (forward primer reverse complement of DW46-2: DW46-3: CTCCGGGCCTTTCG **GAATTAGATCT**CTCGAG**G**, DW46-4: CAGACGCGTTTCGAAGTCGA TTACTTGTACAGCTC). Three piece Gibson clones were screened by sanger sequencing with following

primers: PGK-fwd: CATTCTGCACGCTTCAAAAG, PGK-rev: TTTGAAGCGTGCAGAATGCC, IRES-rev:CCTCGACTAAACACATGT, EGFP-C: CATGGTCCTGCTGGAGTTCGTG.

Next, PIG-3xHA was made with Gibson ligation through digesting PIG with XhoI and PCR amplified 3xHA. 3xHA sequence was purchased from IDT: TACCCATACGATGTTCCA GATTACGCTGGCTATCCCTATGACGTCCCGGACTATGCAGGATCA TATCCATATGACGTTCCAGATTACGCTGTTGCG, and amplified for overhangs to Gibson into PIG, while implementing 4 kozak sequences: HA- V1-F: GGAATTAGATCTCTCGAGGCCACCATGGCCTACCCATA CGATGTT, HA-V2-F: GGAATTAGATCTCTCGAGTCCGCCATGTACC CATACGATGTTCCA, HA-V3F: GGAATTAGATCTCTCGAGGCCACCG TGGCCTACCCATACGATGTT, HA-V4-F: GGAATTAGATCTCTCGAG TCCGCCGTGTACCCATACGATGTTCCA. All four PCRs had the same reverse primer, for addition of a BstEII cloning site (red) for cloning of cDNA. HA-R: GGGGGGGGGGGCGGAATTCTGGTTACCTCGCAACA GCGTAATCTG. Cloning was validated through sanger sequencing with PGK-fwd primer.

Next, PIP4K coding sequences were added to PIG-3xHA through BstEII site. Coding sequences were amplified for Gibson cloning, overlap in italics. PIP4K2A-F: *CCAGATTACGCTGTTGCGAGTATC*ATCGCGAC CCCCGGC, PIP4K2A-R: *GGGGCGGAATTCTGGTTACC*TTACGTCAA GATGTGGCC, PIP4K2B-F: *CCAGATTACGCTGTTGCGAGTATC*ATC TCGTCCAACTGCACC, PIP4K2B-R: *GGGGCGGAATTCTGGTTACC* CTACGTCAGGATGTTG, PIP4K2C-F: *CCAGATTACGCTGTTGCGAG TATC*ATCGCGTCCTCCTCGG, PIP4K2C-R: *GGGGCGGAATTCTGG*

*TTACC*TTAGGCAAAGATGTTG. Colonies were screened by sanger sequencing with PGK-fwd.

Next, we generated mutations in PIP4K cDNA using QuikChange (Agilent 200522). For kinase dead residues primers were as follows: PIP4K2A-D273N-F: CCAGCTGAAGCTCATGAACTACAGTCTGCT GGTGGGAATTCAT, PIP4K2A-D273N-R: ATGAATTCCCACCAGCA GACTGTAGTTCATGAGCTTCAGCTGG, PIP4K2B-D278N-F: ACAGCTGAAGATCATGAACTACAGCCTGCTGGTGGGCATCCAC, PIP4K2B-D278N-R: GTGGATGCCCACCAGCAGGCTGTAGTTCATG ATCTTCAGCTGT, PIP4K2C-D280N-F: AGTGCAGCTGAAGATCATGA ACTACAGCCTTCTGCTAGGCATCC, PIP4K2C-D280N-R: GGATGCC TAGCAGAAGGCTGTAGTTCATGATCTTCAGCTGCACT, PIP4K2A-D359N-F: TAGGAAGGAGGTGTACTTCATGGCAATTATTAACATC CTTACTCATT, PIP4K2A-D359N-R: AATGAGTAAGGATGTTAATAAT TGCCATGAAGTACACCTCCTTCCTA, PIP4K2B-D369N-F: GTATTT CATGGCCATCATTAATATCCTCACGCCATACGATA, PIP4K2B-D369N-R: TATCGTATGGCGTGAGGATATTAATGATGGCCAT GAAATAC, PIP4K2C-D374N-F: CCAGAAGGAGGTCTACTTCATGG GCCTCATTGATATCCTTACACAGPIP4K2C-D374N-R: CTGTGTAAG GATATCAATGAGGCCCATGAAGTAGACCTCCTTCTGG.

For introduction of wobble in PIP4K2A and PIP4K2B to make sequences hairpin-resistant, the following primers were used: 2A-650/665F: GCATGTACCGGCTTAATGTTGATGGTGTAGAGATTTAC GTCATTGTAACTAGGAACGTATTCAGCCACCGTTTGTCTGTGTATA GG, 2A-650/665R:CCTATACACAGACAAACGGTGGCTGAATACGT TCCTAGTTACAATGACGTAAATCTCTACACCATCAACATTAAGCCG

GTACATGC, 2A-948F: CTTCCGTAACCTGCGGGAAAGATTCGGTA TAG, ACGACCAAGATTTCCAGAATTCCCTG, 2A-948R: CAGGGAAT TCTGGAAATCTTGGTCGTCTATACCGAATCTTTCCCGCAGGTTACG GAAG, 2B-130F: CATTGATATCCTCACCCCTTATGACACTAAAAAAA AAGCTGCACATGCTGCCAAAAC, 2B-130R: GTTTTGGCAGCATGTG CAGCTTTTTTTTTAGTGTCATAAGGGGTGAGGATATCAATG, 2B-868F:CCAGCGAGGACGTGGCGGAGATGCATAATATATTGAAAAAG TACCACCAGTTTATAG, 2B-868R: CTATAAACTGGTGGTACTTTTT CAATATATTATGCATCTCCGCCACGTCCTCGCTGG. No mutations needed for PIP4K2C since all hairpins targeted the 3' UTR.

Analysis of cellular phosphoinositides. Cellular phosphoinositides were metabolically labeled for 48 hours in inositol-free DMEM (Thermo ICN1642954) supplemented with 1x Glutamine (Life Technologies 51985034), 10% dialyzed FBS (Life Technologies 26400044), and 10 μCi/ mL ^{3}H myo-inositol (Perkin Elmer NET114A005MC). Cells were washed with PBS and then transferred on ice. Cells were killed and then harvested by scraping using 1.5 mL ice-cold aqueous solution (1M HCl, 5 mM Tetrabutylammonium bisulfate, 25 mM EDTA). 2 mL of ice cold MeOH and 4mL of CHCl3 were added to each sample. After ensuring each vial is tightly capped, samples were vortexed and then centrifuged at 1000 rpm for 5 min. If a significant intermediate layer was visible, sample were gently agitated and spun again, until there were predominately two clear layers. The organic layer (lower) was cleaned using theoretical upper, while the aqueous layer was cleaned using theoretical lower (theoretical upper and lower made by combining CHCl3: MeOH : aqueous solution in 8:4:3 v/v ratio). Organic phases

were collected and dried under nitrogen gas. Lipids were deacylated using monomethylamine solution (47% Methanol, 36% of 40% Methylamine, 9% butanol, and 8% H2O, by volume). Samples were incubated at 55° for 1 hour and subsequently dried under nitrogen gas. To the dried vials, 1 mL of theoretical upper and 1.5 mL of theoretical lower were added (theoretical upper and lower made by combining CHCl3:MeOH:H2O in 8:4:3 v/v ratio). Samples were vortexed and spun at 1000rpm. The aqueous phase (upper) was collected and dried under nitrogen gas. Samples were resuspended in 150 µL Buffer A (1mM EDTA), filtered through a 0.22 µM column (Sigma CLS8169) and transferred to Agilent polypropylene tubes (5182-0717, 5 190-2242). Samples were analyzed by anion-exchange HPLC using Partisphere SAX column (Whatman, VWR 01946-560). The compounds were eluted with a gradient starting at 100% Buffer A (1mM EDTA) and increasing Buffer B (1mM EDTA, 1M NaH2PO4) over time: 0-1 min 100% Buffer A, 1-30 min 98% Buffer A/2% Buffer B, 30-31 min 86% Buffer A/ 14% Buffer B, 31-60 min 70% Buffer A/ 30% Buffer B, 60-80 min 34% Buffer A/ 66 % Buffer B, 80-85 min 100% Buffer B, 85-120 min 100% Buffer A. Buffers were pumped at 1 mL/min through column. Eluate from the HPLC column flowed into an on-line continuous flow scintillation detector (Perkin Elmer Radiomatic 150TR) for isotope detection. The detector was set to observe events between 10 minutes and 85 minutes, with scintillation fluid (Ultima Flo AP, Perkin Elmer 6013599) flowing at 4 mL/min.

2.4 RESULTS

2.4.1 GENERATION OF CELL LINES WITH LOSS OF PIP4K

We predicted candidate shRNA target sequences against *PIP4K2A, PIP4K2B*, and *PIP4K2C* using Splash RNA, (http://splashrna.mskcc.org/)[76]. We cloned oligonucleotides containing miR-E based stem-loop structures into the LT3GEPIR vector, which has a puromycin selection marker, expresses rtTA3, and provides a doxycycline-inducible expression of GFP-tagged hairpin expression through the TRE3G promoter[78]. Next, we cloned a second and third shRNA in tandem, to produce different combinations targeting one, two, or all three members of the PIP4K family.

We tested knockdown efficiency in 3T3 cells, using a medium-throughput assay called SENSOR[77]. Briefly, the SENSOR assays uses a surrogate gene with an artificially designed 3' UTR sequence containing candidate shRNA target sequences. The surrogate gene is dTomato, allowing for changes in fluorescent intensity to be used for quantifying potency of knockdown (Figure 2.2, Figure 2.3). Our finalized set of constructs provided at least two unique hairpins sets for each knockdown, to control for off-target effects (Table 2.1, Table 2.2). We use a series of non-targeting Renilla hairpins to control for off-target effects of viral infection and loading of RNAi processing machinery. We proceeded to validate knockdown efficiency through western blot analysis for protein levels of PIP4K. After transducing 293T cells and

performing puromycin selection for three days, cells were treated with doxycycline for 7 days and then harvested (Figure 2.4).

Table 2.1 shRNA sequences targeting PIP4K isoforms

Hairpin IDs	Targeted alleles	Target sequence
Ren	N/A (Renilla)	TAGATAAGCATTATAATTCCTA
A650	*PIP4K2A*	TATCACATATATTTCAACTCCA
A665	*PIP4K2A*	TACATTTCTTGTAACTATCACA
B130	*PIP4K2B*	TTTCTTCTTTGTATCGTATGGC
B868	*PIP4K2B*	TATTTCTTTAAGATGTTGTGCA
C1406	*PIP4K2C*	TTGAACATCAGAGAGAACCAGG
C3036	*PIP4K2C*	TTCTAAAGAGCAATGGTTGCTG
C3165	*PIP4K2C*	TATTATTATAGTAACAGGAGCA
A948	*PIP4K2A/B*	TTGATCATCAATTCCAAACCTC

Table 2.2 Optimized tandem shRNA series

Hairpin code	Hairpin IDs
Ren	Ren
Ren2	Ren; Ren
Ren3	Ren; Ren; Ren
A1	A650
A2	A665
B1	B130
B2	B868
C1	C1406
C2	C3036
AB1	A650; B868
AB2	A665; B130
BC1	B130; C3165
BC2	B868; C1406
AC1	A650; C3165
AC2	A665; C3036
ABC1	A650; B130; C1406
ABC2	A665; B868; C3036
ABC3	A948; C3165

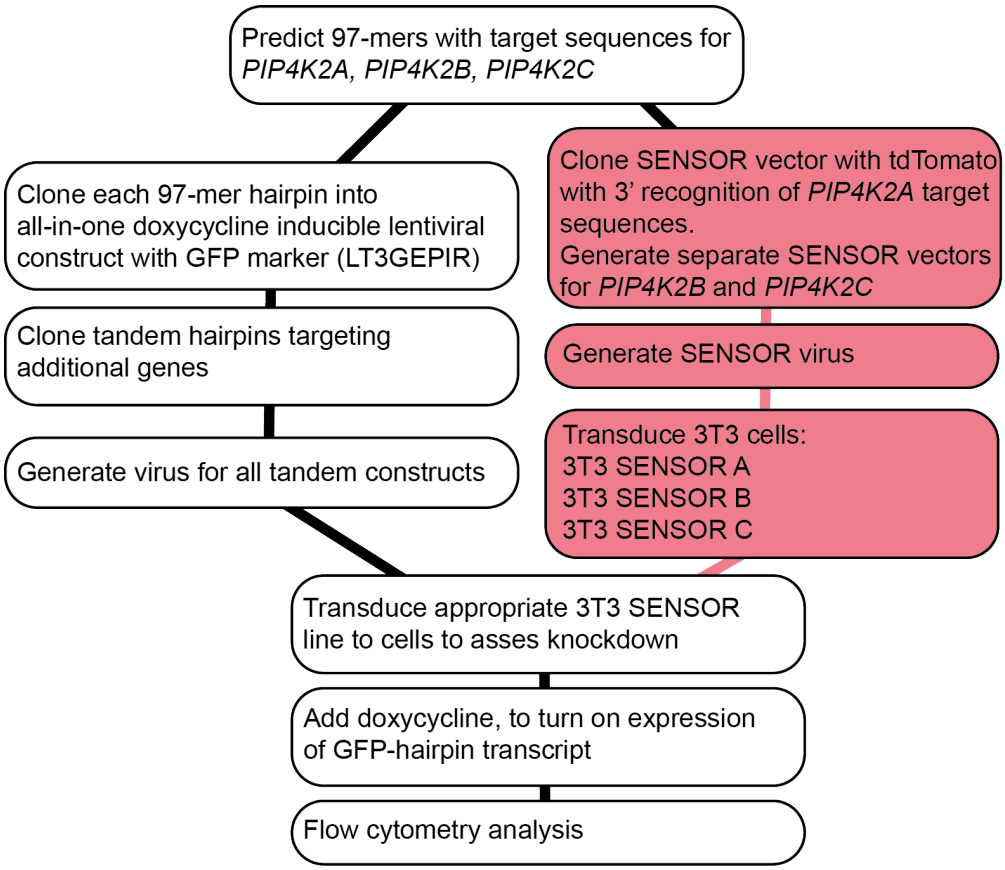

Figure 2.2 SENSOR assay workflow.
Summary of steps for SENSOR assay, adapted from protocol in Fellman et al., 2011.

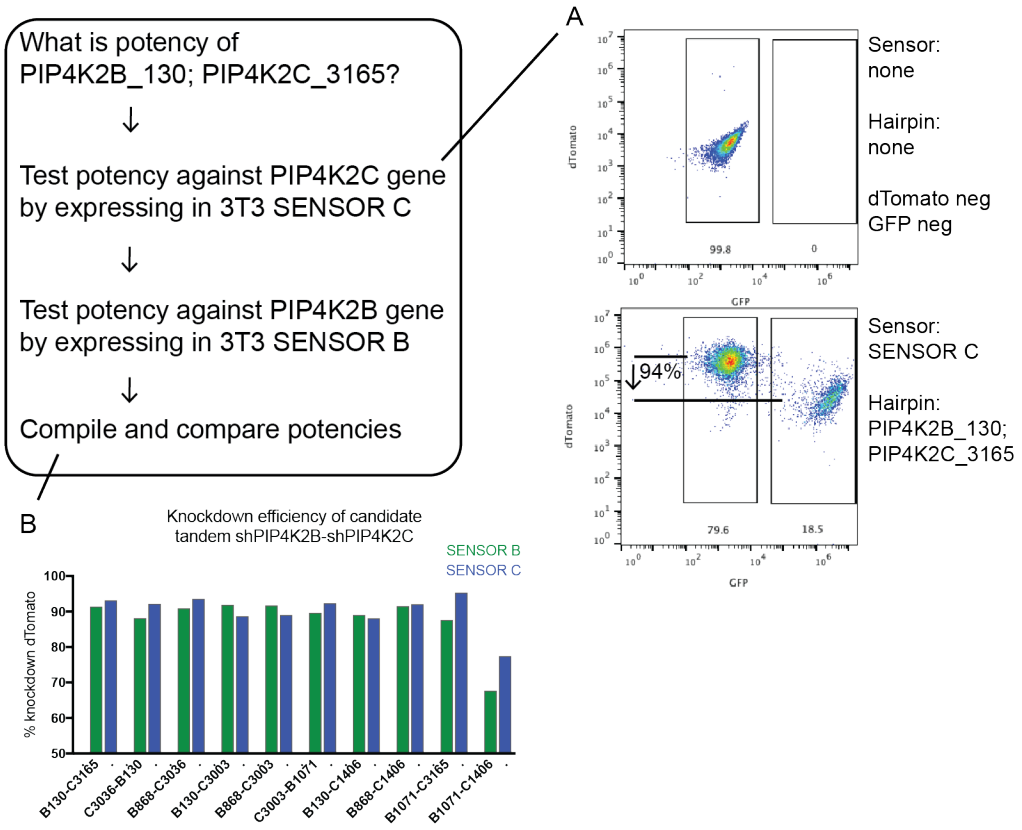

Figure 2.3 Implementing SENSOR assay.
(A) Flow cytometry analysis of hairpin with 94% knockdown of PIP4K2C. **(B)** Comparison of knockdown potency across all candidate tandem hairpins for double knockdown of PIP4K2B-PIP4K2C

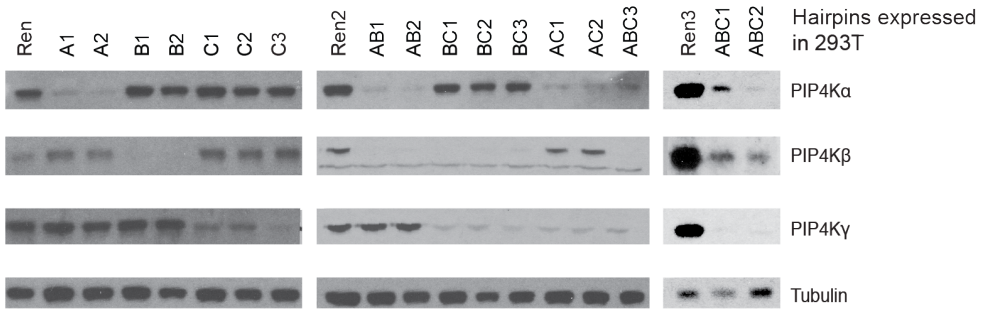

Figure 2.4 Knockdown of PIP4K isoforms in 293T cells.
Hairpins in LT3GEPIR vector were expressed in 293T cells. Cells were collected after seven days doxycycline treatment.

2.4.2 KNOCKDOWN OF PIP4K IS NOT LETHAL

We characterized our knockdown system by monitoring the kinetics of knockdown in 293T cells. Transduced 293T cells were puromycin selected, and pulsed with 24 hours of doxycycline for the purpose of sorting for the brightest GFP population. After two days of recovery in doxycycline-naïve media, cells were placed on 1 ug/mL doxycycline and lysates were harvested every two days. Efficient knockdown of PIP4K requires at least five days of doxycycline treatment (Figure 2.5). This is consistent with unbiased global protein half-life measurements, where PIP4K has an estimated $t_{1/2}$ of ~60 hours[79].

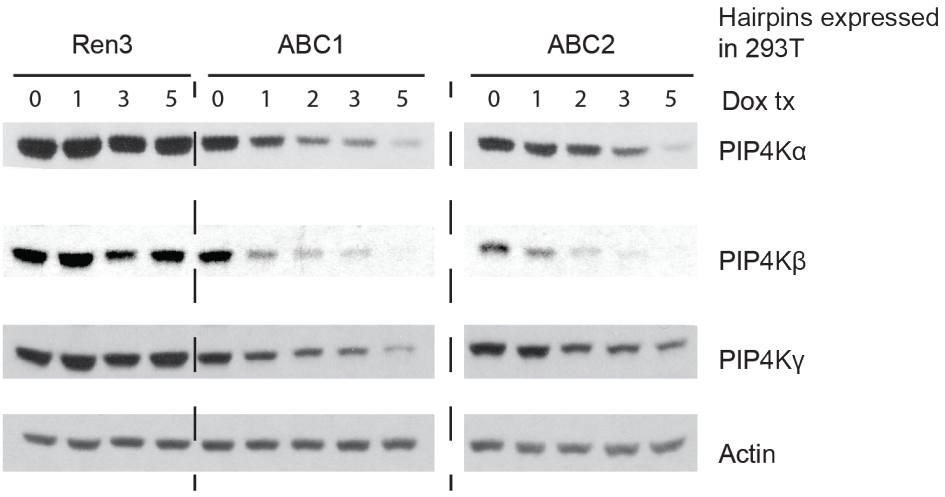

Figure 2.5 Kinetics of shRNA mediated knockdown of PIP4K. 293T cells expressing doxycycline-inducible hairpins against all three isoforms of PIP4K. Lysates were collected over the course of 5 days of doxycycline treatment.

In order to monitor how cell proliferation is affected by knockdown of these enzymes, we performed competition assays over the course of 14 days. After transducing 293T cells, we set aside a population that remained naïve to puromycin selection. In these cells, we monitored the ratio of GFP positive (GFP^+) cells. Doxycycline treatment induces expression of GFP in cells that are expressing hairpin constructs, so seeing a decline in the GFP^+ population would indicate a relative decrease in fitness compared to un-transduced cells. Over the course of two weeks, one of two shPIP4K2B/2C double knockdown cell lines showed a decrease in fitness by about 30% (Figure 2.6). We knocked down PIP4K in PaTu8988t cells (Figure 2.6), a mutant p53 pancreatic adenocarcinoma, and did not see changes in cell proliferation that could be robustly observed across unique hairpins. At this point, we moved from doxycycline inducible hairpins to constitutive hairpin expression for two reasons (Figure 2.7). One, we believed cells could proliferate normally with PIP4K knockdown. Two, we wanted to avoid using doxycycline, a drug known to disrupt cellular metabolism[80]. We constitutively knocked down PIP4K in a panel of cell lines (Figure 2.8) and did not observe gross changes in viability.

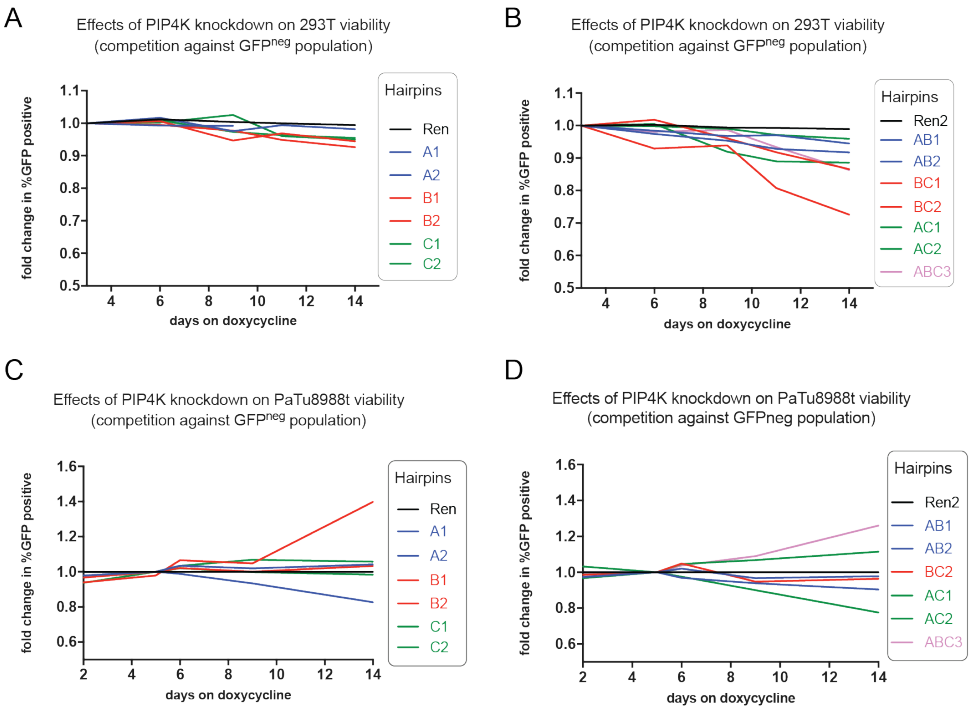

Figure 2.6 Competition assay tracking changes in cell fitness. Doxycycline treatment induces expression of both GFP and hairpins. Over the course of 14 days, cells were tracked with flow cytometry to monitor GFP+ population. Changes in 293T cells, with single isoform PIP4K knockdown **(A)**, or multiple PIP4K isoform knockdown **(B)**. Changes in PaTu8988t cells, with single isoform PIP4K knockdown **(C)**, or multiple PIP4K isoform knockdown **(D)**. All ratios normalized to day one GFP^{+} ratio, and further normalized to non-targeting control Ren or Ren2. Experiments were performed n=1.

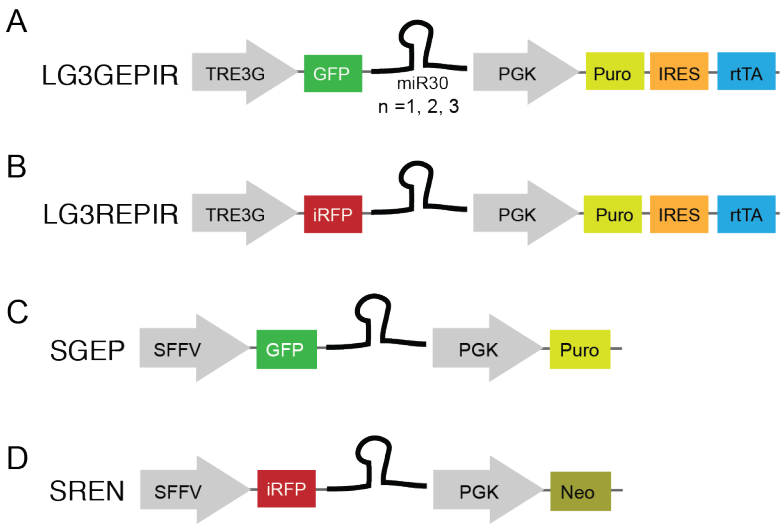

Figure 2.7 Modular use of hairpins in a variety of vectors. Schematic of vectors with doxycycline inducible control of hairpin expression **(A,B)**, or constitutive hairpin expression **(C,D)**. Hairpin expression can be concatemerized with GFP or infrared RFP (iRFP).

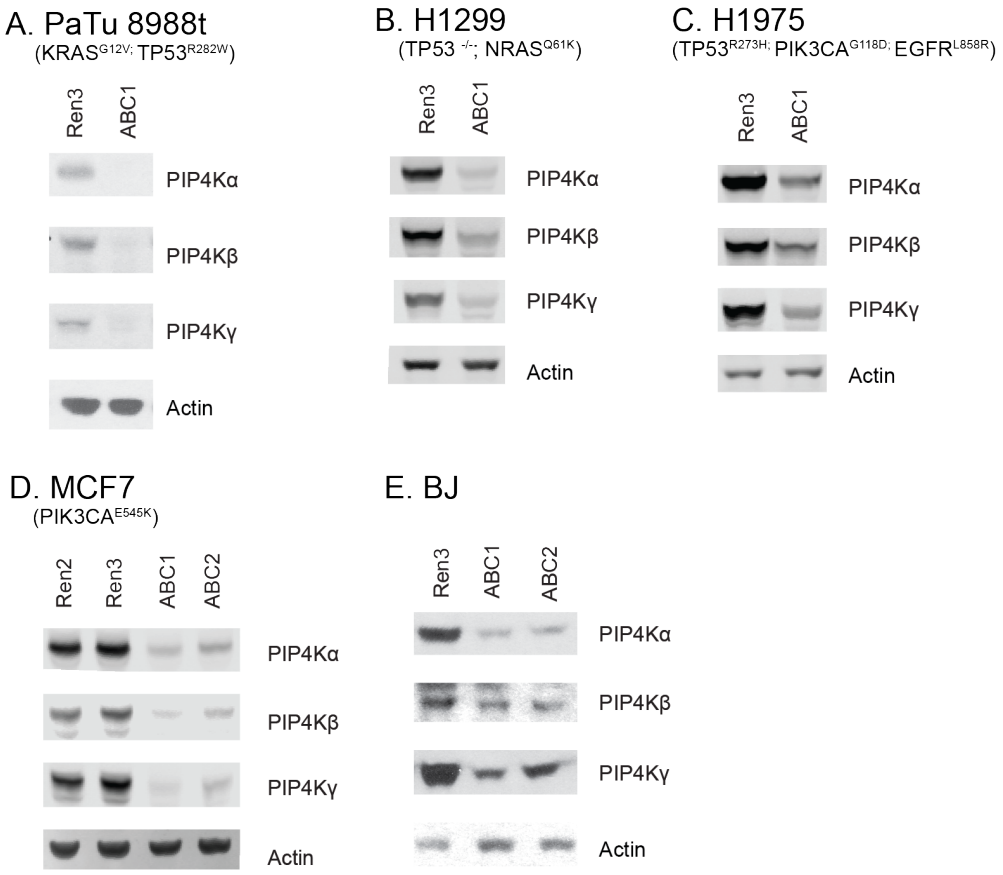

Figure 2.8 Knockdown of PIP4K in a panel of cell lines.
(A) PaTu8988t are derived from human pancreatic adenocarcinoma. **(B,C)** H1299 and H1975 are derived from human lung adenocarcinoma. **(D**) MCF7 are derived from estrogen positive (ER+) human breast adenocarcinoma. **(E)** BJ fibroblast are untransformed human foreskin fibroblasts. Mutations reported from Cancer Cell Line Encyclopedia (CCLE).

2.4.3 GENERATION OF PIP4K TRIPLE KNOCKOUT (TKO) CELL LINES

While our shRNA tools provide potent knockdown of PIP4K, there is residual protein that may confound interpretation of our results. We made cell lines with genetic knockouts of PIP4K, to use as a complementary system. Candidate CRISPR guides were predicted and cloned according to the methods described in Ran et al, 2013. We transfected guides against all three isoforms in 293T cells and performed single cell sorting into a 96-well plate. Clonal populations were screened through western blot analysis and subsequent sequencing of amplified gDNA near the CRISPR cut site (Table 2.3). We successfully validated multiple triple knockout (TKO) clones (Figure 2.9).

Table 2.3 CRISPR guides targeting *PIP4K2A, PIP4K2B, PIP4K2C*

Target	Target sequence
g_PIP4K2A-1	TCATCTGGCATCAACATAAC(AGG)
g_PIP4K2A-2	GAATAGGCTTTGAAGTCATC(TGG)
g_PIP4K2B-1	TCATCTGGCATTAGCATGAC(AGG)
g_PIP4K2B-2	GTCCACCTTGATCTTGCTGT(AGG)
g_PIP4K2C	ATCTGGCAGCAGCATCACCG(GGG)

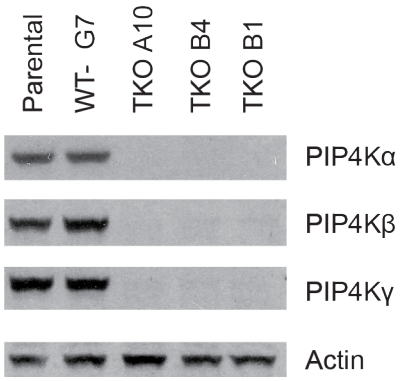

Figure 2.9 Validation of PIP4K TKO cells.
Clonal populations of 293T cells with CRISPR mediated knockout of *PIP4K2A, PIP4K2B, PIP4K2C*.

2.4.4 VALIDATION OF PREVIOUSLY REPORTED PHENOTYPES WHEN PIP4K IS LOST

Loss of PIP4K has been previously reported to increase insulin sensitivity[10,65]. We confirmed that knockdown in Hela cells conferred increased activation of the PI3K pathway upon insulin stimulation (Figure 2.10). Loss of all three PIP4K isoforms is also expected to abolish conversion of PI(5)P into PI(4,5)P_2, thereby causing an increase in PI(5)P levels[14]. Indeed, high pressure liquid chromatography (HPLC) analysis of phosphoinositide species demonstrated a two- to three- fold increase in PI(5)P in the setting of PIP4K deficiency (Figure 2.11).

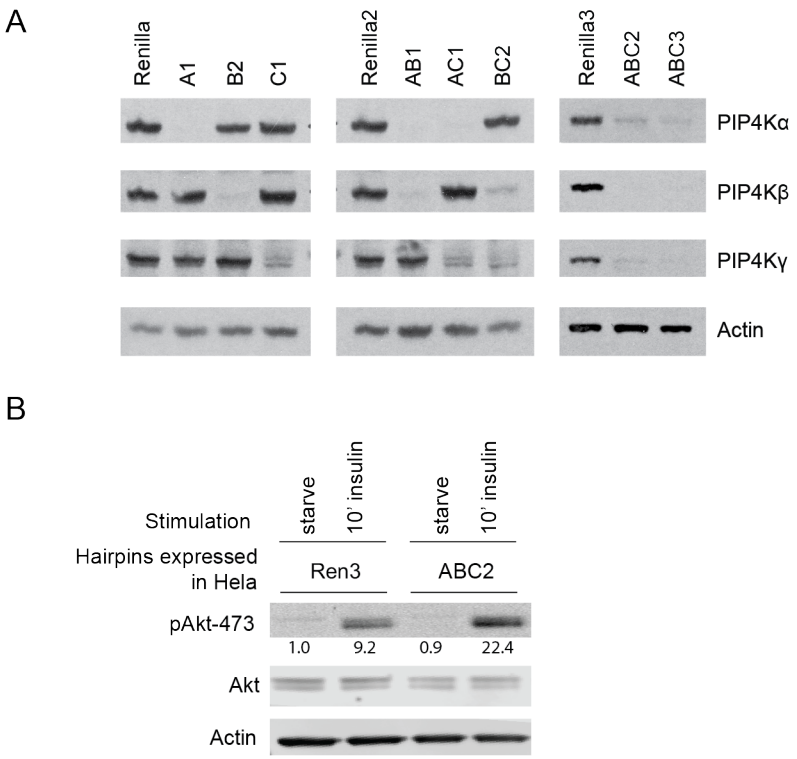

Figure 2.10 Knockdown of PIP4K enhances insulin signaling. **(A)** Validation of PIP4K in triple knockdown (TKD) Hela cells. **(B)** Hela cells were serum starved overnight and stimulated with 500 ng/mL insulin for 10 minutes.

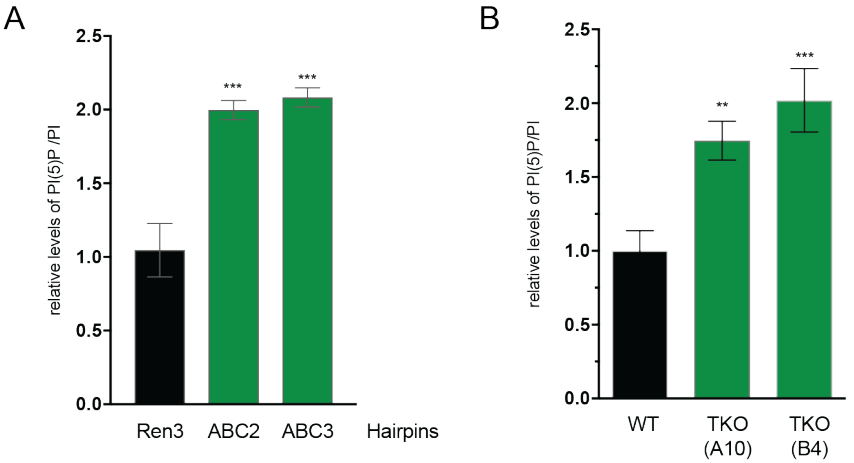

Figure 2.11 PI(5)P increases in cells with loss of PIP4K. HPLC measurement of PI(5)P levels in Hela TKD **(A)** or 293T CRISPR TKO **(B)**. Level of PI(5)P normalized to PI and parental cell line. Significance calculated using ANOVA with Holm-Sidak multiple comparisons to control cell line. **p<0.01, ***p<0.001

2.4.5 PI(4,5)P2 LEVELS INCREASE AND PI(4)P LEVELS DECREASE WHEN PIP4K IS LOST

Upon measurement of phosphoinositide species, we unexpectedly observed that cells with loss of PIP4K exhibit a profound increase in $PI(4,5)P_2$, concomitant with a decrease in PI(4)P (Figure 2.12, Appendix A). Because PIP5K provides the majority of $PI(4,5)P_2$, we would expect that eliminating PIP4K, the non-canonical pathway for $PI(4,5)P_2$ synthesis, would *not* significantly change $PI(4,5)P_2$. Additionally, analysis of $PI(4,5)P_2$ levels in cells with single or double knockdown of PIP4K isoforms shows that there is an additive effect amongst all three isoforms (Figure 2.13). This observation is robustly seen in tumor lines of various tissue origin and mutational backgrounds (Figure 2.14).

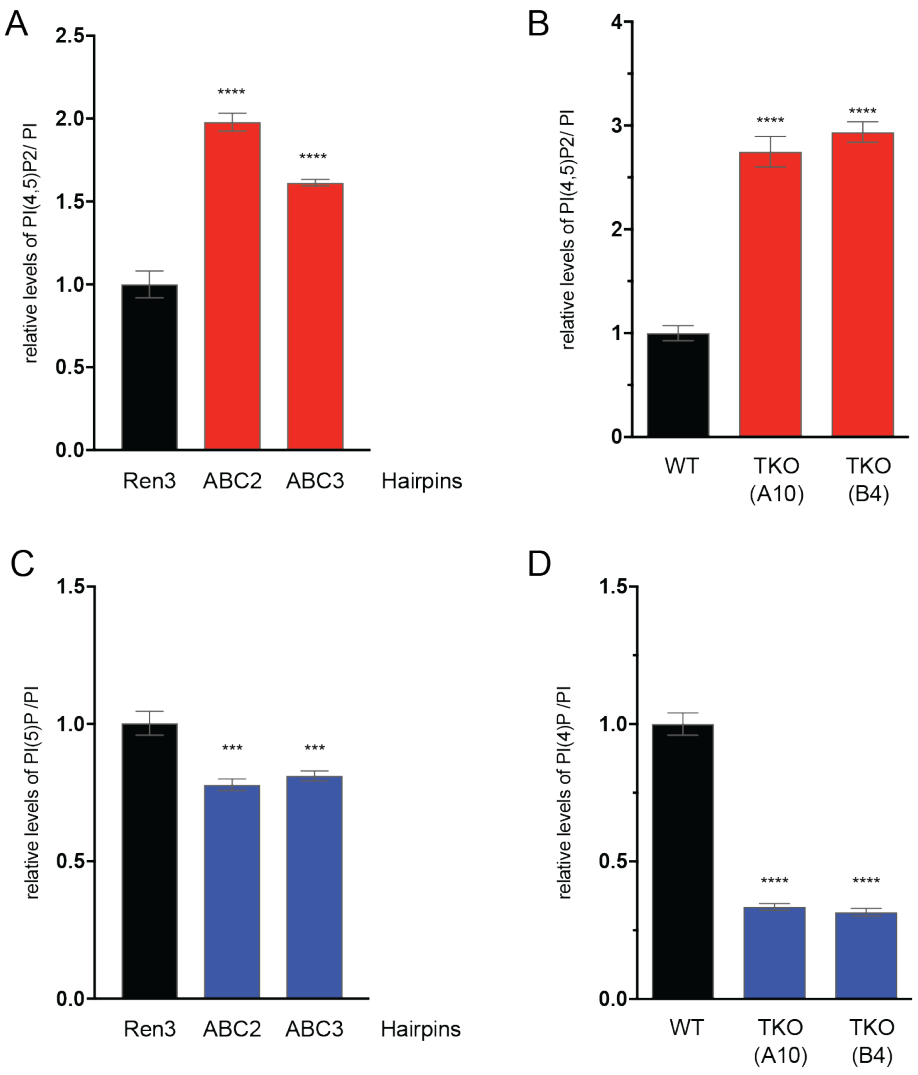

Figure 2.12 PI(4,5)P_2 increaseds and PI(4)P decreaseds in cells with loss of PIP4K.
HPLC measurement of PI(4,5)P_2 levels in Hela TKD **(A)** or 293T CRISPR TKO lines **(B**). Measurement of PI(4)P levels in Hela TKD **(C)** or 293T CRISPR TKO lines **(D**). Levels of phosphoinositides normalized to PI and parental cell line. Significance calculated using ANOVA with Holm-Sidak multiple comparisons to control cell line. ***p<0.001, ****p<0.0001

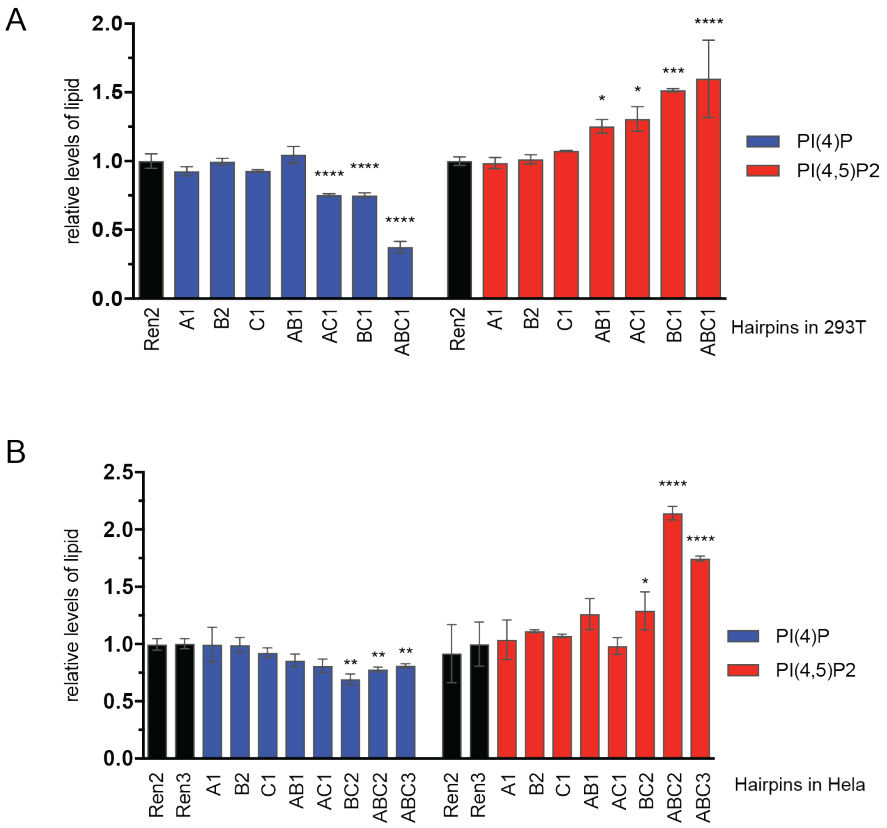

Figure 2.13 Single and double knockdown of PIP4K isoforms. Levels of PI(4)P and PI(4,5)P_2 in 293T cells **(A)** and Hela cells **(B)** with one, two, or three isoforms of PIP4K knocked down. Significance calculated using ANOVA with Holm-Sidak multiple comparisons to control cell line. *p<0.05, **p<0.01, ***p<0.001, ****p<0.0001

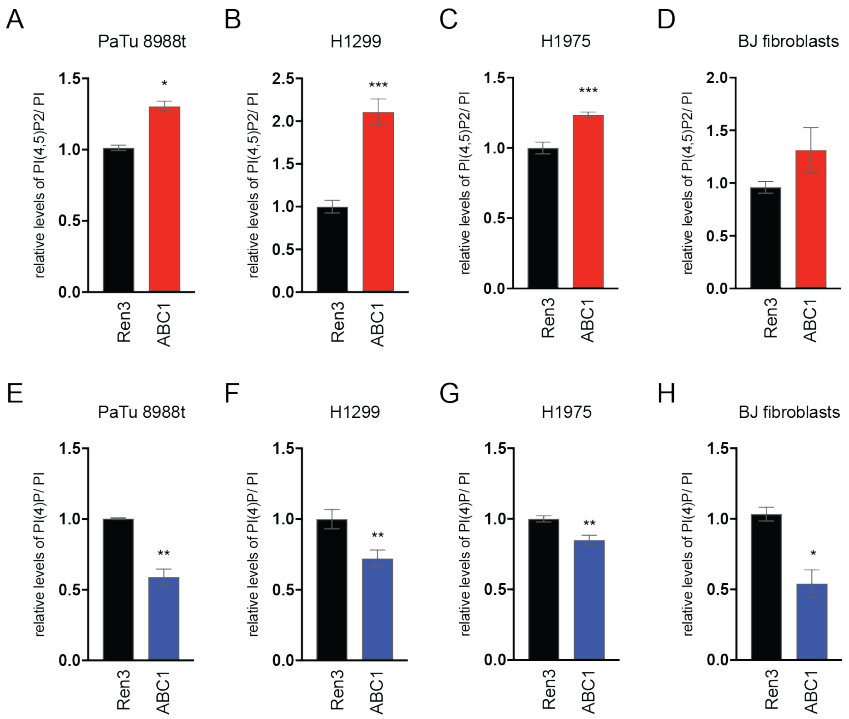

Figure 2.14 Phosphoinositide levels in a panel of cell lines with triple knockdown of PIP4K.
(A,B,C,D) PI(4,5)P_2 and **(E,F,G,H)** PI(4)P levels in a panel of tumor lines of various tissue origin and mutational backgrounds. Significance calculated using ANOVA with Holm-Sidak multiple comparisons to control cell line. *p<0.05, **p<0.01, ***p<0.001

2.4.6 PIP4K HAS A CATLALYTIC INDEPENDENT ROLE IN MODULATING PI(4,5)P2

Analysis of PI(4,5)P_2 levels in cells with single or double knockdown of PIP4K isoforms shows that there is an additive effect amongst all three isoforms. (Figure 2.13). Members of the PIP4K family have dramatically different catalytic activity, with PIP4Kα displaying 1000-fold higher activity than the nearly-dead PIP4Kγ[8]. We observed that double knockdown of the most catalytically active isoforms, PIP4K2A/2B, did not phenocopy the triple knockdown, suggesting a

role for these enzymes which may not be mediated by catalytic function.

To test this, we reconstituted 293 triple knockdown cells with kinase active or dead PIP4K isoforms using lentiviral construct pLenti-3x-FLAG. We expressed hairpin-resistant coding sequences driven by a CMV promoter (Figure 2.15). Endogenous levels of PIP4K were somewhat rescued by overexpression of kinase dead PIP4Kα or PIP4Kβ, complicating the interpretation of the ability of kinase-dead enzymes to restore normal levels of cellular phosphoinositides.

We designed a vector to provide a setting that enabled levels of transgene expression closely resembling endogenous levels. In the vector PIG-3xHA, PIP4K is driven by a PGK promoter with variations in the Kozak sequence, as well as an IRES-GFP feature (Figure 2.16). The Kozak sequence is recognized by the ribosome and therefore a sub-optimal Kozak will decrease initiation of translation. Because GFP expression is driven from the same promoter, GFP intensity reflects the lentiviral copy number integrated as well as variations in the efficiency of transcription from the integration site in the genome. Vector variants were empirically tested and cells were empirically sorted for various GFP levels to achieve near-endogenous levels of reconstitution (Figure 2.17) in 293T and Hela cells with PIP4K knockout and knockdown, respectively.

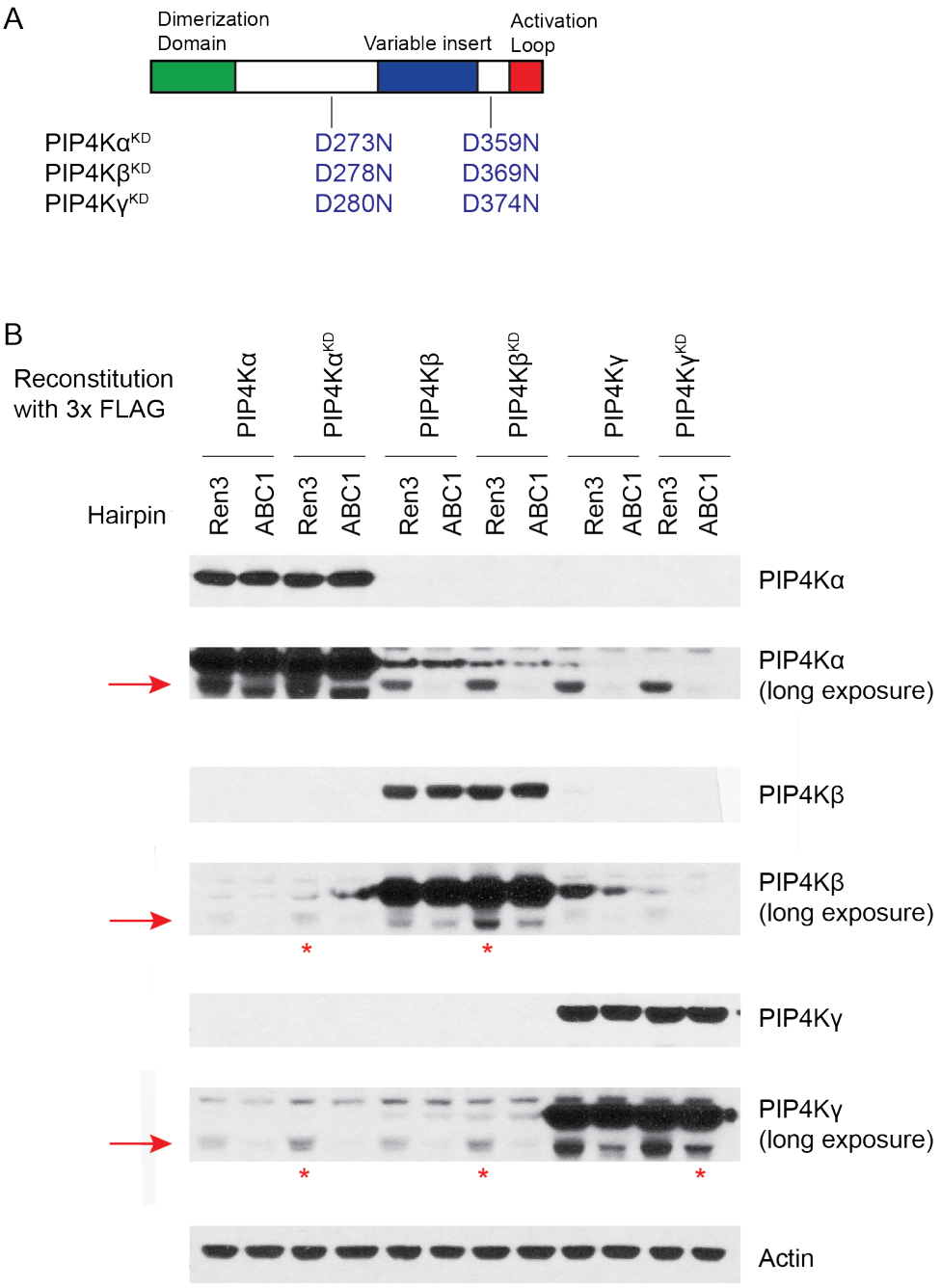

Figure 2.15 Reconstitution of PIP4K in 293T PIP4K knockdown cells. **(A)** Schematic of kinase dead mutations in PIP4K. **(B)** Control cells with non-targeting hairpins (Ren3) and TKD cells (ABC1) were reconstituted with 3x-FLAG tagged wild type or kinase dead isoforms of PIP4K. Long exposure detects the farther migrating endogenous PIP4K (in red arrows). Red asterisks indicate stabilization of endogenous PIP4K.

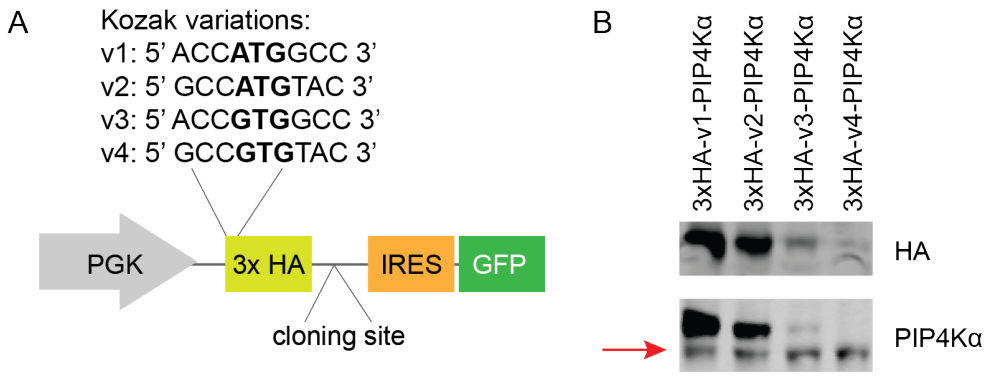

Figure 2.16 Designing endogenous levels reconstitution vector.
(A) PIG 3xHA vector with variations of the Kozak at the start site of N-terminal 3xHA tag.
(B) 293T cells expressing variations of the PIG-3xHA-PIP4Kα. Red arrow indicates endogenous PIP4Kα.

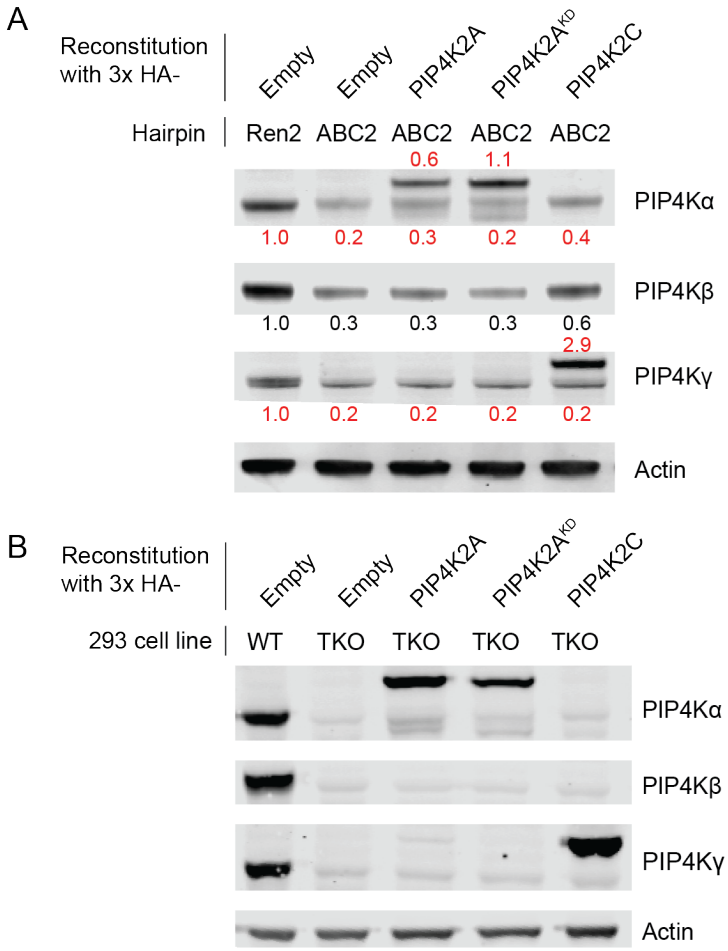

Figure 2.17 Reconstitution of PIP4K to near-endogenous levels. **(A)** TKD Hela cells were reconstituted with hairpin resistant PIP4K isoforms. Relative levels of expression were quantified and normalized to control cell line. **(B)** 293T TKO cells were reconstituted with PIP4K isoforms.

We measured levels of phosphoinositides in these cells. We observed that reconstitution of either kinase active or dead PIP4Ks fully restored levels of PI(4,5)P_2 (Figure 2.18). Moreover, PI(4)P levels were also restored to normal levels with reconstitution of either active or dead PIP4K. In contrast, only the active PIP4Kα reduced PI(5)P to normal levels, indicating that the elevation in this lipid in is due to the loss of PIP4K enzymatic activity.

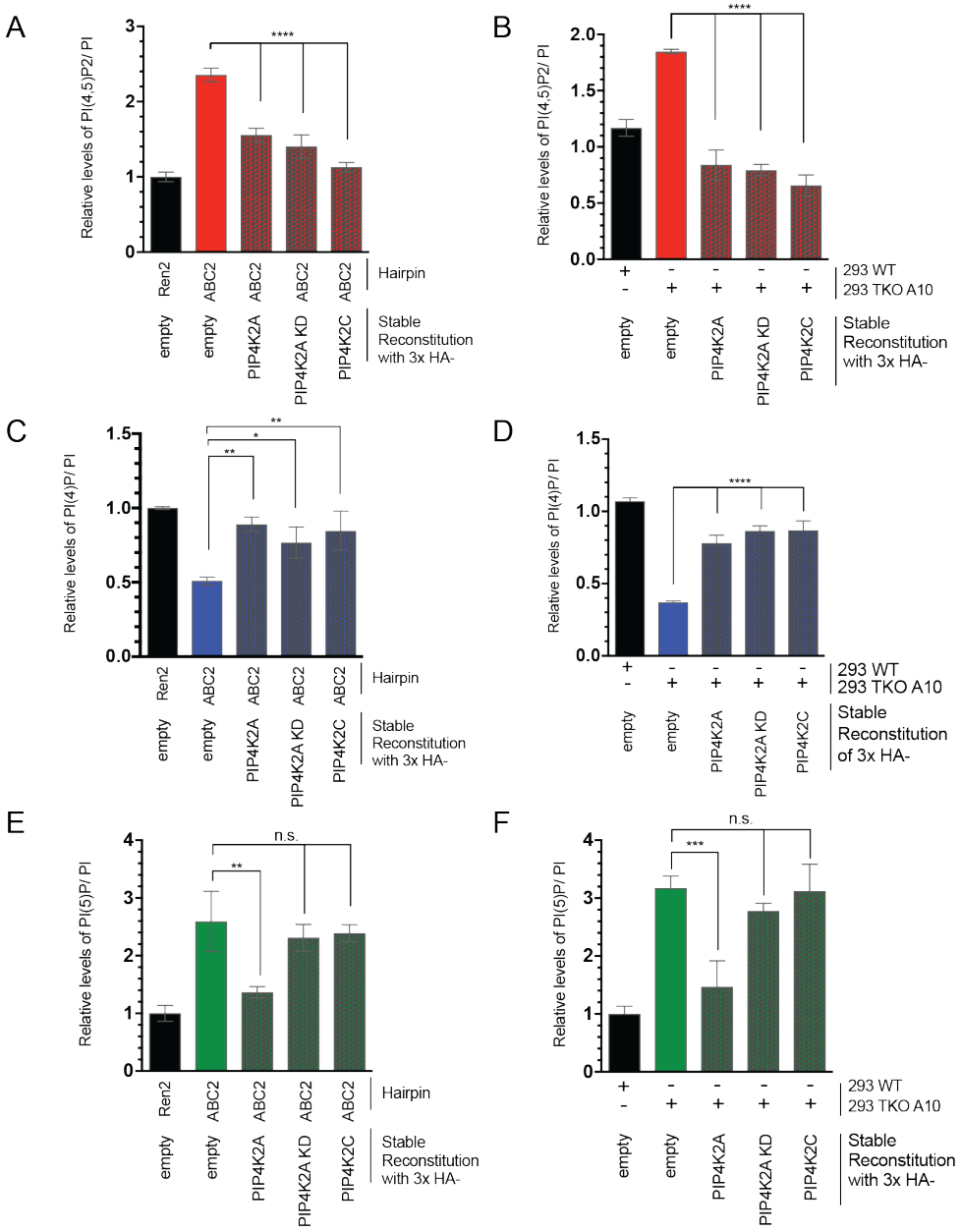

Figure 2.18 PI(4)P and PI(4,5)P_2 are restored to normal levels by reconstitution of catalytic active or dead PIP4K.
Levels of PI(4,5)P_2 upon reconstitution of PIP4K in Hela TKD **(A)** or 293T TKO **(B).** Levels of PI(4)P upon reconstitution of PIP4K in Hela TKD **(C)** or 293 TKO **(D).** PI(5)P levels upon reconstitution of PIP4K in Hela TKD **(E)** or 293 TKO **(F)**.. Significance calculated using ANOVA with Holm-Sidak multiple comparisons to control cell line. *p<0.05, **p<0.01, ***p<0.001, ****p<0.0001, n.s. not significant.

2.4.7 MODULATION OF PI(5)P DOES NOT ALTER PI(4,5)P2

To further corroborate our findings that PIP4K kinase activity is not significantly affecting total cellular $PI(4,5)P_2$, we evaluated the effect of artificially increasing PI(5)P with an exogenous 4-phosphatase, and evaluated the phosphoinositide levels in normal and PIP4K TKO or TKD cells. This would be an additional way to confirm that loss of enzymatic activity of PIP4K is not mediating the unexpected increase in $PI(4,5)P_2$. Transient expression of bacterial Ipgd, a 4-position phosphatase on $PI(4,5)P_2$, dramatically increases cellular PI(5)P[62,63] with only a modest decline in $PI(4,5)P_2$. We transiently expressed Ipgd or an empty vector, and performed HPLC analysis of phosphoinositides in 293T cells (Figure 2.19) as well as Hela cells (Figure 2.20). While Ipgd induced a greater increase in PI(5)P than seen in PIP4K TKO, this was not accompanied by a decrease in PI(4)P. Additionally, Ipgd transfections in TKD or TKO cells did not cause an exacerbated increase in $PI(4,5)P_2$ or decrease in PI(4)P. These results further argue that the increase in PI(5)P is not causing the decline in PI(4)P in cells was loss of PIP4K.

From these observations, we concluded that the catalytic activity of PIP4Ks does not account for the observed decrease in PI(4)P and increase in cellular $PI(4,5)P_2$, and that the PIP4Ks play a scaffolding role in addition to their enzymatic function.

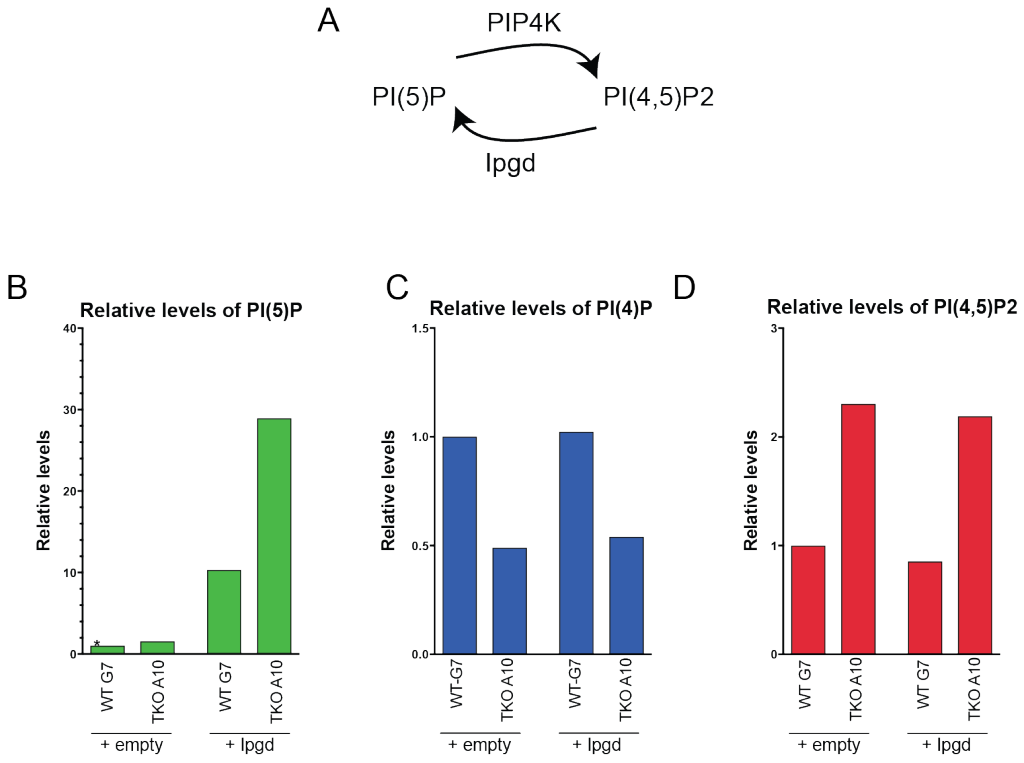

Figure 2.19 Increasing cellular PI(5)P by expressing a PI(4,5)P_2 4-phosphatase does not phenocopy loss of PIP4K in 293T cells. **(A)** Schematic for mechanism by which Ipgd increases PI(5)P. HPLC analysis of PI(5)P **(B),** PI(4)P **(C),** or PI(4,5)P_2 **(D)** levels in 293T wild type or triple knockout cells, with transfection of empty vector or Ipgd vector.

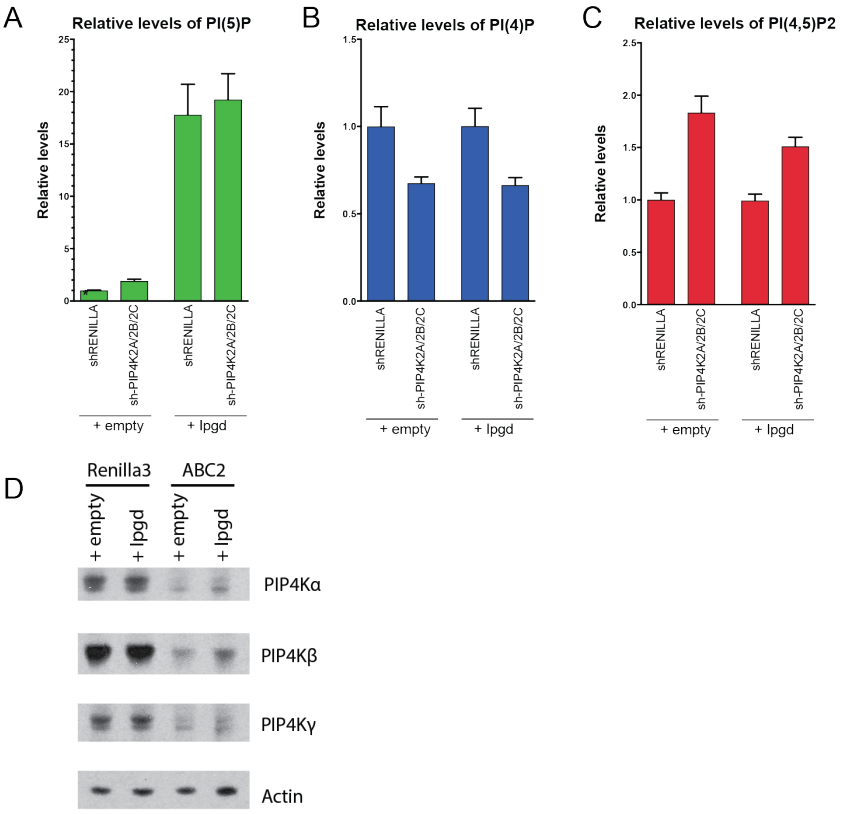

Figure 2.20 Increasing cellular PI(5)P by expressing a PI(4,5)P_2 4-phosphatase does not phenocopy knockdown of PIP4K in Hela cells. HPLC analysis of PI(5)P **(A)**, PI(4)P **(B)**, or PI(4,5)P_2 **(C)** levels in Hela cells. **(D)** Knockdown efficiency was verified in transfection conditions.

2.5 DISCUSSION

We successfully generated tools to knockdown various subsets of the PIP4K family. We successfully validated that loss of PIP4K increases PI(5)P and increases sensitivity to insulin stimulation—both previously reported phenotypes[10,14].

However, we could not validate other phenotypes. We expected severe growth defects in the setting of PIP4K2A/2B double knockdown, or PIP4K2B/2C knockdown, since these double knockout mice could never be generated[12]. However, it appears that cell lines grown in tissue culture do not require PIP4K for proliferation. Additionally, we were ready to observe a synthetic lethality between loss of PIP4K and deficient p53 signaling[12]. However, after knocking down PIP4K in a panel of tumor cell lines with intact, mutant, or deleted *TP53*, we conclude that there are no significant changes in cell viability. Cell lines grown in 2D plates experience much less stress than their *in-vivo* ancestors. Perhaps there are conditions such as nutrient or hypoxic stress that promotes synthetic lethality between loss of PIP4K and p53.

Another explanation for this discrepancy is that our knockdowns allow for residual PIP4K to remain, and would therefore be sufficient to convert enough PI(5)P into $PI(4,5)P_2$. We learn from our artificial induction of PI(5)P, through expression of a 4-phosphatase on $PI(4,5)P_2$, that residual PIP4K has the ability to turnover large quantities of PI(5)P. This is because we see more Ipgd-induced PI(5)P accumulate when PIP4K is genetically knocked out. In contrast, accumulation of PI(5)P is approximately the same when PIP4K is knocked down. Moving forward, it is important to remember that

catalytic-dependent functions of PIP4K may be hidden when using short-hairpin systems to knockdown enzymes.

We were interested to ask if elimination of any PIP4K isoform would influence levels of the other isoforms. Our results show that single or double knockdowns did not destabilize the isoforms that were not targeted, though overexpression of catalytically inactive PIP4Ks stabilized endogenous PIP4K isoforms. A prior study noted that knockout of PIP4K2B caused destabilization of PIP4K2A[65]. In this study, they used DT40 cells, which are B cells derived from chickens. It is possible that this was a cell-type specific observation, or that PIP4K biology is different in chickens, since there is no evidence of PIP4Kγ in birds.

Depletion of all three isoforms of PIP4K causes a significant decrease in PI(4)P and increase in PI(4,5)P_2, as demonstrated in a panel of cell lines of various tissue origin and mutational backgrounds. We were able to use the single and double knockdowns to investigate if loss of one member of the PIP4K accounts for changes in these phosphoinositides. We find that there is an additive effect when more isoforms are depleted, without a robust preference for any particular member. We expect that the ratio of various PIP4K family members is different from cell line to cell line. Perhaps depletion of the most abundant isoform(s) causes more elevation in PI(4,5)P_2 and decrease in PI(4)P.

Our reconstitution studies using vectors with strong promoters serve as a warning for those who try to draw conclusions from experiments using vectors to massively overexpress PIP4K. There

were interesting observations from those experiments that may not be artifacts—overexpression of kinase dead PIP4Kα made cells vacuolated and sick after multiple passages. This was also seen to a lesser degree in overexpression of kinase dead PIP4Kβ. All active reconstitutions and dead PIP4Kγ reconstitutions grew fine and were morphologically normal by brightfield microscopy. Surprisingly, massive overexpression of active PIP4Kγ seemed to decrease PI(4)P and increase PI(4,5)P_2, as if to exacerbate the triple knockdown. We assume this to be an artifact of massive non-physiological expression. Perhaps specific isoforms, if catalytically inactive, have a predisposition to aggregate. We did not investigate these observation since it was not reproduced with the endogenous-level active PIP4Kγ reconstitution. Our results show that reconstitution of endogenous-level active PIP4Kα, dead PIP4Kα, and PIP4Kγ can restore levels of PI(4)P and PI(4,5)P2.

We conclude that all three isoforms of PIP4K share structural features to mediate homeostasis of PI(4)P and PI(4,5)P_2. These experiments establish a novel catalytic-independent function for all members of the PIP4K family. There has been one prior report describing catalytic-independent functions of PIP4K. In drosophila, loss of dPIP4K results in accumulation of photoreceptors on Rab5 positive vesicles, which is reversed upon kinase-dead dPIP4K reconstitution[35]. It is possible that this phenotype is related to changes in PI(4)P and PI(4,5)P_2. The drosophila did not exhibit a significant increase in PI(4,5)P_2 upon loss of dPIP4K, but perhaps the drosophila tissues examined have a different balance or lipid kinases and phosphatases.

Accumulation of $PI(4,5)P_2$ could be masked through rapid conversion into another phosphoinositide species, or hydrolysis into IP_3. We investigate the mechanistic underpinnings of this finding in Chapter 3, and examine how the structural role of PIP4K impacts cell signaling.

2.6 ACKNOWLEDGEMENTS AND CONTRIBUTIONS

Diana Wang designed experiments and interpreted experimental results with the help of Lukas Dow. Diana Wang performed the experiments with assistance from Oksana Mashadova, Solomon Amadiume, and Janet Sun.

CHAPTER THREE: THE PIP4K FAMILY MEMBERS INHIBIT CELLULAR PIP5K ACTIVITY, THEREBY SUPRESSING PI3K SIGNALING

3.1 ABSTRACT

In the previous chapter, we demonstrated a novel, catalytic-independent role for the PIP4K enzymes in regulating cellular PI(4)P and PI(4,5)P_2. In this chapter, we begin to uncover the mechanism underlying these changes. We find that there is enhanced PIP5K activity in cells with deleted PIP4K, which is reversed upon reconstitution of catalytic dead PIP4K.

Because PI(4,5)P_2 is an important lipid in mediating many cellular functions, dysregulation of PI(4,5)P_2 is expected to have far reaching consequences. In this chapter, we focus on how catalytic-independent functions of PIP4K modulate PI3K signaling. We observe an increase in insulin-stimulated PI(3,4,5)P_3 in the PIP4K knockdown cells, which is reversed upon reconstitution of catalytic dead PIP4K. This is consistent with a model in which increased amounts of PI(4,5)P_2 support increased PI(3,4,5)P_3 production.

3.2 INTRODUCTION

Many cellular processes are controlled by $PI(4,5)P_2$. and therefore cells have mechanisms to fine tune the localization and flux of this lipid. $PI(4,5)P_2$ is enriched at the plasma membrane, and is primarily formed by the PIP5K family enzymes[2]. Various pools of $PI(4,5)P_2$ are tightly controlled through lipid kinases, lipid phosphatases, and phospholipases[81,82]. Regulation of PIP5K has been well studied— all three isoforms of PIP5K are stimulated by phosphatidic acid (PA) and regulated by small G-proteins[6,83-85]. Rac has been shown to directly bind and activate PIP5K[86].

Levels of $PI(4,5)P_2$ are remarkably stable[75], yet, as shown in Chapter 2, deletion of the PIP4K family members results in nearly two-fold changes in PI(4)P and $PI(4,5)P_2$. A two-fold increase in $PI(4,5)P_2$ is expected to disrupt many processes. Insulin activation of the PI3K pathway is initiated at the plasma membrane, where conversion of $PI(4,5)P_2$ into $PI(3,4,5)P_3$ recruits effector proteins Akt and Pdk1 to propagate signaling cascades (Figure 1.5)[87].

Local production of $PI(4,5)P_2$ near RTKs is a mechanism to support RTK activation of $PI(3,4,5)P_3$ production. In B cells, BTK constitutively binds to PIP5K, and activation of the B cell receptor enables BTK recruitment of PIP5K to support $PI(4,5)P_2$ and $PI(3,4,5)P_3$ production at the plasma membrane[88]. In a separate example, IQGAP1 acts as a scaffold for PI4KIIIα, PIP5Kα, and PI3K[89]. Through this complex, PI can be sequentially converted to PI(4)P, $PI(4,5)P_2$, and $PI(3,4,5)P_3$. Loss of IQGAP1 impairs insulin-activation of the PI3K signaling pathway.

Manipulation of PIP4K has been previously reported to modulate the PI3K/Akt/mTOR pathway[10]. It is possible that accumulation of PI(5)P, as a consequence of PIP4K inhibition, inhibits a $PI(3,4,5)P_3$ phosphatase[61] or directly activates class 1A PI3K[63]. In this chapter, we test the hypothesis that the catalytic-independent ability of PIP4K to suppress $PI(4,5)P_2$ production is mediated through inhibiting PIP5K activity, thereby limiting insulin activation of and $PI(3,4,5)P_3$ production.

3.3 METHODS

Western blot for PIP5K. Lysates were prepared as described in methods from chapter 2 (2.3). Antibodies purchased from CST (PIP5K1A 9693) and Abcam (PIP5K1C ab109192).

Collection of RNA for RNAseq. RNA was harvested with Trizol (Invitrogen 15596018) and then treated with DNAse (Ambion AM1907) before a second round of purification with Qiagen RNease kit (Qiagen 74104). The WCMC genomics core confirmed high RNA quality via Agilent Bioanalyzer QC nanogel, and prepared a stranded mRNA library. The genomics core performed HiSeq paired end reads with 4 samples per lane, giving 150 million reads per sample.

Cellular PIP5K activity assay and thin layer chromatography. Cells were trypsinized and normalized for cell number. Pellets were resuspended in HNE buffer (20 mM HEPES pH 7.4, 100mM NaCl, 0.5mM EGTA), and sonicated in the presence of ^{32}P-γ-ATP, and liposomes (4ug PS, 2 ug PI(4)P in 30mM HEPES pH 7.4, 1mM EGTA). Reactions were stopped by added 50uL of 4N HCL. To extract lipids, 100 µL of MeOH:CHCl3 (1:1) was added and samples were vortexed 2x 30 seconds. Samples were spun down at top speed for 2 min and the organic phase containing phosphatidylinositol lipids (bottom) were separated using thin-layer chromatography (TLC) using 1-propanol: 2N acetic acid (65:35 v/v). TLC plates (Sigma Z193275) were prepared ahead of time by coating with 1% Potassium Oxalate (Sigma P0963). Phosphorylated lipids were visualized by autoradiography (GE Typhoon FLA 7000) and quantified using ImageQuant TL software.

Purified PIP5K *in-vitro* kinase assay. Similar to protocol described above. Instead of using cell pellet resuspended in HNE buffer, this assay uses E. Coli purified PIP5K resuspended in HNE buffer. Thin layer chromatography protocol is same as above.

Quantification of relative molarity of E. Coli purified protein. Purified protein concentration were estimated via measurement of A280 absorbance. Volumes for equal molarity were loaded on SDS-PAGE gel, next two various BSA standards. Gel was processed with SYPRO Ruby (Invitrogen S12000) according to steps in manufacturer's protocol.

3.4 RESULTS

3.4.1 ASSESSING CHANGES IN PIP5K

As discussed in Chapter 2, in cells depleted of PIP4K, we observed a concomitant decrease in PI(4)P with increase in PI(4,5)P_2. We hypothesized that increased PIP5K activation could consume increased amounts of its substrate, PI(4)P, to form PI(4,5)P_2. Protein levels of PIP5Kα and PIP5Kγ were not consistently altered in response to knockdown or knockout of the PIP4K family (Figure 3.1). RNA-seq did not detect statistically significant changes in members of the PIP5K family (Appendix A).

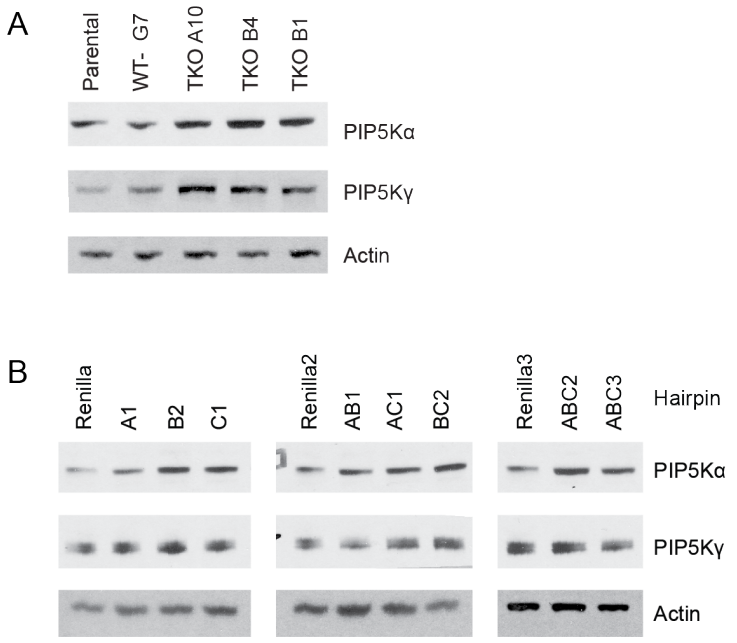

Figure 3.1 Western blot quantifying levels of PIP5K.
(A) PIP5Kα and PIP4Kγ levels in 293T CRISPR TKO clones.
(B) PIP5Kα and PIP4Kγ levels in Hela TKD cells.

PIP5K activity can be assayed in whole cell lysates. Cells are lysed in the absence of detergents, and upon addition of exogenous PI(4)P and ^{32}ATP, radioactive PI(4,5)P_2 is produced. To quantify differences in PI(4,5)P_2 production, lipids are extracted and separated using thin layer chromatography (TLC). Alternatively, the lipids can be deacylated and detected upon separation using HPLC. Indeed, we found through HPLC analysis, that there is increased radioactive PI(4,5)P_2 production in TKO cells, consistent with our model that PIP5K activity is higher in the absence of PIP4K. This observation is reversed when cells are reconstituted with either active or kinase dead PIP4K isoforms, indicating it is not dependent on the enzymatic activity of these enzymes (Figure 3.2).

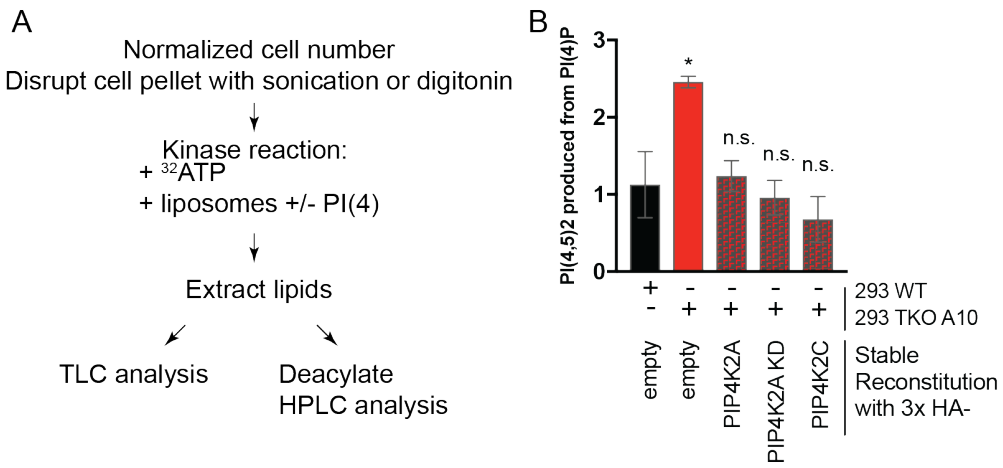

Figure 3.2 Changes in PIP5K activity in 293T cells.
(A) Schematic of protocol to assay changes in cellular PIP5K activity.
(B) HPLC quantification of radioactive PI(4,5)P_2 produced in cell lysates with drop in of exogenous PI(4)P. Significance calculated using ANOVA with Holm-Sidak multiple comparisons to control cell line. *p<0.05, n.s. not significant.

3.4.2 CHANGES IN PI(4,5)P2 LEVELS ARE ACCOMPANIED WITH CHANGES IN INSULIN SENSITIVITY

We observe concomitant changes in PI(4,5)P_2 and PI(3,4,5)P_3. In cells depleted of PIP4K, we observed an increase in levels of PI(3,4,5)P_3 (Figure 3.3). We hypothesized that accumulation of PI(4,5)P_2 could increase PI3K production of PI(3,4,5)P_3, thereby increasing PI3K signaling. 293T cells have detectable PI(3,4,5)P_3 levels, and therefore it is possible to quantify changes in PI(3,4,5)P_3 upon insulin stimulation. Cells were serum starved and stimulated with 50 ng/mL insulin for 5 minutes. TKO cells generated more than two-fold more PI(3,4,5)P_3 upon insulin stimulation, which is rescued upon reconstitution with either active or dead PIP4Kα, or PIP4Kγ (Figure 3.3).

To confirm that the changes in PI3K activity is being transmitted down the PI3K pathway to downstream targets, we used pAkt-473 as a readout for Akt activation (Figure 3.4). There are a plethora of Akt targets that are well characterized, such as pGSK3α and pPRAS40[90]. We see that insulin stimulation of cells with loss of PIP4K results in increased activation of Akt and downstream targets (Figure 3.5), and reconstitution with either kinase dead PIP4Kα or PIP4Kγ reverses the enhanced insulin sensitivity. Our results suggest that loss of allosteric inhibition of PIP4K on PIP5K drives overproduction of PI(4,5)P_2 in plasma membrane pools that are used by PI3K during insulin signaling.

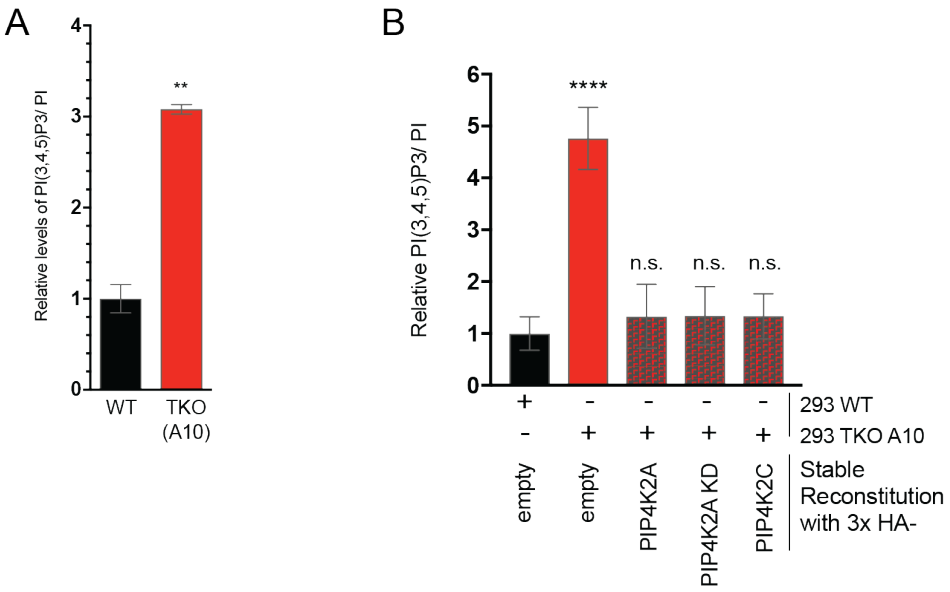

Figure 3.3 Catalytic independent role of PIP4K modulates PI(3,4,5)P_3 production.
(A) HPLC measurement of PI(3,4,5)P_3 levels in 293T TKO cells, harvested in serum-replete conditions. Significance calculated using student's t-test, **p<0.01. **(B)** After overnight serum starvation, 293T cells were stimulated with 50 ng/mL of insulin for 5 minutes. HPLC measurement of PI(3,4,5)P_3 levels analyzed with HPLC. Significance calculated with ANOVA using Holm-Sidak multiple comparisons to control cell line. ****p<0.0001, n.s. not significant.

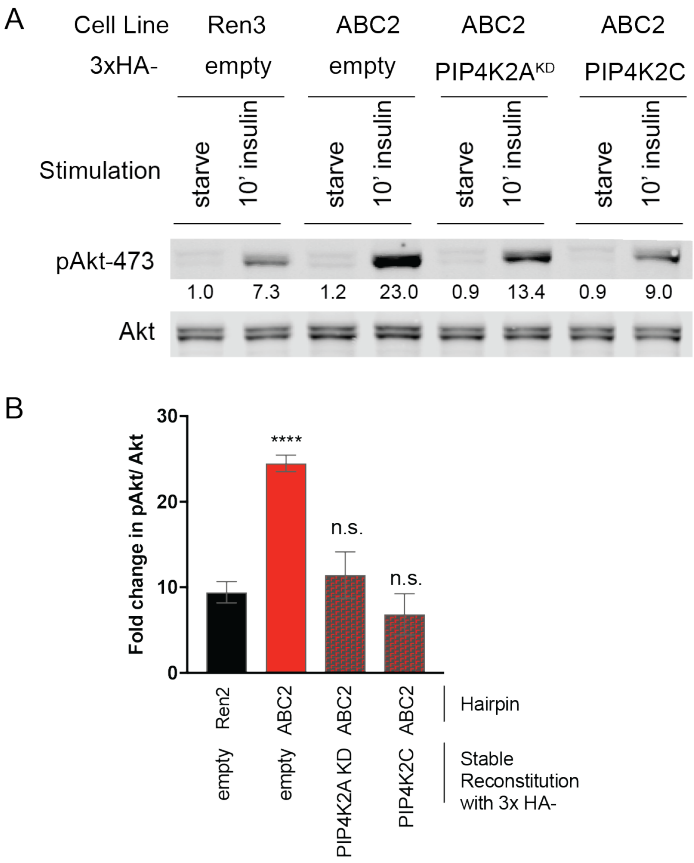

Figure 3.4 Insulin mediated Akt activation is modulated by catalytic independent functions of PIP4K.
(A) Hela cells with triple knockdown of PIP4K and reconstituted with kinase dead PIP4Kα or active PIP4Kγ were serum starved overnight, and stimulated with 500 ng/mL of insulin for 10 minutes. **(B)** Quantification of pAkt-473 levels normalized to total Akt, n=3. Significance calculated using ANOVA with Holm-Sidak multiple comparisons to control cell line. ****p<0.0001, n.s. not significant.

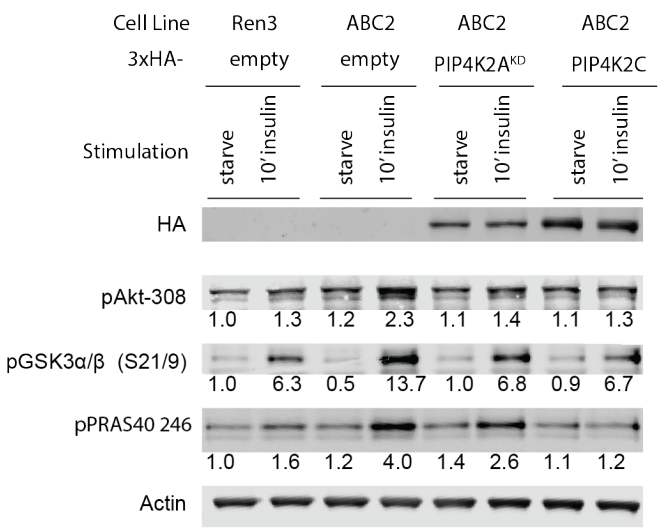

Figure 3.5 Insulin stimulation of the PI3K pathway is modulated by catalytic independent functions of PIP4K.
Hela cells with triple knockdown of PIP4K and reconstituted with kinase dead PIP4Kα or active PIP4Kγ were serum starved overnight, and stimulated with 500 ng/mL insulin for 10 minutes. Signal intensities were normalized to actin and further normalized to starved control cell line.

3.5 DISCUSSION

Our results in Chapter 3 shed light on the mechanism underlying how PIP4Ks modulate PI(4,5)P_2 levels through catalytic-independent means. In the absence of PIP4K, we observe that PIP5K enzymatic activity is enhanced. These results suggest that the PIP4K family can negatively regulate PIP5K.

While a decrease in the ratio of PI(4)P to PI(4,5)P_2 may be explained by our observation that PIP5K activity is enhanced, there could be additional mechanisms enhancing the changes in PI(4)P and PI(4,5)P_2. For example, it is possible that loss of a 5-phosphatase activity could decrease conversion of PI(4,5)P_2 to PI(4)P. However, humans have ten genes that have 5-phosphatase activity, and therefore

it is unlikely that decreased activity in one gene could greatly affect the ratio of PI(4)P to PI(4,5)P_2[91]. Additionally, there are possible mechanisms where reduction of PI(4)P is not coupled to increased PI(4,5)P_2. For example, the decrease in PI(4)P could be attributed to reduced PI4K activity, or increased Sac1 phosphatase activity. Increased PI(4,5)P_2 could be due to reduced hydrolysis by PLC. We have not tested these theories yet, but it is worth exploring in the future if we uncover additional phenotypes which suggest a primary defect in these other mechanisms.

PI3K activation can be direct assessed through measurement of PI(3,4,5)P_3, and indirectly assessed through monitoring downstream signaling proteins. Through both approaches, we were able to demonstrate that loss of PIP4K increases PI3K activation, which is reversed upon reconstitution of either active or dead PIP4K isoforms. We propose that loss of allosteric inhibition of PIP5K by PIP4K enables overproduction of PI(4,5)P_2 which can be limiting during insulin stimulated activation of PI3K signaling. Our findings implicate novel ways to manipulate PIP4K biology to increase systemic insulin sensitivity and potentially treat patients with metabolic syndrome.

Our results provide a mechanism that explains the increased insulin sensitivity observed in *Pip4k2b* knockout mice at the level of PI(4,5)P_2 generation[10]. While *Pip4k2a* knockout and *Pip4k2c* knockout did not exhibit increased insulin sensitivity in insulin tolerance tests or glucose tolerance tests[11,12], it is possible that most tissues can readily compensate when there is deletion of a single isoform of PIP4K. Skeletal muscle has higher expression of PIP4Kβ than other PIP4K

family members (unpublished RNA seq), and therefore it is possible that skeletal muscle relies heavily of PIP4Kβ to modulate PIP5K.

3.6 ACKNOWLEDGEMENTS AND CONTRIBUTIONS

Diana Wang and Marcia Paddock designed experiments and performed most of the experiments with assistance from Janet Sun. Diana Wang and Marcia Paddock interpreted experimental results.

CHAPTER FOUR: CONCLUDING REMARKS

4.1 SUMMARY

This thesis has outlined the design and use of tools to study PIP4K family enzymes, and provides new insight into the biological importance of PIP4K in modulating signaling at the plasma membrane. This body of work describes how PIP4K has a catalytic-independent role for controlling levels of $PI(4,5)P_2$, an important lipid for mediating many processes, including cell signaling. Loss of catalytic-independent functions of PIP4K causes increased activity of PIP5K and insulin stimulated activation of PI3K (Figure 4.1).

4.2 FUTURE DIRECTIONS

Our experiments suggest that members of the PIP4K family share common structural features to inhibit PIP5Ks.The amino acid sequences of the PIP4K family are well conserved (~80%), and comparison of crystal structures corroborates that all three isoforms share common features. We have yet to fully characterize the biochemical mechanism by which PIP4K can inhibit PIP5K.

PIP5K family members were not found to be significantly upregulated in our RNA-seq data (Appendix B) and proteomics data (Appendix C). Furthermore, our RNA-seq and proteomics data did not reveal hits relevant to previously described modulators of PIP5K. PIP5K is known to be stimulated by phosphatidic acid (PA), Rac, and Arf6-GTP[92-95]. We did not observe higher levels of PA using whole cell

lipidomics (Figure 4.2). In fact, PA levels are approximately the same or decreased when PIP4K is lost.

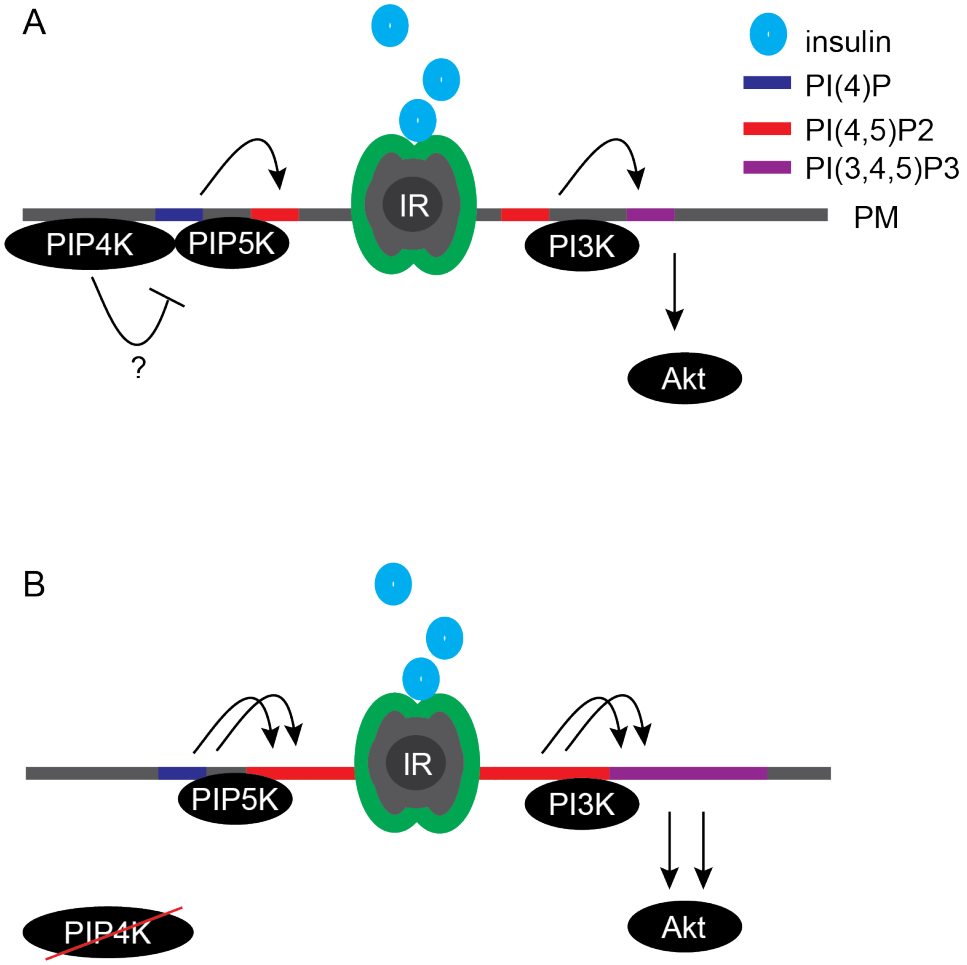

Figure 4.1 Working Model.
Loss of PIP4K drives PI(4,5)P_2 production and enhanced insulin stimulation of the PI3K pathway. **(A)** PIP4K directly binds, and inhibits PIP5K to control production of PI(4,5)P_2. **(B)** Loss of PIP4K allows for full activation of PIP5K and increases availability of PI(4,5)P_2 for enhanced PI(3,4,5)P_3 production. PI(3,4,5)P_3 increases recruitment and activation of Akt and other downstream effector proteins.

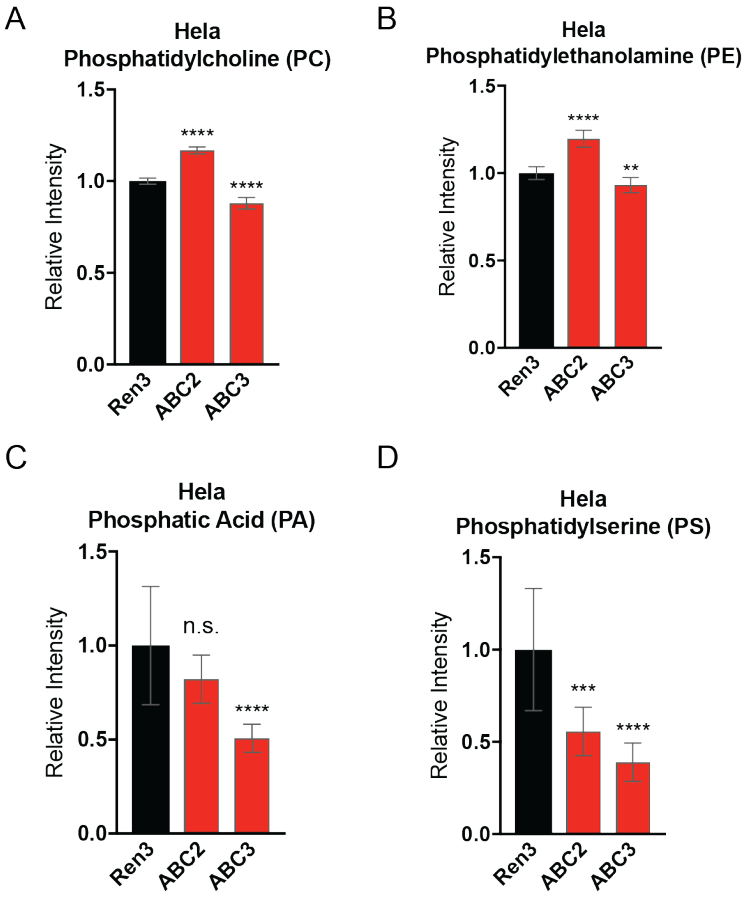

Figure 4.2 PIP4K TKD cells do not have higher levels of PA. To quantify anionitc cellular phospholipids, we performed lipidomics. Hela control (Ren3) and triple knockdown (ABC2, ABC3) cells were normalized by cell number and lipids were extracted via Bligh-Dyer extraction. (**A,B**) Levels of PC and PE are in excess of other phospholipids, and reflect cell number. (**C,D**) Levels of PA and PS are unchanged, or lower in cells with PIP4K knockdown. Significance calculated using ANOVA with Holm-Sidak multiple comparisons to control cell line. ***p<0.001, ****p<0.0001, n.s. not significant.

Phospholipase D (PLD) cleaves phosphatidylcholine (PC) to generate PA. We speculated that there could be increased generation of PA without whole-cell elevation of PA, but we did not observe an increase PLD activity (Figure 4.3)[96]. In fact, there was a trend towards decreased PLD activity in cells with loss of PIP4K.

In order to test if Rac mediates changes in PIP5K when PIP4K is lost, we used isogenic H1299 cells, with Rac1 CRISPR knockout (KO). Knockdown of PIP4K in H1299 wild type or isogenic Rac1 KO cells both showed the same phenotype—where PI(4)P decreases and PI(4,5)P_2 increases (Figure 4.4). Therefore we conclude that the increase in PIP5K activity in cells with loss of PIP4K is not due to PA, PLD, or Rac. Interestingly, H1299 cells had an increase in protein levels of PIP5Kα and PIP5Kγ (Figure 4.4). It is possible that loss of PIP4K causes stabilization of PIP5K in certain cell lines, such as H1299, but not in 293T or Helas, as shown in Figure 3.1.

It remains to be seen loss of PIP4K causes increased PIP5K due to other known mechanisms, such as Arf6 activation, or changes in Rho family GTPases[97-99].

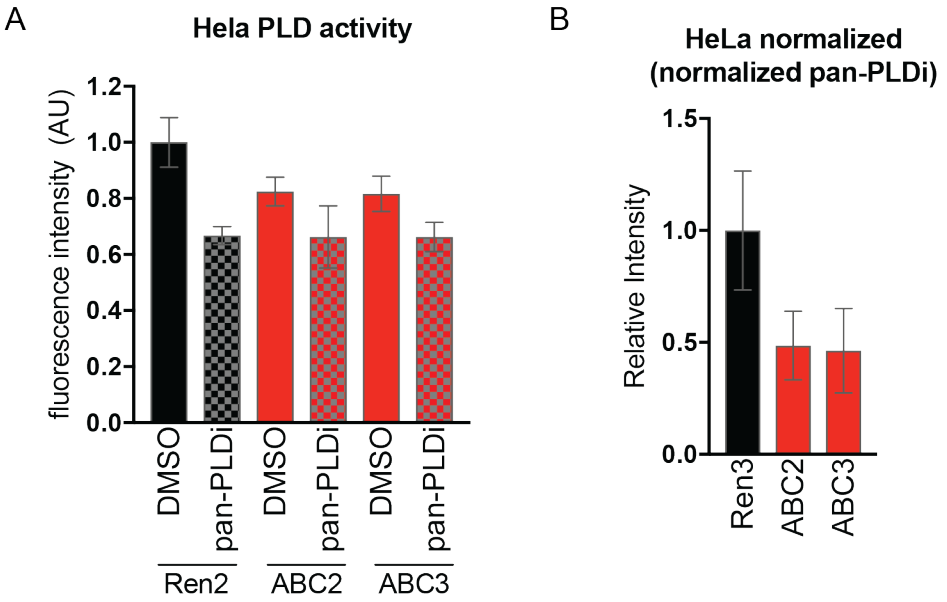

Figure 4.3 PIP4K knockdown cells do not have higher PLD activity. Quantification of PLD activity using clickable substrates. PLD uses BODIPY conjugated azidoalcohol as a substrate, resulting in covalent labeling reflecting PLD activity[96,100]. Hela cells were incubated with substrate in the presence or absence of 750 nM FIPI, a pan PLD inhibitor. **(A)** After washout, cells were analyzed via flow cytometry for GFP intensity. **(B)** Intensity values normalized after subtraction of background, and further normalized to control cell line.

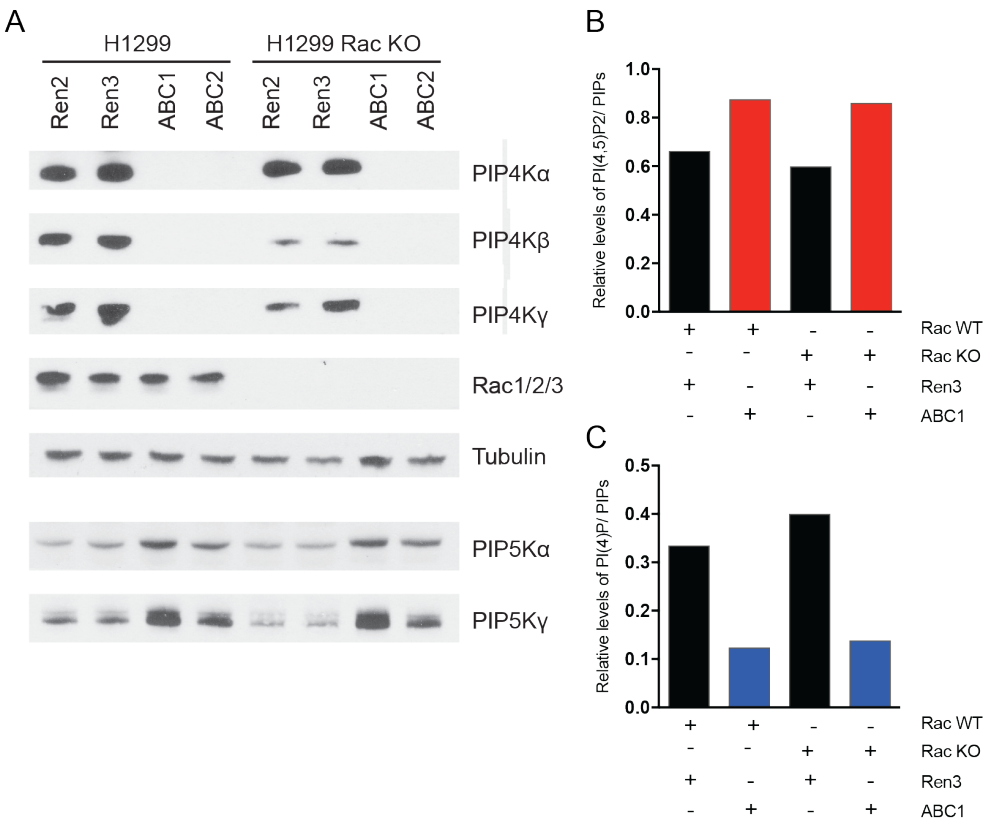

Figure 4.4 Rac does not mediate changes in PIP5K activity in cells with PIP4K depletion.
(A) Western blot validation of H1299 wild type and Rac knockout, with triple knockdown of PIP4K isoforms. **(B)** HPLC measurement of $PI(4,5)P_2$ levels. **(C)** Measurement of PI(4)P levels. Experiment was performed n=1, values normalized to total PIPs.

Members of the PIP4K and PIP5K family have been previously reported to directly complex to each other, but the importance of this interaction was not explored[101]. Additionally, in an unbiased, high throughput mass spectrometry screen, there is evidence of interaction between PIP5Kα and PIP4Kα[102]. Such an interaction would be an opportunity for PIP4K to directly inhibit PIP5K. To test whether the altered activity of PIP5K could be a result of a direct interaction, we

performed in-vitro kinase reactions and found that PIP4Kγ can directly inhibit PIP5Kα activity (Figure 4.5). We titrated levels of PIP4Kγ and found that a dose-dependent ability of PIP4Kγ to inhibit PIP5Kα. This effect was eliminated by denaturing PIP4Kγ, suggesting that intact protein is required to mediate this effect. To determine if PIP4K2A and PIP5K1A can directly interact *in-vivo*, we co-expressed 3xHA-tagged PIP5K1A or 3xHA-empty with 3xFLAG-tagged PIP4K2A. Cells were cross-linked and mechanically lysed. Immunoprecipitated proteins were boiled before western blot analysis. FLAG-PIP4K2A is enriched when tagged-PIP5K1A is immunoprecipitated (Figure 4.5).

We speculate that the interactions between PIP4K and PIP5K occur only in the presence of membranes. While cellular PIP5K activity is higher, immunoprecipitation (IP) of tagged PIP5K1A in wild type and TKO 293T cells does not exhibit differential activity in-vitro (data not shown). We expect that detergents during the IP disrupted these protein complexes, thereby relieving PIP4K inhibition of PIP5K.

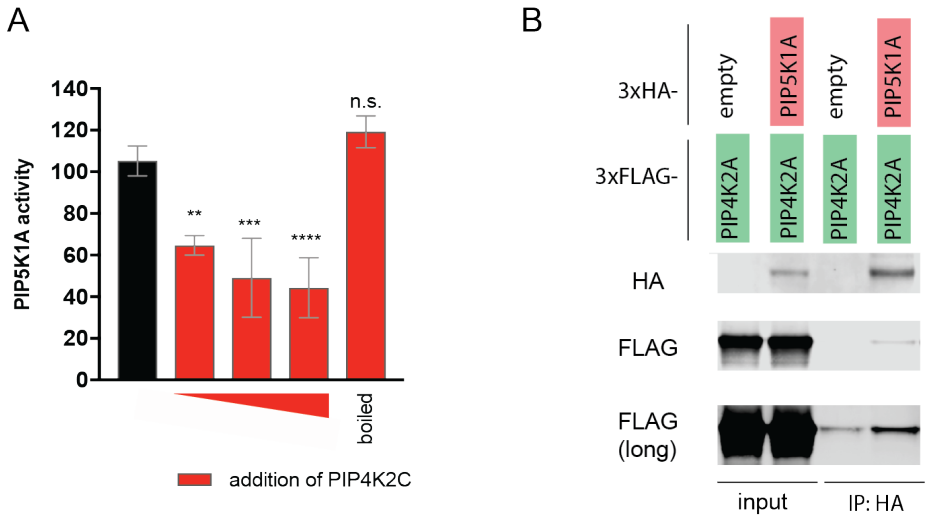

Figure 4.5 PIP4Ks can directly inhibit PIP5Kα
(A) Quantification of PIP5Kα activity from *in-vitro* kinase assays. Titrations were performed at 1:10 and 1:50 dilutions. Significance calculated using ANOVA with Holm-Sidak multiple comparisons to control cell line. **p<0.01, ***p<0.001, ****p<0.0001, n.s. not significant.
(B) 293T TKO cells expressing 3xHA tagged PIP5K1A and 3xFLAG tagged PIP4K2A. FLAG tagged PIP4K2A is detected in pulldown of HA tagged PIP5K1A.

We hypothesized that PIP4K influences membrane $PI(4,5)P_2$ homeostasis through a mechanism which requires PIP4K to be properly localized to membrane. Therefore, disruption of PIP4K recruitment to its native membranes should phenocopy PIP4K deletion. To test this, we made point mutations in PIP4Kγ which abrogates key basic resides predicted to mediate membrane interactions (Figure 4.6). In 293T TKO cells, wild type PIP4Kγ but not mutant PIP4Kγ ($PIP4K2C^{5E}$) rescued levels of $PI(4,5)P_2$. We have yet validate that these mutations cause PIP4K to freely diffuse as cytosolic proteins, and we have yet to test which subset of residues is most important for mediating membrane recruitment.

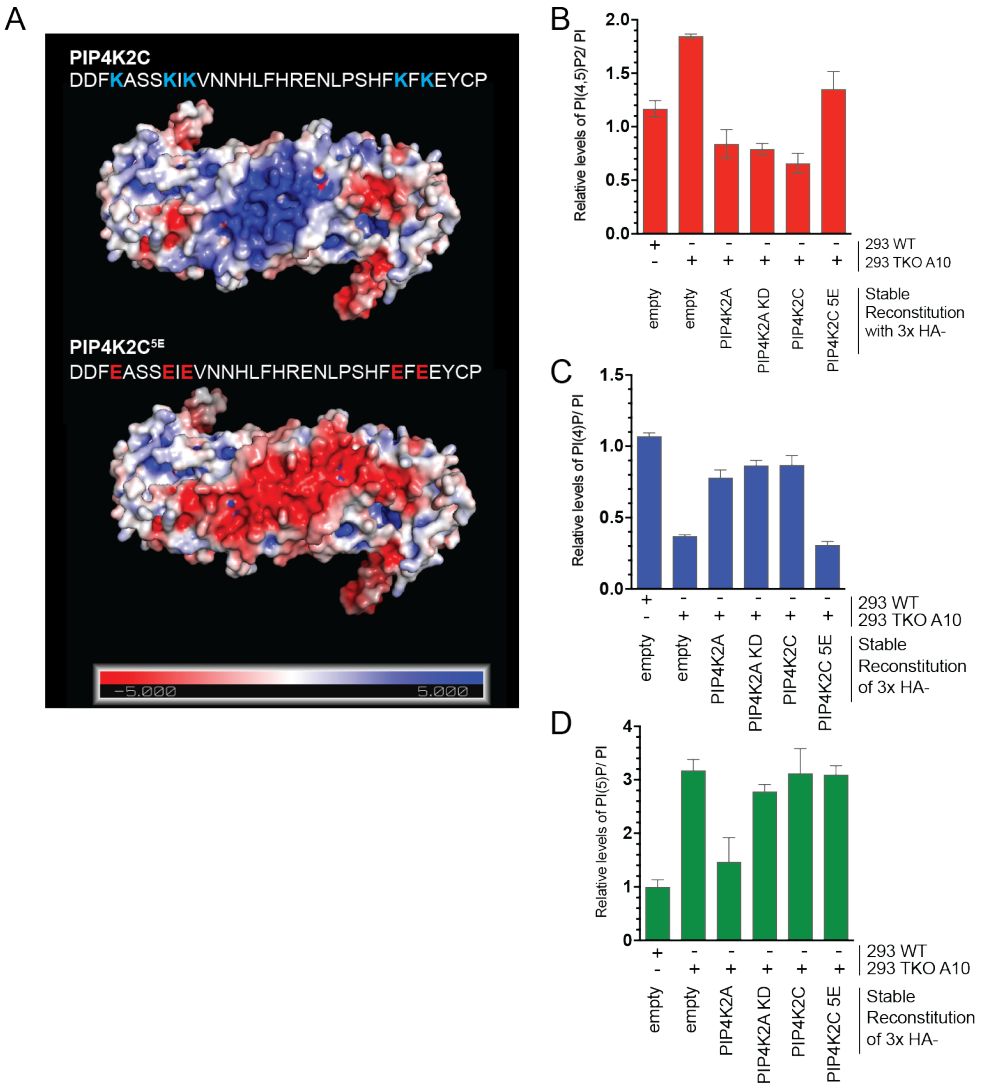

Figure 4.6 PIP4K recruitment to negatively charged membranes may be required for inhibition of PIP5K.
(A) Membrane facing view of PIP4Kγ with electrostatic potential mapped on the solvent accessible surface. Blue indicates positive surface charge while red indicates negative surface charge. Mutations indicated in PIP4K2C^{5E} abrogate positively charged interface. Calculations were made with PyMol APBS[103]. **(B,C,D)** Quantified phosphoinositide species are modified from Figure 2.17 to include PIP4K2C^{5E} rescue cell line.

It will be interesting to identify the exact structural features which mediate this interaction, but it is likely that the interaction between PIP5K and PIP4K is weak, because both families of lipid kinases reside on negatively charged membranes that recruit and enrich for both parties. When two weakly associated proteins are limited to stochastic diffusion along 2 dimensions, rather than 3 dimensions, the two proteins are more likely to associate. It may be difficult to co-immunoprecipitate PIP4Ks with PIP5Ks since lipid membranes represent the 2 dimensional setting, and disruption of membranes with detergents will cause the enzymes to exist in 3 dimensions.

Protein copy numbers of PIP4K family members are in 10 to 50-fold excess to that of PIP5K family members across a panel of cell lines, well in excess of the amount needed to inhibit PIP5K *in-vitro*[104]. We propose that a fraction of PIP4K is directly interacting with PIP5K activity at the plasma membrane, and inhibiting its activity, though attempts to directly visualize the PIP4Ks have been inconclusive.

Lastly, it will be important to characterize how accumulation of $PI(4,5)P_2$ in our system affects other cellular processes, such as signaling through other receptor tyrosine kinases and cell migration and adhesion. While our functional readout from insulin signaling points to a plasma membrane or endocytic compartment that has accumulated $PI(4,5)P_2$, we speculate that nuclear $PI(4,5)P_2$ may also be higher.

There is a body of literature that describes the importance of PIP4K in the nucleus[105-108], and there is growing evidence that phosphoinositides may exist outside of membranous structures[109,110]. Nuclear $PI(4,5)P_2$ made from PIP5K1A has been reported to control

mRNA polyadenylation[111]. It remains to be seen, how non-conventional roles of phosphoinositides regulate biology in the nucleus.

4.3 PIP4K AS A THERAPEUTIC TARGET

Our findings implicate novel ways to manipulate PIP4K biology to increase systemic insulin sensitivity and potentially treat patients with metabolic syndrome. Development of a small molecule to specifically disrupt allosteric inhibition of PIP5K by PIP4K would be a clever way to promote insulin sensitivity while preserving the catalytic function of PIP4K for autophagosome-lysosome fusion[13]. Recent advances in small molecule conjugated proteasome adaptors enable rapid degradation of specific targets[112]. Because covalent PIP4K inhibitors are already under development, it is possible to engineer and repurpose these small molecules to eliminate PIP4K family proteins. It will be interesting to see if this approach can enhance insulin sensitivity.

It remains unclear if targeting PIP4K would be a suitable strategy for cancer therapeutics. We did not appreciate changes in cell growth upon PIP4K knockdown or knockout. Inhibition of PIP5K activity may be a strategy to restrain tumor growth, as demonstrate in a prostate cancer study[113]. Perhaps development of a small molecule to *enhance* allosteric inhibition of PIP5K by PIP4K could be used in cancer therapeutics to downregulate oncogenic PI3K signaling.

Inhibition of PIP4K catalytic activity could be beneficial for treating patients with autoimmune diseases. While loss of PIP4Kγ alone conferred increased inflammation through activation of mTOR, loss of

the sole drosophila isoform reduced mTOR signaling[11,14]. We predict that loss of all three mammalian isoforms would phenocopy loss of the sole copy in Drosophila, raising the possibility that PIP4Kγ has dominant negative effects on PIP4Kα and PIP4Kβ. In the Drosophila system, kinase dead rescue was not sufficient to restore mTOR signaling, which supports the model where conversion of PI(5)P to PI(4,5)P_2 enhances mTOR signaling.

PIP4K is emerging as a critical regular of metabolism through modulating phosphoinositide homeostasis. In this thesis, we define a novel catalytic-independent function for the PIP4K family. As their catalytic roles have been the primary focus of previous studies, these data represent a major shift in our understanding of the function of PIP4K and should impact the way researchers target PIP4K for therapeutic intervention. This understanding of catalytically independent PIP4K activity improves our understanding of how structural features of PIP4Ks modulate PIP5K activity, providing new avenues for intervention.

4.4 ACKNOWLEDGEMENTS AND CONTRIBUTIONS

Diana Wang and Marcia Paddock designed and performed most of the experiments with assistance from Janet Sun. Cindy Hodakoski generated H1299 Rac knockout cell line. Jeremy Baskin and Timothy Bumpus performed and analyzed lipidomics, and provided reagents for measurement of PLD activity. RNA-seq in Appendix B was performed

by Diana Wang and the WCMC genomics core, and subsequently analyzed by Charlie Murphy. Proteomics in Appendix C was performed by Diana Wang, Benjamin Stein, and the WCMC metabolomics core, and subsequently analyzed by Benjamin Stein.

APPENDICES

APPENDIX A: HPLC chromatograph of 293 WT vs TKO

Superimposed HPLC trace files for analysis of phosphoinositides in 293 WT (blue) or 293 TKO (red). Calculations are normalized to total phosphatidylinositol-phosphate species, rather than PI.

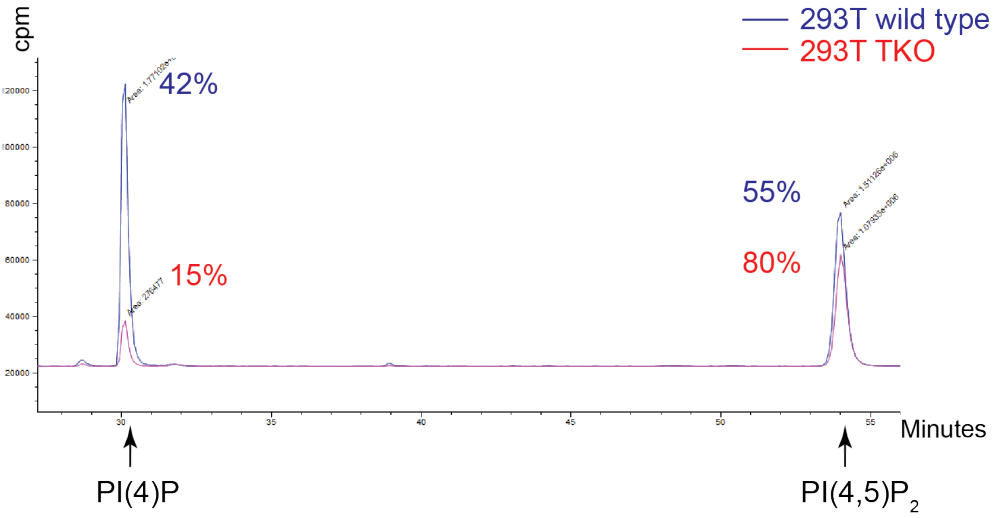

APPENDIX B: RNA-seq analysis of differential gene expression. Comparison of 293T non-targeting control and triple knockdown of PIP4K isoforms. Results filtered for Padj < 0.05 and sorted for ascending log2FoldChange where a negative number denotes lower expression in the triple PIP4K knockdown.

Gene	log2FoldChange	padj	Gene Description
PIP4K2C	-1.408387908	4.00E-18	PIP4Kgamma
PIP4K2B	-1.390011051	1.46E-39	PIP4Kbeta
PIP4K2A	-1.219750261	5.47E-13	PIP4Kalpha
NPIPB13	-0.866220964	1.58E-05	Nuclear Pore Complex Interacting Protein Family, Member B13
BMPER	-0.751503168	3.35E-07	BMP Binding Endothelial Regulator
UBE2QL1	-0.663762027	0.002	Ubiquitin Conjugating Enzyme E2 Q Family Like 1
TCAM1P	-0.652458318	0.002	Testicular Cell Adhesion Molecule 1, Pseudogene
FBN2	-0.627185283	6.28E-07	Fibrillin 2
EMILIN2	-0.607279637	0.005	Elastin Microfibril Interfacer 2
NEK7	-0.589149295	0.002	NIMA Related Kinase 7
OCA2	-0.57558744	0.001	OCA2 Melanosomal Transmembrane Protein
MAMLD1	-0.572334476	0.001	Mastermind Like Domain Containing 1
THBS4	-0.54472776	0.006	Thrombospondin 4
KCNJ14	-0.527273508	0.001	Potassium Voltage-Gated Channel Subfamily J Member 14
ARNT	-0.523098517	0.001	Aryl Hydrocarbon Receptor Nuclear Translocator
OTUD4	-0.519632361	0.000	OTU Deubiquitinase 4
FBLN5	-0.513768898	0.001	Fibulin 5
IL6R	-0.49776544	0.001	Interleukin 6 Receptor
SFRP1	-0.4910494	0.009	Secreted Frizzled Related Protein 1
ENO2	-0.472239972	0.006	Enolase 2
LGALS8	-0.469348772	0.001	Galectin 8
OVGP1	-0.457273503	0.007	Oviductal Glycoprotein 1
GALNT12	-0.445742874	0.005	Polypeptide N-Acetylgalactosaminyltransferase 12
VPS4B	-0.432029195	0.000	Vacuolar Protein Sorting 4 Homolog B
PMEPA1	-0.410844436	0.008	Prostate Transmembrane Protein, Androgen Induced 1
MRS2	-0.402331554	0.000	MRS2, Magnesium Transporter
NUP43	-0.399720942	0.000	Nucleoporin 43
MAP2K4	-0.393322205	0.002	Mitogen-Activated Protein Kinase Kinase 4
ZIC5	-0.386177899	2.74E-05	Zic Family Member 5
ADI1	-0.374327709	0.008	Acireductone Dioxygenase 1
ARL4C	-0.373774372	0.002	ADP Ribosylation Factor Like GTPase 4C
GDF7	-0.372994763	0.001	Growth Differentiation Factor 7
NFIB	-0.372891921	0.002	Nuclear Factor I B
CNN3	-0.357938254	0.002	Calponin 3
SALL1	-0.357499803	0.001	Spalt Like Transcription Factor 1
NUDT21	-0.351602361	0.005	Nudix Hydrolase 21
TMBIM6	-0.34960252	1.26E-05	Transmembrane BAX Inhibitor Motif Containing 6
MEX3A	-0.346807254	0.001	Mex-3 RNA Binding Family Member A
SMAD7	-0.343228616	0.001	SMAD Family Member 7

TMED8	-0.337075883	0.005	Transmembrane P24 Trafficking Protein Family Member 8
RAB39B	0.280077167	0.010	RAB39B, Member RAS Oncogene Family
MEF2C	0.328503256	0.008	Myocyte Enhancer Factor 2C
ITGA6	0.351325191	0.004	Integrin Subunit Alpha 6
NR6A1	0.375502341	0.000	Nuclear Receptor Subfamily 6 Group A Member 1
TCP11L1	0.377995307	0.001	T-Complex 11 Like 1
NDRG1	0.405034134	0.000	N-Myc Downstream Regulated 1
BMP6	0.407225445	0.002	Bone Morphogenetic Protein 6
PVT1	0.41048126	0.003	Pvt1 Oncogene (Non-Protein Coding)
TP53I3	0.451244812	0.008	Tumor Protein P53 Inducible Protein 3
DNAJC22	0.457834613	0.010	DnaJ Heat Shock Protein Family (Hsp40) Member C22
NOL4	0.472913112	0.001	Nucleolar Protein 4
FGF9	0.474592859	0.001	Fibroblast Growth Factor 9
TMTC1	0.477185964	2.92E-06	Transmembrane And Tetratricopeptide Repeat Containing 1
SPRY2	0.47972153	0.000	Sprouty RTK Signaling Antagonist 2
HHAT	0.491689022	0.000	Hedgehog Acyltransferase
ARHGAP24	0.500041112	0.006	Rho GTPase Activating Protein 24
ALDH1A2	0.508375732	0.007	Aldehyde Dehydrogenase 1 Family Member A2
CHODL	0.51099374	0.004	Chondrolectin
PCYT1B	0.51494933	0.001	Phosphate Cytidylyltransferase 1, Choline, Beta
HPGD	0.515067623	0.000	Hydroxyprostaglandin Dehydrogenase 15-(NAD)
SEMA3A	0.523234251	0.002	Semaphorin 3A
SPATA18	0.536027688	0.004	Spermatogenesis Associated 18
VAV1	0.548708665	0.002	Vav Guanine Nucleotide Exchange Factor 1
ZMAT3	0.562054413	8.28E-07	Zinc Finger Matrin-Type 3
SLC4A8	0.562557788	0.004	Solute Carrier Family 4 Member 8
NHLH2	0.565963347	0.005	Nescient Helix-Loop-Helix 2
PCDH17	0.573529181	0.000	Protocadherin 17
COL13A1	0.58737847	0.008	Collagen Type XIII Alpha 1 Chain
SCN9A	0.588524328	0.000	Sodium Voltage-Gated Channel Alpha Subunit 9
PDE1A	0.612273153	0.002	Phosphodiesterase 1A
TMEFF2	0.616368169	0.004	Transmembrane Protein With EGF Like And Two Follistatin Like Domains 2
INSC	0.62271113	0.010	Inscuteable Homolog (Drosophila)
CRIP3	0.623018001	0.001	Cysteine Rich Protein 3
CLVS2	0.625800127	0.003	Clavesin 2
EBF1	0.629376273	0.003	Early B-Cell Factor 1
CEL	0.634724964	0.002	Carboxyl Ester Lipase
PCDH10	0.649829648	0.005	Protocadherin 10
TLR6	0.650629503	0.001	Toll Like Receptor 6
SEMA3E	0.653250085	7.05E-06	Semaphorin 3E
DUSP6	0.655294842	0.005	Dual Specificity Phosphatase 6
MYB	0.657492001	0.000	MYB Proto-Oncogene, Transcription Factor
PARM1	0.65918507	2.67E-07	Prostate Androgen-Regulated Mucin-Like Protein 1
TLL1	0.659632678	0.000	Tolloid Like 1
NDUFA4L2	0.684071868	0.002	NDUFA4, Mitochondrial Complex Associated Like 2

CRB1	0.693103561	0.001	Crumbs 1, Cell Polarity Complex Component
LIF	0.699105844	0.001	LIF, Interleukin 6 Family Cytokine
PPFIA2	0.702380901	4.60E-05	PTPRF Interacting Protein Alpha 2
BMP3	0.705127151	0.000	Bone Morphogenetic Protein 3
EPHA5	0.709535619	0.000	EPH Receptor A5
ABCA1	0.713181738	3.78E-05	ATP Binding Cassette Subfamily A Member 1
INPP4B	0.729215995	0.000	Inositol Polyphosphate-4-Phosphatase Type II B
NPAS3	0.729314796	0.001	Neuronal PAS Domain Protein 3
RPRM	0.760273514	0.000	Reprimo, TP53 Dependent G2 Arrest Mediator Homolog
FAS	0.760753494	1.64E-11	Fas Cell Surface Death Receptor
HIST1H1C	0.763058697	4.30E-06	Histone Cluster 1 H1 Family Member C
CDKN1A	0.772161784	8.85E-05	Cyclin Dependent Kinase Inhibitor 1A
METTL7A	0.786977043	1.87E-10	Methyltransferase Like 7A
SLC2A3	0.788188422	7.80E-09	Solute Carrier Family 2 Member 3
COL14A1	0.796893808	6.17E-08	Collagen Type XIV Alpha 1 Chain
INPP5D	0.860547372	1.69E-05	Inositol Polyphosphate-5-Phosphatase D
GPR50	0.863486565	1.06E-05	G Protein-Coupled Receptor 50
SCN3A	0.886344072	1.06E-05	Sodium Voltage-Gated Channel Alpha Subunit 3
ETV4	1.089182393	1.54E-09	ETS Variant 4
EGR1	1.105066137	1.57E-09	Early Growth Response 1
FRMPD2	1.354384086	9.91E-17	FERM And PDZ Domain Containing 2

APPENDIX C: Quantitative analysis of proteome

SILAC-based analysis for differential proteome expression in 293T non-targeting control and triple knockdown of PIP4K isoforms. Cell lines were metabolically labeled with light or heavy isotopes and proteins were mixed before trypsin digestion. Three biological replicates were performed. Results filtered for BH FDR correction <0.05. The average ratio column indicates quantity in control (Ren3) over triple knockdown (ABC1), and table below was filtered for proteins enriched in ABC1 (average ratio <1). Thousands of proteins with average ratio >1 are not listed in this appendix. Table is sorted for ascending average ratio.

Uniprot	average ratio	t-test pvalue	ratio pvalue	Description
Q86SQ7	0.2	0.020	2.00E-04	Serologically defined colon cancer antigen 8 OS=Homo sapiens GN=SDCCAG8 PE=1 SV=1
Q9HCD6	0.26	0.009	5.00E-05	Protein TANC2 OS=Homo sapiens GN=TANC2 PE=1 SV=3
Q9HCU9	0.44	0.009	5.00E-05	Breast cancer metastasis-suppressor 1 OS=Homo sapiens GN=BRMS1 PE=1 SV=1
Q96ED9	0.44	0.026	4.50E-04	Protein Hook homolog 2 OS=Homo sapiens GN=HOOK2 PE=1 SV=3
Q9H2C0	0.44	0.027	0.03012	Gigaxonin OS=Homo sapiens GN=GAN PE=1 SV=1
P18084	0.48	0.015	0.00653	Integrin beta-5 OS=Homo sapiens GN=ITGB5 PE=1 SV=1
Q9BQS8	0.49	0.000	0.01151	FYVE and coiled-coil domain-containing protein 1 OS=Homo sapiens GN=FYCO1 PE=1 SV=3
Q9P032	0.5	0.002	0.01775	NADH dehydrogenase [ubiquinone] 1 alpha subcomplex assembly factor 4 OS=Homo sapiens GN=NDUFAF4 PE=1 SV=1
Q16822	0.51	0.000	0.03223	Phosphoenolpyruvate carboxykinase [GTP], mitochondrial OS=Homo sapiens GN=PCK2 PE=1 SV=3
Q4VCS5	0.52	0.000	0.04513	Angiomotin OS=Homo sapiens GN=AMOT PE=1 SV=1
O75874	0.56	0.000	0.01048	Isocitrate dehydrogenase [NADP] cytoplasmic OS=Homo sapiens GN=IDH1 PE=1 SV=2
P00491	0.56	0.000	0.02232	Purine nucleoside phosphorylase OS=Homo sapiens GN=PNP PE=1 SV=2
Q9UIU6	0.57	0.000	0.0118	Homeobox protein SIX4 OS=Homo sapiens GN=SIX4 PE=1 SV=2
P51608	0.6	0.010	5.00E-05	Methyl-CpG-binding protein 2 OS=Homo sapiens GN=MECP2 PE=1 SV=1
Q99576	0.6	0.002	0.00376	TSC22 domain family protein 3 OS=Homo sapiens GN=TSC22D3 PE=1 SV=2
Q9H8H3	0.6	0.000	0.01986	Methyltransferase-like protein 7A OS=Homo sapiens GN=METTL7A PE=1 SV=1
O95835	0.62	0.011	5.00E-05	Serine/threonine-protein kinase LATS1 OS=Homo sapiens GN=LATS1 PE=1 SV=1
Q05D32	0.62	0.002	0.00393	CTD small phosphatase-like protein 2 OS=Homo sapiens GN=CTDSPL2 PE=1 SV=2

Q9Y2H0	0.62	0.009	0.00963	Disks large-associated protein 4 OS=Homo sapiens GN=DLGAP4 PE=1 SV=3
P54886	0.62	0.000	0.02747	Delta-1-pyrroline-5-carboxylate synthase OS=Homo sapiens GN=ALDH18A1 PE=1 SV=2
Q9NZ45	0.62	0.000	0.03006	CDGSH iron-sulfur domain-containing protein 1 OS=Homo sapiens GN=CISD1 PE=1 SV=1
O43524	0.63	0.001	0.019	Forkhead box protein O3 OS=Homo sapiens GN=FOXO3 PE=1 SV=1
Q92520	0.63	0.003	0.03522	Protein FAM3C OS=Homo sapiens GN=FAM3C PE=1 SV=1
O43572	0.64	0.011	5.00E-05	A-kinase anchor protein 10, mitochondrial OS=Homo sapiens GN=AKAP10 PE=1 SV=2
Q9Y3B6	0.65	0.016	0.03618	ER membrane protein complex subunit 9 OS=Homo sapiens GN=EMC9 PE=1 SV=3
Q4KWH8	0.66	0.000	3.00E-05	1-phosphatidylinositol 4,5-bisphosphate phosphodiesterase eta-1 OS=Homo sapiens GN=PLCH1 PE=1 SV=1
P51809	0.66	0.000	0.01488	Vesicle-associated membrane protein 7 OS=Homo sapiens GN=VAMP7 PE=1 SV=3
O00400	0.66	0.011	0.01905	Acetyl-coenzyme A transporter 1 OS=Homo sapiens GN=SLC33A1 PE=1 SV=1
Q6PCB8	0.66	0.037	0.02457	Embigin OS=Homo sapiens GN=EMB PE=1 SV=1
Q13315	0.67	0.000	0.00956	Serine-protein kinase ATM OS=Homo sapiens GN=ATM PE=1 SV=4
Q7Z4S6	0.67	0.000	0.01564	Kinesin-like protein KIF21A OS=Homo sapiens GN=KIF21A PE=1 SV=2
Q9H040	0.67	0.045	0.02962	SprT-like domain-containing protein Spartan OS=Homo sapiens GN=SPRTN PE=1 SV=2
Q9Y5N6	0.68	0.000	6.90E-04	Origin recognition complex subunit 6 OS=Homo sapiens GN=ORC6 PE=1 SV=1
Q9H0F7	0.68	0.000	0.00185	ADP-ribosylation factor-like protein 6 OS=Homo sapiens GN=ARL6 PE=1 SV=1
P23193	0.68	0.000	0.01302	Transcription elongation factor A protein 1 OS=Homo sapiens GN=TCEA1 PE=1 SV=2
Q15041	0.68	0.001	0.01826	ADP-ribosylation factor-like protein 6-interacting protein 1 OS=Homo sapiens GN=ARL6IP1 PE=1 SV=2
Q8N2G8	0.69	0.000	0.00499	GH3 domain-containing protein OS=Homo sapiens GN=GHDC PE=1 SV=2
Q9H4B0	0.69	0.000	0.00775	Probable tRNA N6-adenosine threonylcarbamoyltransferase, mitochondrial OS=Homo sapiens GN=OSGEPL1 PE=2 SV=2
Q9P0J1	0.69	0.000	0.02883	[Pyruvate dehydrogenase [acetyl-transferring]]-phosphatase 1, mitochondrial OS=Homo sapiens GN=PDP1 PE=1 SV=3
P86790	0.7	0.002	0.00229	Vacuolar fusion protein CCZ1 homolog B OS=Homo sapiens GN=CCZ1B PE=1 SV=1
P86791	0.7	0.002	0.00229	Vacuolar fusion protein CCZ1 homolog OS=Homo sapiens GN=CCZ1 PE=1 SV=1
Q86YH6	0.7	0.005	0.0043	Decaprenyl-diphosphate synthase subunit 2 OS=Homo sapiens GN=PDSS2 PE=1 SV=2
Q9BU61	0.7	0.000	0.03094	NADH dehydrogenase [ubiquinone] 1 alpha subcomplex assembly factor 3 OS=Homo sapiens GN=NDUFAF3 PE=1 SV=1
Q86VN1	0.71	0.003	0.02868	Vacuolar protein-sorting-associated protein 36 OS=Homo sapiens GN=VPS36 PE=1 SV=1

O94925	0.71	0.000	0.03725	Glutaminase kidney isoform, mitochondrial OS=Homo sapiens GN=GLS PE=1 SV=1
Q86V85	0.72	0.001	0.00542	Integral membrane protein GPR180 OS=Homo sapiens GN=GPR180 PE=2 SV=1
O96011	0.72	0.037	0.00703	Peroxisomal membrane protein 11B OS=Homo sapiens GN=PEX11B PE=1 SV=1
O15321	0.72	0.049	0.00853	Transmembrane 9 superfamily member 1 OS=Homo sapiens GN=TM9SF1 PE=2 SV=2
Q99856	0.72	0.000	0.03473	AT-rich interactive domain-containing protein 3A OS=Homo sapiens GN=ARID3A PE=1 SV=2
O95563	0.72	0.003	0.0452	Mitochondrial pyruvate carrier 2 OS=Homo sapiens GN=MPC2 PE=1 SV=1
Q86WX3	0.73	0.026	0.00443	Active regulator of SIRT1 OS=Homo sapiens GN=RPS19BP1 PE=1 SV=1
Q3SY69	0.73	0.000	0.02743	Mitochondrial 10-formyltetrahydrofolate dehydrogenase OS=Homo sapiens GN=ALDH1L2 PE=1 SV=2
P56177	0.74	0.006	9.00E-04	Homeobox protein DLX-1 OS=Homo sapiens GN=DLX1 PE=2 SV=3
P56178	0.74	0.006	9.00E-04	Homeobox protein DLX-5 OS=Homo sapiens GN=DLX5 PE=1 SV=2
P56179	0.74	0.006	9.00E-04	Homeobox protein DLX-6 OS=Homo sapiens GN=DLX6 PE=2 SV=2
Q07687	0.74	0.006	9.00E-04	Homeobox protein DLX-2 OS=Homo sapiens GN=DLX2 PE=1 SV=2
Q9UDW1	0.74	0.000	0.0071	Cytochrome b-c1 complex subunit 9 OS=Homo sapiens GN=UQCR10 PE=1 SV=3
P56277	0.74	0.019	0.00949	Cx9C motif-containing protein 4 OS=Homo sapiens GN=CMC4 PE=1 SV=1
Q8IYS2	0.74	0.021	0.01837	Uncharacterized protein KIAA2013 OS=Homo sapiens GN=KIAA2013 PE=1 SV=1
O00584	0.74	0.048	0.02482	Ribonuclease T2 OS=Homo sapiens GN=RNASET2 PE=1 SV=2
O95299	0.74	0.000	0.02818	NADH dehydrogenase [ubiquinone] 1 alpha subcomplex subunit 10, mitochondrial OS=Homo sapiens GN=NDUFA10 PE=1 SV=1
Q6P4Q7	0.75	0.010	0.04458	Metal transporter CNNM4 OS=Homo sapiens GN=CNNM4 PE=1 SV=3
O60344	0.76	0.012	0.00163	Endothelin-converting enzyme 2 OS=Homo sapiens GN=ECE2 PE=1 SV=4
Q6ZSJ8	0.76	0.001	0.00638	Uncharacterized protein C1orf122 OS=Homo sapiens GN=C1orf122 PE=4 SV=2
Q9Y2H1	0.76	0.001	0.00809	Serine/threonine-protein kinase 38-like OS=Homo sapiens GN=STK38L PE=1 SV=3
P52657	0.76	0.046	0.01689	Transcription initiation factor IIA subunit 2 OS=Homo sapiens GN=GTF2A2 PE=1 SV=1
Q9NVS9	0.76	0.000	0.04227	Pyridoxine-5'-phosphate oxidase OS=Homo sapiens GN=PNPO PE=1 SV=1
Q99943	0.77	0.001	0.00805	1-acyl-sn-glycerol-3-phosphate acyltransferase alpha OS=Homo sapiens GN=AGPAT1 PE=1 SV=2
O14949	0.77	0.000	0.01103	Cytochrome b-c1 complex subunit 8 OS=Homo sapiens GN=UQCRQ PE=1 SV=4
Q32NB8	0.77	0.035	0.02388	CDP-diacylglycerol--glycerol-3-phosphate 3-phosphatidyltransferase, mitochondrial OS=Homo sapiens GN=PGS1 PE=2 SV=1

P58004	0.77	0.000	0.03087	Sestrin-2 OS=Homo sapiens GN=SESN2 PE=1 SV=1
P51151	0.77	0.000	0.03358	Ras-related protein Rab-9A OS=Homo sapiens GN=RAB9A PE=1 SV=1
Q6ZRI6	0.78	0.001	1.30E-04	Uncharacterized protein C15orf39 OS=Homo sapiens GN=C15orf39 PE=1 SV=3
Q9H2H9	0.78	0.009	0.01542	Sodium-coupled neutral amino acid transporter 1 OS=Homo sapiens GN=SLC38A1 PE=1 SV=1
Q9H7B2	0.78	0.000	0.01812	Ribosome production factor 2 homolog OS=Homo sapiens GN=RPF2 PE=1 SV=2
P49748	0.78	0.000	0.04518	Very long-chain specific acyl-CoA dehydrogenase, mitochondrial OS=Homo sapiens GN=ACADVL PE=1 SV=1
O75414	0.79	0.008	8.30E-04	Nucleoside diphosphate kinase 6 OS=Homo sapiens GN=NME6 PE=1 SV=3
Q658Y4	0.79	0.002	0.0091	Protein FAM91A1 OS=Homo sapiens GN=FAM91A1 PE=1 SV=3
Q8NC60	0.79	0.034	0.0264	Nitric oxide-associated protein 1 OS=Homo sapiens GN=NOA1 PE=1 SV=2
Q15629	0.8	0.023	0.02287	Translocating chain-associated membrane protein 1 OS=Homo sapiens GN=TRAM1 PE=1 SV=3
Q9UFW8	0.8	0.000	0.02345	CGG triplet repeat-binding protein 1 OS=Homo sapiens GN=CGGBP1 PE=1 SV=2
P21796	0.8	0.000	0.02973	Voltage-dependent anion-selective channel protein 1 OS=Homo sapiens GN=VDAC1 PE=1 SV=2
Q9H2J7	0.8	0.002	0.03213	Sodium-dependent neutral amino acid transporter B(0)AT2 OS=Homo sapiens GN=SLC6A15 PE=1 SV=1
Q8WVE0	0.81	0.005	0.00222	Protein-lysine N-methyltransferase N6AMT2 OS=Homo sapiens GN=N6AMT2 PE=1 SV=1
O14656	0.81	0.022	0.01646	Torsin-1A OS=Homo sapiens GN=TOR1A PE=1 SV=1
Q9NX62	0.81	0.023	0.02139	Inositol monophosphatase 3 OS=Homo sapiens GN=IMPAD1 PE=1 SV=1
Q9BRU9	0.81	0.005	0.02809	rRNA-processing protein UTP23 homolog OS=Homo sapiens GN=UTP23 PE=1 SV=2
Q8TAM2	0.82	0.039	2.00E-04	Tetratricopeptide repeat protein 8 OS=Homo sapiens GN=TTC8 PE=1 SV=2
O14734	0.82	0.000	0.01138	Acyl-coenzyme A thioesterase 8 OS=Homo sapiens GN=ACOT8 PE=1 SV=1
Q8NI35	0.82	0.004	0.02128	InaD-like protein OS=Homo sapiens GN=INADL PE=1 SV=3
O75143	0.83	0.001	5.30E-04	Autophagy-related protein 13 OS=Homo sapiens GN=ATG13 PE=1 SV=1
O00418	0.83	0.026	0.00213	Eukaryotic elongation factor 2 kinase OS=Homo sapiens GN=EEF2K PE=1 SV=2
Q9UMR5	0.83	0.000	0.00238	Lysosomal thioesterase PPT2 OS=Homo sapiens GN=PPT2 PE=1 SV=4
Q6ZRV2	0.83	0.043	0.0088	Protein FAM83H OS=Homo sapiens GN=FAM83H PE=1 SV=3
Q2TBE0	0.83	0.043	0.00889	CWF19-like protein 2 OS=Homo sapiens GN=CWF19L2 PE=1 SV=4
Q96LA8	0.83	0.003	0.00985	Protein arginine N-methyltransferase 6 OS=Homo sapiens GN=PRMT6 PE=1 SV=1
B7ZAQ6	0.83	0.000	0.01057	Golgi pH regulator A OS=Homo sapiens GN=GPR89A PE=1 SV=2

P0CG08	0.83	0.000	0.01057	Golgi pH regulator B OS=Homo sapiens GN=GPR89B PE=1 SV=1
O75027	0.83	0.009	0.03199	ATP-binding cassette sub-family B member 7, mitochondrial OS=Homo sapiens GN=ABCB7 PE=1 SV=2
Q9Y512	0.83	0.000	0.03778	Sorting and assembly machinery component 50 homolog OS=Homo sapiens GN=SAMM50 PE=1 SV=3
Q86YS6	0.84	0.043	2.00E-04	Ras-related protein Rab-43 OS=Homo sapiens GN=RAB43 PE=1 SV=1
Q53R41	0.84	0.000	0.00416	FAST kinase domain-containing protein 1 OS=Homo sapiens GN=FASTKD1 PE=1 SV=1
Q14376	0.84	0.001	0.0057	UDP-glucose 4-epimerase OS=Homo sapiens GN=GALE PE=1 SV=2
Q9UQN3	0.84	0.005	0.02043	Charged multivesicular body protein 2b OS=Homo sapiens GN=CHMP2B PE=1 SV=1
Q9NYY8	0.84	0.000	0.02838	FAST kinase domain-containing protein 2 OS=Homo sapiens GN=FASTKD2 PE=1 SV=1
P30622	0.84	0.000	0.03949	CAP-Gly domain-containing linker protein 1 OS=Homo sapiens GN=CLIP1 PE=1 SV=2
O95816	0.84	0.000	0.04623	BAG family molecular chaperone regulator 2 OS=Homo sapiens GN=BAG2 PE=1 SV=1
Q9Y448	0.85	0.000	8.70E-04	Small kinetochore-associated protein OS=Homo sapiens GN=KNSTRN PE=1 SV=2
Q9NTG7	0.85	0.003	0.004	NAD-dependent protein deacetylase sirtuin-3, mitochondrial OS=Homo sapiens GN=SIRT3 PE=1 SV=2
Q15072	0.85	0.004	0.00483	Zinc finger protein OZF OS=Homo sapiens GN=ZNF146 PE=1 SV=2
Q8N983	0.85	0.021	0.01333	39S ribosomal protein L43, mitochondrial OS=Homo sapiens GN=MRPL43 PE=1 SV=1
Q13614	0.85	0.032	0.01946	Myotubularin-related protein 2 OS=Homo sapiens GN=MTMR2 PE=1 SV=4
Q8NDV7	0.85	0.013	0.0217	Trinucleotide repeat-containing gene 6A protein OS=Homo sapiens GN=TNRC6A PE=1 SV=2
Q9H7S9	0.85	0.000	0.02598	Zinc finger protein 703 OS=Homo sapiens GN=ZNF703 PE=1 SV=1
O14686	0.85	0.001	0.02684	Histone-lysine N-methyltransferase 2D OS=Homo sapiens GN=KMT2D PE=1 SV=2
Q9HAS0	0.85	0.005	0.03245	Protein Njmu-R1 OS=Homo sapiens GN=C17orf75 PE=1 SV=2
P52789	0.85	0.000	0.03533	Hexokinase-2 OS=Homo sapiens GN=HK2 PE=1 SV=2
Q8WY91	0.86	0.025	5.00E-05	THAP domain-containing protein 4 OS=Homo sapiens GN=THAP4 PE=1 SV=2
P53611	0.86	0.000	0.00307	Geranylgeranyl transferase type-2 subunit beta OS=Homo sapiens GN=RABGGTB PE=1 SV=2
Q15172	0.86	0.005	0.00474	Serine/threonine-protein phosphatase 2A 56 kDa regulatory subunit alpha isoform OS=Homo sapiens GN=PPP2R5A PE=1 SV=1
O94864	0.86	0.005	0.00726	STAGA complex 65 subunit gamma OS=Homo sapiens GN=SUPT7L PE=1 SV=1
Q9P2M7	0.86	0.003	0.02249	Cingulin OS=Homo sapiens GN=CGN PE=1 SV=2

Q96TA2	0.86	0.002	0.03778	ATP-dependent zinc metalloprotease YME1L1 OS=Homo sapiens GN=YME1L1 PE=1 SV=2
P33908	0.87	0.001	3.00E-05	Mannosyl-oligosaccharide 1,2-alpha-mannosidase IA OS=Homo sapiens GN=MAN1A1 PE=1 SV=3
Q8WVC6	0.87	0.006	0.0057	Dephospho-CoA kinase domain-containing protein OS=Homo sapiens GN=DCAKD PE=1 SV=1
P20073	0.87	0.000	0.00938	Annexin A7 OS=Homo sapiens GN=ANXA7 PE=1 SV=3
O43615	0.87	0.000	0.04582	Mitochondrial import inner membrane translocase subunit TIM44 OS=Homo sapiens GN=TIMM44 PE=1 SV=2
P62068	0.88	0.006	9.00E-04	Ubiquitin carboxyl-terminal hydrolase 46 OS=Homo sapiens GN=USP46 PE=1 SV=1
Q99595	0.88	0.020	0.00243	Mitochondrial import inner membrane translocase subunit Tim17-A OS=Homo sapiens GN=TIMM17A PE=1 SV=1
Q8N5P1	0.88	0.021	0.00247	Zinc finger CCCH domain-containing protein 8 OS=Homo sapiens GN=ZC3H8 PE=1 SV=2
Q9NUJ3	0.88	0.030	0.0236	T-complex protein 11-like protein 1 OS=Homo sapiens GN=TCP11L1 PE=1 SV=1
Q70UQ0	0.88	0.011	0.02768	Inhibitor of nuclear factor kappa-B kinase-interacting protein OS=Homo sapiens GN=IKBIP PE=1 SV=1
Q9Y277	0.88	0.000	0.03012	Voltage-dependent anion-selective channel protein 3 OS=Homo sapiens GN=VDAC3 PE=1 SV=1
O15091	0.88	0.017	0.03356	Mitochondrial ribonuclease P protein 3 OS=Homo sapiens GN=KIAA0391 PE=1 SV=2
O60830	0.88	0.030	0.03712	Mitochondrial import inner membrane translocase subunit Tim17-B OS=Homo sapiens GN=TIMM17B PE=1 SV=1
Q4L235	0.89	0.009	3.00E-04	Acyl-CoA synthetase family member 4 OS=Homo sapiens GN=AASDH PE=1 SV=3
Q9UG56	0.89	0.014	4.30E-04	Phosphatidylserine decarboxylase proenzyme, mitochondrial OS=Homo sapiens GN=PISD PE=2 SV=4
Q8NEZ2	0.89	0.039	0.01279	Vacuolar protein sorting-associated protein 37A OS=Homo sapiens GN=VPS37A PE=1 SV=1
O75600	0.89	0.005	0.01885	2-amino-3-ketobutyrate coenzyme A ligase, mitochondrial OS=Homo sapiens GN=GCAT PE=1 SV=1
Q96BW5	0.89	0.013	0.0191	Phosphotriesterase-related protein OS=Homo sapiens GN=PTER PE=1 SV=1
Q00765	0.89	0.003	0.02156	Receptor expression-enhancing protein 5 OS=Homo sapiens GN=REEP5 PE=1 SV=3
P24390	0.89	0.029	0.02361	ER lumen protein-retaining receptor 1 OS=Homo sapiens GN=KDELR1 PE=1 SV=1
Q16527	0.89	0.003	0.02677	Cysteine and glycine-rich protein 2 OS=Homo sapiens GN=CSRP2 PE=1 SV=3
Q8N0Z6	0.89	0.004	0.02756	Tetratricopeptide repeat protein 5 OS=Homo sapiens GN=TTC5 PE=1 SV=2
Q92558	0.89	0.047	0.02907	Wiskott-Aldrich syndrome protein family member 1 OS=Homo sapiens GN=WASF1 PE=1 SV=1
P61604	0.89	0.000	0.03477	10 kDa heat shock protein, mitochondrial OS=Homo sapiens GN=HSPE1 PE=1 SV=2

P54578	0.89	0.000	0.03858	Ubiquitin carboxyl-terminal hydrolase 14 OS=Homo sapiens GN=USP14 PE=1 SV=3
Q8WUK0	0.9	0.008	2.30E-04	Phosphatidylglycerophosphatase and protein-tyrosine phosphatase 1 OS=Homo sapiens GN=PTPMT1 PE=1 SV=1
Q8IYL3	0.9	0.000	0.00178	UPF0688 protein C1orf174 OS=Homo sapiens GN=C1orf174 PE=1 SV=2
Q9UH62	0.9	0.001	0.01383	Armadillo repeat-containing X-linked protein 3 OS=Homo sapiens GN=ARMCX3 PE=1 SV=1
Q7Z6B7	0.9	0.030	0.01433	SLIT-ROBO Rho GTPase-activating protein 1 OS=Homo sapiens GN=SRGAP1 PE=1 SV=1
Q96FK6	0.9	0.017	0.02139	WD repeat-containing protein 89 OS=Homo sapiens GN=WDR89 PE=2 SV=1
P45880	0.9	0.000	0.03217	Voltage-dependent anion-selective channel protein 2 OS=Homo sapiens GN=VDAC2 PE=1 SV=2
Q13011	0.9	0.000	0.03703	Delta(3,5)-Delta(2,4)-dienoyl-CoA isomerase, mitochondrial OS=Homo sapiens GN=ECH1 PE=1 SV=2
Q9NVH0	0.9	0.047	0.04279	Exonuclease 3'-5' domain-containing protein 2 OS=Homo sapiens GN=EXD2 PE=1 SV=2
Q6NVY1	0.91	0.000	0.03188	3-hydroxyisobutyryl-CoA hydrolase, mitochondrial OS=Homo sapiens GN=HIBCH PE=1 SV=2
P06280	0.91	0.000	0.03324	Alpha-galactosidase A OS=Homo sapiens GN=GLA PE=1 SV=1
O95834	0.91	0.006	0.03788	Echinoderm microtubule-associated protein-like 2 OS=Homo sapiens GN=EML2 PE=1 SV=1
Q96CU9	0.92	0.044	5.00E-05	FAD-dependent oxidoreductase domain-containing protein 1 OS=Homo sapiens GN=FOXRED1 PE=1 SV=2
Q9Y2S7	0.92	0.014	0.02913	Polymerase delta-interacting protein 2 OS=Homo sapiens GN=POLDIP2 PE=1 SV=1
Q9Y3P9	0.92	0.013	0.03565	Rab GTPase-activating protein 1 OS=Homo sapiens GN=RABGAP1 PE=1 SV=3
O75439	0.92	0.000	0.04901	Mitochondrial-processing peptidase subunit beta OS=Homo sapiens GN=PMPCB PE=1 SV=2
P49069	0.93	0.009	0.00147	Calcium signal-modulating cyclophilin ligand OS=Homo sapiens GN=CAMLG PE=1 SV=1
Q9NWU5	0.93	0.045	0.02431	39S ribosomal protein L22, mitochondrial OS=Homo sapiens GN=MRPL22 PE=1 SV=1
Q9BQD3	0.94	0.028	3.00E-04	KxDL motif-containing protein 1 OS=Homo sapiens GN=KXD1 PE=1 SV=2
O43427	0.94	0.015	0.0019	Acidic fibroblast growth factor intracellular-binding protein OS=Homo sapiens GN=FIBP PE=1 SV=3
P36542	0.94	0.000	0.01747	ATP synthase subunit gamma, mitochondrial OS=Homo sapiens GN=ATP5C1 PE=1 SV=1
P12235	0.94	0.004	0.04551	ADP/ATP translocase 1 OS=Homo sapiens GN=SLC25A4 PE=1 SV=4
Q9NYM9	0.95	0.000	1.20E-04	BET1-like protein OS=Homo sapiens GN=BET1L PE=1 SV=1
O15260	0.95	0.045	0.00908	Surfeit locus protein 4 OS=Homo sapiens GN=SURF4 PE=1 SV=3
Q9UKS6	0.95	0.011	0.01283	Protein kinase C and casein kinase substrate in neurons protein 3 OS=Homo sapiens GN=PACSIN3 PE=1 SV=2

Q15075	0.95	0.001	0.02929	Early endosome antigen 1 OS=Homo sapiens GN=EEA1 PE=1 SV=2
Q02978	0.95	0.015	0.03529	Mitochondrial 2-oxoglutarate/malate carrier protein OS=Homo sapiens GN=SLC25A11 PE=1 SV=3
P27144	0.96	0.046	0.02926	Adenylate kinase 4, mitochondrial OS=Homo sapiens GN=AK4 PE=1 SV=1
P38646	0.98	0.001	0.03869	Stress-70 protein, mitochondrial OS=Homo sapiens GN=HSPA9 PE=1 SV=2

BIBLIOGRPAPHY

1 Fruman, D. A., Meyer, R. E. & Cantley, L. C. Phosphoinositide kinases. *Annu Rev Biochem* (1998).

2 Balla, T. Phosphoinositides: tiny lipids with giant impact on cell regulation. *Physiol Rev* **93**, 1019-1137, doi:10.1152/physrev.00028.2012 (2013).

3 Homma, K. *et al.* Phosphatidylinositol-4-phosphate 5-kinase localized on the plasma membrane is essential for yeast cell morphogenesis. *Journal of Biological Chemistry* **273**, 15779-15786 (1998).

4 Doughman, R. L., Firestone, A. J. & Anderson, R. A. Phosphatidylinositol phosphate kinases put PI4,5P(2) in its place. *J Membr Biol* **194**, 77-89, doi:10.1007/s00232-003-2027-7 (2003).

5 van den Bout, I. & Divecha, N. PIP5K-driven PtdIns(4,5)P2 synthesis: regulation and cellular functions. *J Cell Sci* **122**, 3837-3850, doi:10.1242/jcs.056127 (2009).

6 Funakoshi, Y., Hasegawa, H. & Kanaho, Y. Regulation of PIP5K activity by Arf6 and its physiological significance. *J Cell Physiol* **226**, 888-895, doi:10.1002/jcp.22482 (2011).

7 Schramp, M., Hedman, A., Li, W., Tan, X. & Anderson, R. PIP kinases from the cell membrane to the nucleus. *Subcell Biochem* **58**, 25-59, doi:10.1007/978-94-007-3012-0_2 (2012).

8 Clarke, Jonathan H. & Irvine, Robin F. Evolutionarily conserved structural changes in phosphatidylinositol 5-phosphate 4-kinase (PI5P4K) isoforms are responsible for differences in enzyme activity and localization. *Biochemical Journal* **454**, 49-57, doi:10.1042/bj20130488 (2013).

9 Rameh, L. E., Tolias, K. F., Duckworth, B. C. & Cantley, L. C. A new pathway for synthesis of phosphatidylinositol-4,5-bisphosphate. *Nature* **390**, 192-196 (1997).

10 Lamia, K. A. *et al.* Increased insulin sensitivity and reduced adiposity in phosphatidylinositol 5-phosphate 4-kinase beta-/- mice. *Mol Cell Biol* **24**, 5080-5087, doi:10.1128/MCB.24.11.5080-5087.2004 (2004).

11 Shim, H. *et al.* Deletion of the gene Pip4k2c, a novel phosphatidylinositol kinase, results in hyperactivation of the immune system. *Proc Natl Acad Sci U S A* **113**, 7596-7601, doi:10.1073/pnas.1600934113 (2016).

12 Emerling, B. M. *et al.* Depletion of a putatively druggable class of phosphatidylinositol kinases inhibits growth of p53-null tumors. *Cell* **155**, 844-857, doi:10.1016/j.cell.2013.09.057 (2013).

13 Lundquist, M. R. *et al.* Phosphatidylinositol-5-Phosphate 4-Kinases Regulate Cellular Lipid Metabolism By Facilitating Autophagy. *Molecular Cell* **70**, 531-544.e539, doi:10.1016/j.molcel.2018.03.037 (2018).

14 Gupta, A. *et al.* Phosphatidylinositol 5-phosphate 4-kinase (PIP4K) regulates TOR signaling and cell growth during Drosophila development. *PNAS* (2013).

15 Ciruela, A., Hinchliffe, K. A., Divecha, N. & Irvine, R. F. Nuclear targeting of the B isoform of Type II phosphatidylinositol phosphate kinase (phosphatidylinositol 5 phosphate 4-kinase) by its a-helix 7. *Biochem J.* **345**, 587-591 (2000).

16 Wang, M. *et al.* Genomic tagging reveals a random association of endogenous PtdIns5P 4-kinases IIalpha and IIbeta and a partial nuclear localization of the IIalpha isoform. *Biochem J* **430**, 215-221, doi:10.1042/BJ20100340 (2010).

17 Boronenkov, I. V., Loijens, J. C., Umeda, M. & Anderson, R. A. Phosphoinositide Signaling Pathways in Nuclei Are Associated with Nuclear Speckles Containing Pre-mRNA Processing Factors. *Molecular Biology of the Cell* **9**, 3547-3560 (1998).

18 Bulley, S. J., Clarke, J. H., Droubi, A., Giudici, M. L. & Irvine, R. F. Exploring phosphatidylinositol 5-phosphate 4-kinase function. *Adv Biol Regul* **57**, 193-202, doi:10.1016/j.jbior.2014.09.007 (2015).

19 Richardson, J. P., Wang, M., Clarke, J. H., Patel, K. J. & Irvine, R. F. Genomic tagging of endogenous type IIbeta phosphatidylinositol 5-phosphate 4-kinase in DT40 cells reveals a nuclear localisation. *Cell Signal* **19**, 1309-1314, doi:10.1016/j.cellsig.2007.01.010 (2007).

20 Clarke, J. H., Emson, P. C. & Irvine, R. F. Localization of phosphatidylinositol phosphate kinase IIgamma in kidney to a membrane trafficking compartment within specialized cells of the nephron. *Am J Physiol Renal Physiol* **295**, F1422-1430, doi:10.1152/ajprenal.90310.2008 (2008).

21 Bultsma, Y., Keune, W. J. & Divecha, N. PIP4Kbeta interacts with and modulates nuclear localization of the high-activity PtdIns5P-4-kinase isoform PIP4Kalpha. *Biochem J* **430**, 223-235, doi:10.1042/BJ20100341 (2010).

22 Rao, V. D., Misra, S., Boronenkov, I. V., Anderson, R. A. & Hurley, J. H. Structure of Type IIB Phosphatidylinositol phosphate kinase: A protein kinase fold flattened for interfacial phosphorylation. *Cell* **94**, 829-839 (1998).

23 Kunz, J. *et al.* The Activation Loop of Phosphatidylinositol Phosphate Kinases Determines Signaling Specificity. *Mol Cell* **5**, 1-11 (2000).

24 Kunz, J., Fuelling, A., Kolbe, L. & Anderson, R. A. Stereo-specific Substrate Recognition by Phosphatidylinositol Phosphate Kinases Is Swapped by Changing a Single Amino Acid Residue. *Journal of Biological Chemistry* **277**, 5611-5619, doi:10.1074/jbc.M110775200 (2001).

25 Castellino, A. M., Parker, G. J., Boronenkov, I. V., Anderson, R. A. & Chao, M. V. A novel interaction between the Juxtamembrane region of the p55 tumor necrosis factor receptor and phosphatidylinositol-4-phosphate-5-kinase. *J Biol Chem* **272**, 5861-5870 (1997).

26 Mackey, A. M., Sarkes, D. A., Bettencourt, I., Asara, J. M. & Rameh, L. E. PIP5Kg is a substrate for mTORC1 that maintains basal mTORC1 signaling during starvation. *Science Signaling* **7**, 1-11 (2014).

27 Zheng, L. & Conner, S. D. PI5P4Kgamma functions in DTX1-mediated Notch signaling. *Proc Natl Acad Sci U S A*, doi:10.1073/pnas.1712142115 (2018).

28 Itoh, T., Ijuin, T. & Takenawa, T. A Novel Phosphatidylinositol-5-phosphate 4-kinase (Phosphatidylinositol-phosphate Kinase IIγ) is phosphorylated in the Endoplasmic Reticulum in Response to Mitogenic Signals. *J Biol Chem* **273**, 20292-20299 (1998).

29 Yang, S. *et al.* MANF regulates hypothalamic control of food intake and body weight. *Nat Commun* **8**, 579, doi:10.1038/s41467-017-00750-x (2017).

30 Clarke, J. H. & Irvine, R. F. The activity, evolution and association of phosphatidylinositol 5-phosphate 4-kinases. *Adv Biol Regul* **52**, 40-45, doi:10.1016/j.advenzreg.2011.09.002 (2012).

31 He, K. *et al.* Dynamics of phosphoinositide conversion in clathrin-mediated endocytic traffic. *Nature* **552**, 410-414, doi:10.1038/nature25146 (2017).

32 Choy, C. H., Han, B. K. & Botelho, R. J. Phosphoinositide Diversity, Distribution, and Effector Function: Stepping Out of the Box. *Bioessays* **39**, doi:10.1002/bies.201700121 (2017).

33 Itoh, T. *et al.* Role of the ENTH domain in phosphatidylinositol-4,5-bisphosphate binding and endocytosis. *Science* **291**, 1047-1051 (2001).

34 Chang-Ileto, B. *et al.* Synaptojanin 1-mediated PI(4,5)P2 hydrolysis is modulated by membrane curvature and facilitates membrane fission. *Dev Cell* **20**, 206-218, doi:10.1016/j.devcel.2010.12.008 (2011).

35 Kamalesh, K. *et al.* Phosphatidylinositol 5-phosphate 4-kinase regulates early endosomal dynamics during clathrin-mediated endocytosis. *J Cell Sci* **130**, 2119-2133, doi:10.1242/jcs.202259 (2017).

36 Farhan, H. *et al.* MAPK signaling to the early secretory pathway revealed by kinase/phosphatase functional screening. *J Cell Biol* **189**, 997-1011, doi:10.1083/jcb.200912082 (2010).

37 Wang, H. *et al.* GABARAPs regulate PI4P-dependent autophagosome:lysosome fusion. *Proceedings of the National Academy of Sciences*, 201507263, doi:10.1073/pnas.1507263112 (2015).

38 De Leo, M. G. *et al.* Autophagosome-lysosome fusion triggers a lysosomal response mediated by TLR9 and controlled by OCRL. *Nat Cell Biol* **18**, 839-850, doi:10.1038/ncb3386 (2016).

39 Bai, J., Tucker, W. C. & Chapman, E. R. PIP2 increases the speed of response of synaptotagmin and steers its membrane-penetration activity toward the plasma membrane. *Nat Struct Mol Biol* **11**, 36-44, doi:10.1038/nsmb709 (2004).

40 Vicinanza, M. *et al.* PI(5)P regulates autophagosome biogenesis. *Mol Cell* **57**, 219-234, doi:10.1016/j.molcel.2014.12.007 (2015).

41 Raucher, D. *et al.* Phosphatidylinositol 4,5-bisphosphate functions as a second messenger that regulates cytoskeleton-plasma membrane adhesion. *Cell* **100**, 221-228 (2000).

42 Hammond, G. R. & Balla, T. Polyphosphoinositide binding domains: Key to inositol lipid biology. *Biochim Biophys Acta* **1851**, 746-758, doi:10.1016/j.bbalip.2015.02.013 (2015).

43 Hammond, G. R. *et al.* PI4P and PI(4,5)P2 are essential but independent lipid determinants of membrane identity. *Science* **337**, 727-730, doi:10.1126/science.1222483 (2012).

44 Ueno, T., Falkenburger, B. J., Pohlmeyer, C. & Inoue, T. Triggering Actin Comets versus membrane ruffles: Distinctive Effects of phosphoinositides on Actin Reorganization. *Science Signaling* (2011).

45 Sengelaub, C. A., Navrazhina, K., Ross, J. B., Halberg, N. & Tavazoie, S. F. PTPRN2 and PLCbeta1 promote metastatic breast cancer cell migration through PI(4,5)P2-dependent actin remodeling. *EMBO J* **35**, 62-76, doi:10.15252/embj.201591973 (2016).

46 Halberg, N. *et al.* PITPNC1 Recruits RAB1B to the Golgi Network to Drive Malignant Secretion. *Cancer Cell* **29**, 339-353, doi:10.1016/j.ccell.2016.02.013 (2016).

47 Clark, E. A., Golub, T. R., Lander, E. S. & Hynes, R. O. Genomic analysis of metastasis reveals an essential role for RhoC. *Nature* **406**, 532-535 (2000).

48 Ling, K., Schill, N. J., Wagoner, M. P., Sun, Y. & Anderson, R. A. Movin' on up: the role of PtdIns(4,5)P(2) in cell migration. *Trends Cell Biol* **16**, 276-284, doi:10.1016/j.tcb.2006.03.007 (2006).

49 Akil, A. *et al.* Septin 9 induces lipid droplets growth by a phosphatidylinositol-5-phosphate and microtubule-dependent mechanism hijacked by HCV. *Nat Commun* **7**, 12203, doi:10.1038/ncomms12203 (2016).

50 Haugsten, E. M., Oppelt, A. & Wesche, J. Phosphatidylinositol 5-phosphate is a second messenger important for cell migration. *Commun Integr Biol* **6**, e25446, doi:10.4161/cib.25446 (2013).

51 Oppelt, A. *et al.* Production of phosphatidylinositol 5-phosphate via PIKfyve and MTMR3 regulates cell migration. *EMBO Rep* **14**, 57-64, doi:10.1038/embor.2012.183 (2013).

52 Oppelt, A. *et al.* PIKfyve, MTMR3 and their product PtdIns5P regulate cancer cell migration and invasion through activation of Rac1. *Biochem J* **461**, 383-390, doi:10.1042/BJ20140132 (2014).

53 Viaud, J. *et al.* Phosphatidylinositol 5-phosphate regulates invasion through binding and activation of Tiam1. *Nat Commun* **5**, 4080, doi:10.1038/ncomms5080 (2014).

54 Yih, L. H., Wu, Y. C., Hsu, N. C. & Kuo, H. H. Arsenic trioxide induces abnormal mitotic spindles through a PIP4KIIgamma/Rho pathway. *Toxicol Sci* **128**, 115-125, doi:10.1093/toxsci/kfs129 (2012).

55 Jaldin-Fincati, J. R., Pavarotti, M., Frendo-Cumbo, S., Bilan, P. J. & Klip, A. Update on GLUT4 Vesicle Traffic: A Cornerstone of Insulin Action. *Trends Endocrinol Metab* **28**, 597-611, doi:10.1016/j.tem.2017.05.002 (2017).

56 Fruman, D. A. *et al.* The PI3K Pathway in Human Disease. *Cell* **170**, 605-635, doi:10.1016/j.cell.2017.07.029 (2017).

57 Mendoza, M. C., Er, E. E. & Blenis, J. The Ras-ERK and PI3K-mTOR pathways: cross-talk and compensation. *Trends Biochem Sci* **36**, 320-328, doi:10.1016/j.tibs.2011.03.006 (2011).

58 O'Reilly, K. E. *et al.* mTOR inhibition induces upstream receptor tyrosine kinase signaling and activates Akt. *Cancer Res* **66**, 1500-1508, doi:10.1158/0008-5472.CAN-05-2925 (2006).

59 Guittard, G. *et al.* Cutting edge: Dok-1 and Dok-2 adaptor molecules are regulated by phosphatidylinositol 5-phosphate production in T cells. *J Immunol* **182**, 3974-3978, doi:10.4049/jimmunol.0804172 (2009).

60 Wilcox, A. & Hinchliffe, K. A. Regulation of extranuclear PtdIns5P production by phosphatidylinositol phosphate 4-kinase 2alpha. *FEBS Lett* **582**, 1391-1394, doi:10.1016/j.febslet.2008.03.022 (2008).

61 Carricaburu, V. *et al.* The phosphatidylinositol (PI)-5-phosphate 4-kinase type II enzyme controls insulin signaling by regulating PI-3,4,5-trisphosphate degradation. *Proc Natl Acad Sci U S A* **100**, 9867-9872, doi:10.1073/pnas.1734038100 (2003).

62 Niebuhr, D. *et al.* Conversion of PtdIns(4,5)P2 into PtdIns(5)P by the S.flexneri effector IpgD reorganizes host cell morphology. (2002).

63 Pendaries, C. *et al.* PtdIns(5)P activates the host cell PI3-kinase/Akt pathway during Shigella flexneri infection. *EMBO J* **25**, 1024-2034, doi:10.1038/ (2006).

64 Jones, D. R., Foulger, R., Keune, W. J., Bultsma, Y. & Divecha, N. PtdIns5P is an oxidative stress-induced second messenger that regulates PKB activation. *FASEB J* **27**, 1644-1656, doi:10.1096/fj.12-218842 (2013).

65 Bulley, S. J. *et al.* In B cells, phosphatidylinositol 5-phosphate 4-kinase-alpha synthesizes PI(4,5)P2 to impact mTORC2 and Akt signaling. *Proc Natl Acad Sci U S A*, doi:10.1073/pnas.1522478113 (2016).

66 Hong, J. H. *et al.* Convergence of IRBIT, phosphatidylinositol (4,5) bisphosphate and WNK/SPAK kinases in regulation of the NA+-HCO3- cotransporters family. (2013).

67 Kawaai, K. *et al.* Splicing variation of Long-IRBIT determines the target selectivity of IRBIT family proteins. *Proc Natl Acad Sci U S A* **114**, 3921-3926, doi:10.1073/pnas.1618514114 (2017).

68 Ando, H. *et al.* IRBIT Interacts with the Catalytic Core of Phosphatidylinositol Phosphate Kinase Type Ialpha and IIalpha through Conserved Catalytic Aspartate Residues. *PLoS One* **10**, e0141569, doi:10.1371/journal.pone.0141569 (2015).

69 Davis, M. I. *et al.* A homogeneous, high-throughput assay for phosphatidylinositol 5-phosphate 4-kinase with a novel, rapid substrate preparation. *PLoS One* **8**, e54127, doi:10.1371/journal.pone.0054127 (2013).

70 Clarke, J. H. *et al.* The function of phosphatidylinositol 5-phosphate 4-kinase gamma (PI5P4Kgamma) explored using a specific inhibitor that targets the PI5P-binding site. *Biochem J* **466**, 359-367, doi:10.1042/BJ20141333 (2015).

71 Kitagawa, M. *et al.* Dual blockade of the lipid kinase PIP4Ks and mitotic pathways leads to cancer-selective lethality. *Nat Commun* **8**, 2200, doi:10.1038/s41467-017-02287-5 (2017).

72 Al-Ramahi, I. *et al.* Inhibition of PIP4Kgamma ameliorates the pathological effects of mutant huntingtin protein. *Elife* **6**, doi:10.7554/eLife.29123 (2017).

73 Nandez, R. *et al.* A role of OCRL in clathrin-coated pit dynamics and uncoating revealed by studies of Lowe syndrome cells. *Elife* **3**, e02975, doi:10.7554/eLife.02975 (2014).

74 Malek, M. *et al.* PTEN Regulates PI(3,4)P2 Signaling Downstream of Class I PI3K. *Mol Cell* **68**, 566-580 e510, doi:10.1016/j.molcel.2017.09.024 (2017).

75 Nakatsu, F. *et al.* PtdIns4P synthesis by PI4KIIIalpha at the plasma membrane and its impact on plasma membrane identity. *J Cell Biol* **199**, 1003-1016, doi:10.1083/jcb.201206095 (2012).

76 Pelossof, R. *et al.* Prediction of potent shRNAs with a sequential classification algorithm. *Nat Biotechnol* **35**, 350-353, doi:10.1038/nbt.3807 (2017).

77 Fellmann, C. *et al.* Functional identification of optimized RNAi triggers using a massively parallel sensor assay. *Mol Cell* **41**, 733-746, doi:10.1016/j.molcel.2011.02.008 (2011).

78 Fellmann, C. *et al.* An optimized microRNA backbone for effective single-copy RNAi. *Cell Rep* **5**, 1704-1713, doi:10.1016/j.celrep.2013.11.020 (2013).

79 Schwanhausser, B. *et al.* Global quantification of mammalian gene expression control. *Nature* **473**, 337-342, doi:10.1038/nature10098 (2011).

80 Chatzispyrou, I. A., Held, N. M., Mouchiroud, L., Auwerx, J. & Houtkooper, R. H. Tetracycline antibiotics impair mitochondrial function and its experimental use confounds research. *Cancer Res* **75**, 4446-4449, doi:10.1158/0008-5472.CAN-15-1626 (2015).

81 Sun, Y., Thapa, N., Hedman, A. C. & Anderson, R. A. Phosphatidylinositol 4,5-bisphosphate: targeted production and signaling. *Bioessays* **35**, 513-522, doi:10.1002/bies.201200171 (2013).

82 Kwiatkowska, K. One lipid, multiple functions: how various pools of PI(4,5)P(2) are created in the plasma membrane. *Cell Mol Life Sci* **67**, 3927-3946, doi:10.1007/s00018-010-0432-5 (2010).

83 Ishihara, H. *et al.* Type I phosphatidylinositol-4-phosphate 5-kinase. *J Biol Chem* **273**, 8741-8748 (1998).

84 Santarius, M., Lee, C. H. & Anderson, R. A. Supervised membrane swimming: small G-protein lifeguards regulate PIPK signalling and monitor intracellular PtdIns(4,5)P2 pools. *Biochem J* **398**, 1-13, doi:10.1042/BJ20060565 (2006).

85 Weernink, P. A. *et al.* Activation of type I phosphatidylinositol 4-phosphate 5-kinase isoforms by the Rho GTPases, RhoA, Rac1, and Cdc42. *J Biol Chem* **279**, 7840-7849, doi:10.1074/jbc.M312737200 (2004).

86 Tolias, K. F. *et al.* Type Ia phosphatidylinositol-4-phosphate 5-kinase mediates Rac-dependent actin assembly. *Curr Biol* **10**, 153-156 (2000).

87 Manning, B. D. & Toker, A. AKT/PKB Signaling: Navigating the Network. *Cell* **169**, 381-405, doi:10.1016/j.cell.2017.04.001 (2017).

88 Saito, K. *et al.* BTK regulates PtdIns-4,5-P2 synthesis: Importance for Calcium Signaling and PI3K activity. *Immunity* **19**, 669-678 (2003).

89 Choi, S. *et al.* Agonist-stimulated phosphatidylinositol-3,4,5-trisphosphate generation by scaffolded phosphoinositide kinases. *Nat Cell Biol* **18**, 1324-1335, doi:10.1038/ncb3441 (2016).

90 Sancak, Y. *et al.* PRAS40 is an insulin-regulated inhibitor of the mTORC1 protein kinase. *Mol Cell* **25**, 903-915, doi:10.1016/j.molcel.2007.03.003 (2007).

91 Hsu, F. & Mao, Y. The structure of phosphoinositide phosphatases: Insights into substrate specificity and catalysis. *Biochim Biophys Acta* **1851**, 698-710, doi:10.1016/j.bbalip.2014.09.015 (2015).

92 Abramovici, H. *et al.* Diacylglycerol kinase zeta regulates actin cytoskeleton reorganization through dissociation of Rac1 from RhoGDI. *Mol Biol Cell* **20**, 2049-2059, doi:10.1091/mbc.E07-12-1248 (2009).

93 Aikawa, Y. & Martin, T. F. ARF6 regulates a plasma membrane pool of phosphatidylinositol(4,5)bisphosphate required for regulated exocytosis. *J Cell Biol* **162**, 647-659, doi:10.1083/jcb.200212142 (2003).

94 Chatah, N. E. & Abrams, C. S. G-protein-coupled receptor activation induces the membrane translocation and activation of phosphatidylinositol-4-phosphate 5-kinase I alpha by a Rac- and Rho-dependent pathway. *J Biol Chem* **276**, 34059-34065, doi:10.1074/jbc.M104917200 (2001).

95 Krauss, M. *et al.* ARF6 stimulates clathrin/AP-2 recruitment to synaptic membranes by activating phosphatidylinositol phosphate kinase type Igamma. *J Cell Biol* **162**, 113-124, doi:10.1083/jcb.200301006 (2003).

96 Bumpus, T. W. & Baskin, J. M. A chemoenzymatic strategy for imaging cellular phosphatidic acid synthesis. (2016).

97 Tolias, K. F., Cantley, L. C. & Carpenter, C. L. Rho Ramily GTPases bind to phosphoinositide kinases. *J Biol Chem* **270**, 17656-17659 (1995).

98 van Hennik, P. B. *et al.* The C-terminal domain of Rac1 contains two motifs that control targeting and signaling specificity. *J Biol Chem* **278**, 39166-39175, doi:10.1074/jbc.M307001200 (2003).

99 Nakano-Kobayashi, A. *et al.* Role of activation of PIP5Kg661 by AP-2 complex in synaptic vesicle endocytosis. *EMBO J* **26**, 1105-1116, doi:10.1038/ (2007).

100 Bumpus, T. W. & Baskin, J. M. Clickable Substrate Mimics Enable Imaging of Phospholipase D Activity. *ACS Cent Sci* **3**, 1070-1077, doi:10.1021/acscentsci.7b00222 (2017).

101 Hinchliffe, K. A., Giudici, M. L., Letcher, A. J. & Irvine, R. F. Type IIa phosphatidylinositol phosphate kinase associates with the plasma membrane via interaction with type I isoforms. *Biochem J* **363**, 563-570 (2002).

102 Huttlin, E. L. *et al.* Architecture of the human interactome defines protein communities and disease networks. *Nature* **545**, 505-509, doi:10.1038/nature22366 (2017).

103 Jurrus, E. *et al.* Improvements to the APBS biomolecular solvation software suite. *Protein Sci* **27**, 112-128, doi:10.1002/pro.3280 (2018).

104 Wisniewski, J. R., Hein, M. Y., Cox, J. & Mann, M. A "proteomic ruler" for protein copy number and concentration estimation without spike-in standards. *Mol Cell Proteomics* **13**, 3497-3506, doi:10.1074/mcp.M113.037309 (2014).

105 Bua, D. J., Martin, G. M., Binda, O. & Gozani, O. Nuclear phosphatidylinositol-5-phosphate regulates ING2 stability at discrete chromatin targets in response to DNA damage. *Sci Rep* **3**, 2137, doi:10.1038/srep02137 (2013).

106 Gozani, O. *et al.* The PHD Finger of the Chromatin-Associated Protein ING2 Functions as a Nuclear Phosphoinositide Receptor. *Cell* **114**, 99-111, doi:10.1016/s0092-8674(03)00480-x (2003).

107 Jones, D. R. *et al.* Nuclear PtdIns5P as a transducer of stress signaling: an in vivo role for PIP4Kbeta. *Mol Cell* **23**, 685-695, doi:10.1016/j.molcel.2006.07.014 (2006).

108 Stijf-Bultsma, Y. *et al.* The Basal Transcription Complex Component TAF3 Transduces Changes in Nuclear Phosphoinositides into Transcriptional Output. *Mol Cell* **58**, 453-467, doi:10.1016/j.molcel.2015.03.009 (2015).

109 Wang, Y. H. *et al.* DNA damage causes rapid accumulation of phosphoinositides for ATR signaling. *Nat Commun* **8**, 2118, doi:10.1038/s41467-017-01805-9 (2017).

110 Blind, R. D. *et al.* The signaling phospholipid PIP3 creates a new interaction surface on the nuclear receptor SF-1. *Proc Natl Acad Sci U S A* **111**, 15054-15059, doi:10.1073/pnas.1416740111 (2014).

111 Mellman, D. L. *et al.* A PtdIns4,5P2-regulated nuclear poly(A) polymerase controls expression of select mRNAs. *Nature* **451**, 1013-1017, doi:10.1038/nature06666 (2008).

112 Bondeson, D. P. & Crews, C. M. Targeted Protein Degradation by Small Molecules. *Annu Rev Pharmacol Toxicol* **57**, 107-123, doi:10.1146/annurev-pharmtox-010715-103507 (2017).

113 Semenas, J. *et al.* The role of PI3K/AKT-related PIP5K1alpha and the discovery of its selective inhibitor for treatment of advanced prostate cancer. *Proc Natl Acad Sci U S A* **111**, E3689-3698, doi:10.1073/pnas.1405801111 (2014).